The University Of Sheffield.

Optimising Blends of Blast Furnace Slag for the Immobilisation of Nuclear Waste

Rebecca Anne Sanderson

A thesis submitted in partial fulfilment of the requirements for the degree of Nuclear Engineering Doctorate

Immobilisation Science Laboratory
Department of Materials Science and Engineering
The University of Sheffield

March 2019

Abstract

The UK nuclear industry uses cement encapsulation as the preferred treatment option for intermediate level waste. The grout is a mix of Portland cement (10-25 wt. %) with blast furnace slag (75-90 wt. %) and is required to conform to strict performance criteria in order to achieve successful encapsulation. However, the supply of cement powder to the nuclear industry has been inconsistent, causing changes in the performance properties of the material over time. The supply of BFS changed from a unique powder specifically designed for the UK nuclear industry to a set of commercially available materials due to economic changes to the cement industry.

A significant difference between the commercial material and the cement powders used historically, is the particle size. The particle size distributions of the commercial powders are much narrower and finer (higher specific surface area). This affects the rheology, fluidity, setting time, bleed and water demand of the cement grouts produced. In order to broaden the particle size distribution of blast furnace slag, a coarse and fine fraction with a similar chemical compositions were mixed together. By blending the two materials, it was possible to produce cement powder blends with a lower specific surface area that mimics the original specification powder.

This research investigates the effect of altering the ratio of fine and coarse materials by monitoring the performance of the blast furnace slag in varying blends. The physical properties were monitored using fluidity, heat of hydration, setting time and the yield stress of the system. The ability of the cement pastes to infill around simulant nuclear waste was also determined using high resolution tomographic analysis. Large scale trials were also undertaken to simulate plant operations. The results found that each extreme of the blend (i.e. at 100 wt. % of either the finer or coarser material), the cement pastes do not conform to the required specification. This confirms the requirement for blending the two materials to produce the ideal particle size for the optimum performance. This will help future-proof the supply of cement powders to the nuclear industry.

Acknowledgements

The first person I would like to mention and express a big thank you to is Prof. John Provis for his continued positivity and encouragement throughout this project. John was always there to offer support and advice, both during my time at Sheffield and via email whilst I was based at NNL. I would also like to thank Gavin Cann who was my second supervisor, for providing valuable industrial input and supporting me during my time based at NNL. I am very grateful to have had expertise from both academia and industry, which has contributed significantly to the progress of this research project.

My biggest thanks you goes to my family and friends who have been a constant support and motivation. A special thank you goes to Dr. Laura Gardner, who has been an amazing friend and colleague throughout the project.

I would like to thank the Immobilisation Science Laboratory group (ISL) at the University of Sheffield and the team at NNL Workington, who all made me feel very welcome and made working at both places much more enjoyable. In particular, Dr. Oday Hussein who helped me at the labs in Sheffield, Dr. Brant Walkley for helping out with the tomography and radiography experiments and Helen Dixon for her continued support and help in the wet lab at NNL.

Thank you to Stefan Michalik and Michael Drakopoulos for their help and advice during the beamtime experiments at the Diamond Light Source and to Helen Farris from Sellafield Ltd. for her support and experienced input during the project.

Finally, I would like to thanks the EPSRC and Sellafield Ltd. for funding this research. It has provided me with the opportunity to work on an industrially focused project and develop skills to further my career.

Publications

Journal Articles

1. R. A. Sanderson, G. M. Cann, J. L. Provis, The effect of blast-furnace slag particle size on the hydration of slag-Portland cement grouts at elevated temperatures, *Advances in Cement Research,* **2018***, 30*: 337-344.
2. R. A. Sanderson, G. M. Cann, J. L. Provis, Comparison of calorimetric methods for the assessment of slag cement hydration, *Advances in Applied Ceramics,* **2017***, 116*: 186-192

Oral Presentations

1. R. A. Sanderson, G. M. Cann, J. L.Provis, Scale-up effects in the use of slag-blended cements for nuclear waste immobilisation, *37th Cement and Concrete Science Conference,* London, Sept 11-12, **2017** (printed proceedings)
2. R. A. Sanderson, G. M. Cann, J. L.Provis, Optimising blends of blast furnace slag for the immobilisation of nuclear waste, *Nuclear Vision Conference,* Workington, June 29th, **2017**
3. R. Sanderson, G. Cann, J. Provis, The Effect of Particle Size on the Hydration of Blast Furnace Slag Blended Grouts for the Immobilisation of Nuclear Waste, *Microdurability The 3rd International RILEM Conference on Microstructure Related Durability of Cementitious Composite,* Nanjing, China , October 24-26th, **2016** (printed proceedings)
4. R. A. Sanderson, G. M. Cann, J. L.Provis, Optimising blends of blast furnace slag for the immobilisation of nuclear waste, *36th Cement and Concrete Science Conference,* Cardiff, Sept 11-12, **2017** (printed proceedings)
5. R. Sanderson, G. Cann & J. Provis, Optimising Blends of Blast Furnace Slag for the Immobilisation of Nuclear Waste, *Waste Management Symposia*, Phoenix, Arizona USA, 6-10th March **2016** (printed proceedings)
6. R. A. Sanderson, G. M. Cann, J. L.Provis, The effect of particle size on the hydration and heat evolution of blast furnace slag blended grouts, *35th Cement and Concrete Science Conference,* Aberdeen, Aug 26th -28th, **2015** (printed proceedings)

Poster Presentations

1. R. A. Sanderson, G. M. Cann, J. L.Provis, Optimising blends of blast furnace slag for the immobilisation of nuclear waste, *European Nuclear Young Generation Forum,* Paris, June 22nd – 26th, **2015**
2. R. A. Sanderson, G. M. Cann, J. L.Provis, Optimising blends of blast furnace slags for the immobilisation of nuclear waste, *35th Cement and Concrete Science Conference,* Sheffield, Sept 14th – 17th, **2014** (printed proceedings)

Awards

Scholarship Recipient – Roy G. Post Scholarship Recipient – *Waste Management Symposium, March 2017*

2nd place - IOM3 Young Persons' Lecture Competition – *Local Society Heat, November 2017*

Industry Events

1. R. A. Sanderson, G. M. Cann, J. L.Provis, Scale-up effects in the use of slag-blended cements for nuclear waste immobilisation, *Waste Packaging & Storage Group Meeting (sponsored by the Nuclear Decommissioning Authority),* Cumbria, Oct 9th, **2017**

Abbreviations

AFm	Alumina, ferric oxide, monosulphate
AGR	Advanced Gas-cooled Reactor
BET	Braunauer-Emmett-Teller
BFS	Blast furnace slag
BNFL	British Nuclear Fuels Ltd
CS	Compressive Strength
C-S-H	Calcium silicate hydrate
DLS	Diamond light source
EARP	Enhanced Actinide Removal Plant
EngD	Engineering Doctorate
FA	Fly ash
GBFS	Ground granulated blast furnace slag
GGBS	Ground granulated blastfurnace slag
GDF	Geological disposal facility
HLW	High level waste
ICC	Isothermal conduction calorimetry
ILW	Intermediate level waste
JEEP	Joint Engineering, Environment and Processing
LLW	Low level waste
LLWR	Low level waste repository
LWR	Light Water Reactor
Magnox	MAGnesium Non-OXidising
MEP	Magnox encapsulation plant
NDA	Nuclear decommissioning authority
NNL	National Nuclear Laboratory
OPC	Ordinary Portland cement
PC	Portland cement
PETF	Product Evaluation Task Force
PSD	Particle size distribution
PTK	Port Talbot GGBS:Calumite:Ketton PC
RWM	Radioactive Waste Management Ltd
SA	Semi-adiabatic

SCM	Supplementary cementitious materials
SCR	Scunthorpe GGBS:Calumite:Ribblesdale PC
SEM	Scanning Electron Microscope
SL	Sellafield Ltd.
SSA	Specific surface area
THORP	Thermal oxide reprocessing plant
VLLW	Very low level waste
w/s	Water to solids content
WEP	Wastes encapsulation plant
WPEP	Waste Packaging and Encapsulation Plant
XRD	X-ray diffraction
XRF	X-ray fluorescence
YODEL	Yield stress model

Contents

1 Introduction

1.1 UK Nuclear Waste

Every industry produces waste, and the nuclear industry is no exception. However, it can be problematic to dispose of the waste produced from the nuclear fuel cycle. Nuclear waste is categorised depending on its radioactivity and degree of heat generation; in the UK there are four categories, which are high-, intermediate-, low and very low level wastes [1]. As of the last UK inventory in 2016, there is estimated to be 4.7 million cubic metres of radioactive waste either existing or forecast to be produced from current facilities and planned future operations [2]. Less than 1% of this is high level waste, just over 9% is intermediate level, and 90% is made up of low and very low level waste [3]. Low level waste (LLW) radioactive content must not exceed greater than 4 GBq per tonne of alpha activity or 12 GBq per tonne of beta/gamma activity and is disposed of at a near surface low level waste repository (LLWR) in Cumbria. Very low level waste (VLLW) is a category within LLW with activity levels low enough to safely dispose of to specific landfill sites. Intermediate level waste (ILW) and high level waste (HLW) both exceed the activity levels to be considered as LLW (i.e. greater than 4 GBq/t of alpha or 12 GBq per tonne of beta/gamma) [2]. However, ILW (e.g. fuel cladding, sludges) does not require heat to be taken into account during disposal, and the current favoured method is encapsulation in 500 L stainless steel drums within a cement matrix [4]. HLW contains material that is significantly heat generating due to its radioactive content (e.g. long lived fission products), which is produced during reprocessing operations at the Sellafield site. The disposal route for HLW is to immobilize the highly active liquor into a molten glass matrix. This process is called vitrification and forms a stable glass wasteform which in encased in stainless steel canisters [3, 5].

One of the biggest challenges faced by the nuclear industry is that although the wastes are categorised according to their radioactivity, within those waste streams the waste exists in a wide variety of different forms. ILW specifically has a broad inventory of waste streams ranging from solid metals to sludge originating from different processes. As a result, the waste has to be processed in slightly different ways whilst taking into consideration safety, radiation stability, physical/chemical properties and long term disposal [6, 7]. Cement grout encapsulation has been the favoured method of processing ILW because it is generally well understood and cement has historically been readily

available, proved to be a durable material whilst providing good shielding, relatively inexpensive, and acts as a diffusion barrier [8].

One of the cement grouts used in the UK for the encapsulation of nuclear waste is a blend of Portland cement (PC) and blast furnace slag (BFS). This cement formulation has been used for nearly 30 years [9]. However, during that period the sources of cement powders have changed, which has in turn altered the performance properties of the cement grout. The performance of the grout is essential in order to produce reliable and stable wasteforms [4]. The waste is encapsulated within a 500 L stainless steel drum, as shown in Figure 1.1.

Figure 1.1. Example of a typical wasteform containing ILW encapsulated in cement grout [10].

1.2 Geological Disposal Facility

Once the waste has been processed, the wasteforms are stored in safe and secure interim storage facilities until long term disposal becomes available. The current plan in the UK is to dispose of the ILW and HLW in a geological disposal facility (GDF). The facility will be highly engineered to isolate the radioactive waste within a multi barrier system to provide protection for long term disposal. It is essential that the engineered design works with the natural barrier that surrounds the GDF to prevent the release of radionuclides into the surrounding environment which could cause harm to life. This

barrier system will comprise of the initial wasteform itself, in which the waste is encapsulated/immobilised into a durable container. The next 'layer' will be in the form of a buffer, which will be cement-based for ILW and clay in the instance of HLW, before the final geological setting of the host rock, which is deep below the surface [10, 11]. The current plan is that the storage facility will be constructed at a depth of between 650 – 1000 m underground and will consist of a series of 'vaults' to store ILW, as shown in Figure 1.2, with an array of tunnels to house the HLW [10]. The depth of the facility will depend on the geology of the site, because at the time of writing, the location of the GDF has not been selected. The footprint of the GDF is estimated to be around 10 - 20 square kilometers.

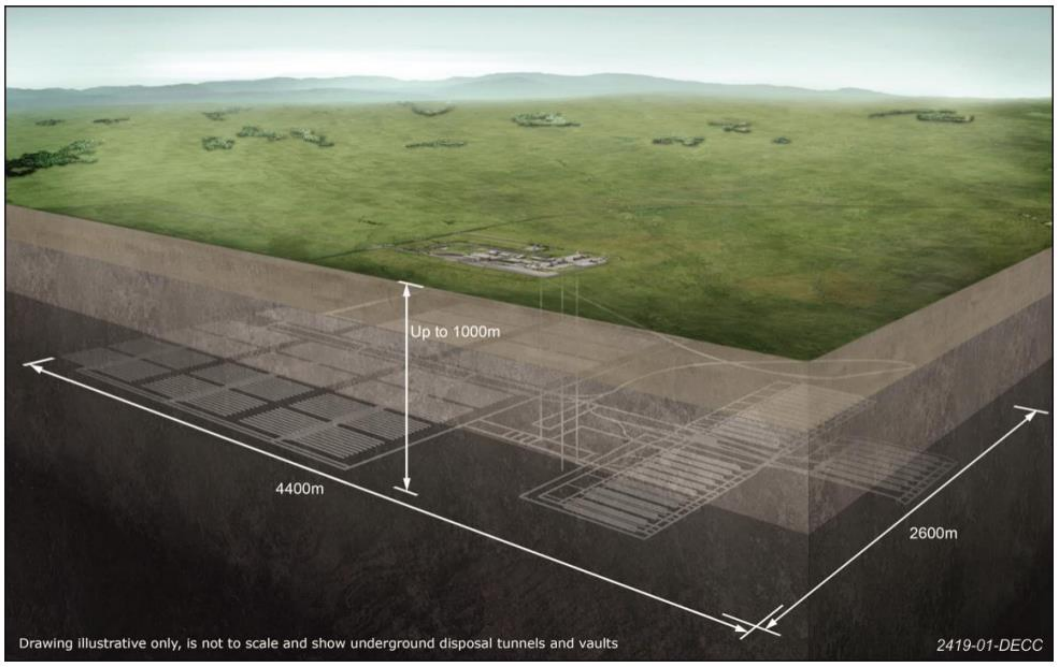

Figure 1.2. Geological disposal facility concept design [10].

1.3 Project Aims

Cement encapsulation is the preferred disposal route for ILW waste in the UK. This has been investigated and developed over a number of years, and the cement grout used has to perform to very specific requirements in order to ensure the production of consistent wasteforms. However, during this timeframe a number of different material sources have been used due to economic challenges within the cement industry. As a result, this change in cement powder source has affected the performance of the grouts produced. The nuclear industry previously used a bespoke special grade of BFS material, but unfortunately this has become unavailable. Alternative cement materials were

considered until a suitable source was found and introduced into the encapsulation plants on a trial basis [12]. The replacement materials were readily available industry standard cement binders and has been a successful alternative, but further optimisation of the blend is required.

The issues with the supply have mainly been with the BFS, and particularly ensuring that the powder being produced meets the Sellafield Ltd (SL) specification. The BFS currently used at Sellafield is a blend of ground granulated blast furnace slag (GGBS) and a coarser fractioned slag called Calumite [13]. The performance of Calumite in a blended format has not been reported in the technical literature, although it is assumed to behave with similar characteristics to a standard slag. The particle size of the cement powders used contributes significantly to the performance properties of the cement matrices, but has not been investigated in depth with regard to nuclear waste encapsulation. The reason this is of high importance is that the powders investigated from different sources exhibit a similar chemical composition but the particle size distributions of the materials differ significantly. Further validation and optimisation of the blend of GGBS and Calumite is required in terms of particle size.

The investigation of the effect of particle size distribution of the precursor cement powders used for nuclear waste encapsulation is presented in this thesis. The aim of the project is to future proof the supply of cement for the UK's nuclear cementation program. This will be achieved by determining how the particle size of the cement powders affects:

- The fresh state properties of the grout
- The heat evolution of the cement pastes during the early stages of the hydration reaction
- The infill process and wasteform production
- The scalability of the cement system from laboratory scale to 500 L plant scale wasteforms

2 Literature Review

This literature review intends to introduce the research under discussion in this thesis. However, further literature and discussion are also presented at the start of each chapter. As a result, this chapter will familiarise the reader with the topic area and the following chapters will complement and expand on the information presented here.

2.1 Cement Products

Cement has been produced for nearly 200 years and now dominates the global construction industry [14]. The total UK consumption of cementitious materials is estimated to be 10 million tonnes a year [15]. The most prominent cement used is Portland cement but other supplementary materials have become popular as suitable substitutes. Supplementary cementitious materials (SCM's) are often industrial by-products such as fly ash and slag cement and they contribute to the properties of the cement product through hydraulic or pozzolanic activity.

2.1.1 Portland Cement

Portland cement (PC) is produced by the calcination of lime such as limestone or chalk and silica/alumina such as clay or shale, at high temperatures of about 1450˚C in a rotary kiln [16]. Clinker is produced and is made up of four major phases called alite (Ca_3SiO_5/C_3S), belite (Ca_2SiO_4/C_2S), tricalcium aluminate ($Ca_3Al_2O_6$/C_3A) and a ferrite phase (Ca_2AlFeO_5/C_4AF). The clinker is combined with gypsum, which regulates the rate of setting and prevents flash setting, before it is ball milled and finely ground to create the final product, Portland cement. Of the four major phases, alite constitutes about 50-70 wt. % of cement and contributes to the majority of the strength development at up to 28 days curing. However, the hydration of alite is a highly exothermic reaction causing a high rate of heat evolution, which is an undesirable quality for the encapsulation of radioactive waste, due to the increased risk of cracking of the wasteform i.e. the waste and grout. The main hydration product from the alite reaction is calcium silicate hydrate (C-S-H), along with portlandite [8, 16]. Belite (15-30 wt. % of the cement) reacts in a similar manner to alite but at a slower rate enhancing longer term strength. The final two phases, tricalcium aluminate (5-10 wt. %) and the ferrite phase (5-15 wt. %) react with the gypsum forming ettringite ($Ca_6Al_2(SO_4)_3(OH)_{12}\cdot 26H_2O$) and monosulphoaluminate ($Ca_4Al_2(SO_4)(OH)_{12}\cdot 6H_2O$) [16].

Portland cement can be blended with supplementary cementitious materials (SCM) to form a composite cement. This is a hydraulic cement (meaning that it hardens and

retains strength even under water as defined in BS EN 197-1 [17]), where the SCM contributes to the hydration reaction causing a change in the hydration product. Examples of SCMs include fly ash (FA), a by-product of coal power stations, other pozzolans, limestone, and granulated blast furnace slag (GBFS) from the iron and steel manufacturing industry. The substitution of Portland cement with SCMs has several advantages: it reduces the CO_2 emissions produced, reduces energy consumption associated with clinker formation because less material is needed, there is increased performance associated with them such as; enhanced durability and improved rheology, and the process utilises industrial wastes [16, 18].

Currently, the nuclear industry utilise composite cements for encapsulation of radioactive waste. Portland cement is blended with either FA or GBFS to form grouts with varying replacement percentages depending on the waste stream intended for disposal [9]. Similarly to Portland cement, composite cements have several characteristics that make them a suitable candidate for use during the encapsulation of nuclear waste. These attributes are that they: [8]

- form a fluid grout suitable for encapsulation of unusual shaped wastes
- set and are durable in their hardened state whilst providing shielding
- modify the pore structure to further reduce transport of radionuclides
- have a lower pH than that of Portland cement to reduce hydrogen release from any encapsulated aluminium or magnesium, whilst still maintaining a high pH to sufficiently decrease radionuclide solubility
- can be processed relatively easily under remote handling conditions
- are readily available and inexpensive
- limit the risk of thermal cracking by reducing heat evolution

2.1.2 Blast Furnace Slag

Blast furnace slag (BFS) is a by-product of iron-ore refinement, and is formed as a molten liquid within a blast furnace. The composition of the BFS varies according to the raw materials used but the key elements include calcium, magnesium, aluminium, and silicon oxides, and sulphide [19]. There are three main types of BFS and these are categorised by their method of cooling. Air-cooled BFS, which produces hard and dense slag suitable for construction aggregate, pelletized BFS that is mainly used in light weight aggregate, and granulated slag forms sand sized particles [20]. It is granulated slags that are of interest in this project.

Granulated BFS is only produced if the molten BFS is cooled relatively rapidly to temperatures below 800˚C. This is achieved by spraying the molten BFS with high

pressure jets of water, forming a wet and sandy material which when dry, can be ground and typically contains over 95 % glass. Although the composition changes depending on the plant of origin, a general overview of the major components are shown in Table 1 [16].

Table 2.1. Blast furnace slag oxide composition [16].

Component	Weight %
MgO	1-18
Al_2O_3	5-33
SiO_2	27-42
CaO	30-50

The grinding technique used significantly influences the BFS cement properties, and a number of studies have investigated the effect of using different methods [21-23]. Many types of grinding mills have been developed such as ball mills, vertical roller mills, airflow mills and high pressure grinding rolls to name a few. Tubular shaped ball mills have traditionally been used for grinding cement either in open or closed circuits [22]. The use of different grinding methods has an effect on the particle size, geometric characteristic and shape of the GGBS produced. Therefore, it is possible for the GGBS to have the same surface area but due to method of grinding, could potentially have different performance characteristics. It is reported that GGBS produced via ball mill grinding has the widest particle size distribution (PSD). It was also found that although some grinding methods produced GGBS with predominantly spherical particles, the ball mill method produces anomalous shaped particles with edges and angles [23]. A typical example of GGBS that has been ground using a ball mill is shown in Figure 2.1. The majority of the GGBS material under investigation in this project is ground in a closed-circuit ball mill. Once it has been through the grinding process, it is then passed through a separator segregating GGBS that conforms to the powder specification from material that does not. The 'rejected' GGBS is then sent for grinding once again [12].

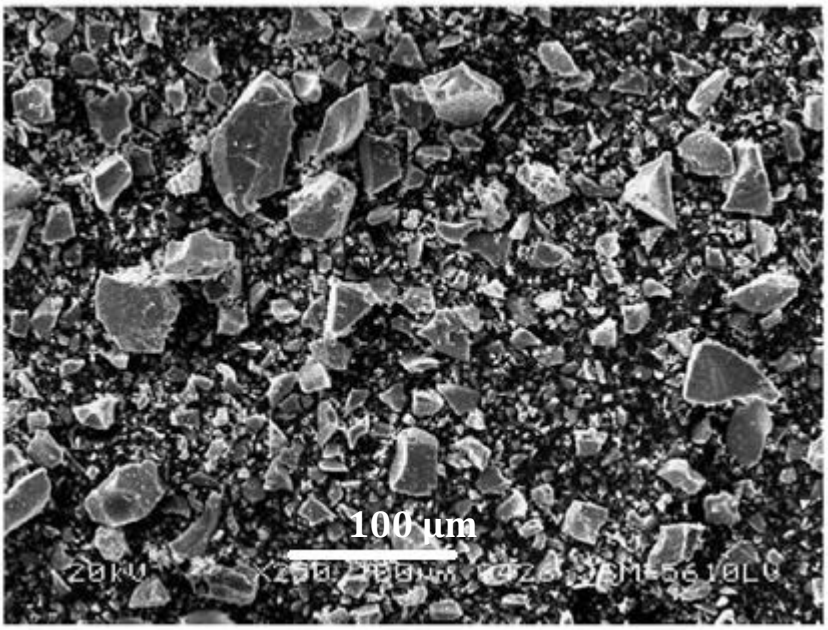

Figure 2.1. SEM IMAGE OF GGBS GROUND IN A BALL MILL [11].

A cementitious system where blast furnace slag (BFS) is combined with ordinary Portland cement (OPC) is used in the UK as a grout for the encapsulation of intermediate level radioactive waste (ILW) [24]. The hydration of the OPC releases alkaline and sulfate components that activate the BFS, forming a fluid cementitious grout [25]. A major advantage of using a BFS/OPC system is the low heat of hydration it offers, which means that heat development is a slower process (compared to a pure OPC system), reducing the risk of thermal cracking [19].

2.1.3 Calumite

Calumite is produced from granulated blast furnace slag and has been reportedly been used for over 25 years, predominantly in the manufacture of glass [26, 27]. Information about Calumite is not widely reported, especially in terms of use for cement grouts. The composition of Calumite is 99 wt. % glassy in nature and is seen as an alumina source but also contains all the major oxides required for glassmaking. The use of Calumite in the manufacture of glass is claimed to lower energy costs and improve the quality of the finished product [26]. The manufacture of Calumite requires a rigorous processing method to maintain quality control and produce a stringent specification. Calumite is processed in a similar manner to GGBS, but instead of grinding the material, it is crushed to less than 0.7 mm [28]. Calumite is used in this project in blends with GGBS, to modify the particle size of the BFS fraction used during encapsulation.

2.1.4 Chemistry of BFS/PC cement

The hydration of PC is complex because it is a multi-component system and a series of reactions occur successively and in parallel, creating an evolution of heat. The rate of hydration depends on the quantities of the four main phases alite, belite, tricalcium aluminate, and ferrite. However, during the hydration of a Portland cement-granulated slag mix it is even more complex because both materials will react with water. The hydration plot of rate vs time for blended BFS/PC systems replicates that of a standard Portland cement. The typical 4 stages of cement hydration are 1) the initial period, 2) the induction period, 3) acceleration period and 4) the deceleration period [29, 30]. To begin with, there is very little reaction observed between the water and the slag as it does not contain C_3S (tricalcium aluminate) or other fast-reacting hydraulic components. It is for this reason that PC becomes a crucial contributor to the reactivity of the cement grout. BFS with water alone does not tend to harden but when finely ground and mixed with an activator, BFS reacts at ambient temperature. PC behaves as the activator for the BFS by releasing hydroxide such as $Ca(OH)_2$, resulting in the formation of strength developing calcium silicate and calcium aluminate compounds [31]. The hydration kinetics of slag is slower than that of PC clinker and requires an alkaline environment which is produced as a result of clinker dissolution [32]. Therefore, the presence of slag in blended cements retards the acceleration period resulting in a lower peak heat. This consequently reduces water consumption during hydration.

The hydration properties of BFS affects the microstructure and phase assemblage of the cement product. In a Portland cement system the main hydration product is C-S-H. However, during slag hydration the C-S-H product incorporates aluminium and becomes a C-A-S-H gel and other products include a hydrotalcite like phase and strätlingite [33-35]. The C-A-S-H product in BFS is more amorphous than the C-S-H in PC. BFS/PC blended systems have a high pH is caused by $Ca(OH)_2$ which results in accelerated dissolution of the glassy phases in the slag and the formation of C-S-H. This helps reduce permeability of the hardened cement.

The characteristics discussed with regards to slag hydration are beneficial for ILW encapsulation because a lower heat of hydration reduces the risk of the cement matrix cracking in the wasteform and also results in a lower water demand minimising corrosion. The effect that BFS has on the hydration products is also advantageous due to a decrease in radionuclide solubility once the wasteforms in produced.

2.2 Properties of Blast Furnace Slag

2.2.1 Effect of Particle Size Distribution

As previously mentioned, the grinding of BFS has a significant impact on the particle shape, size and geometry, and in turn this affects the reactivity and performance of the grout produced from the cement powder. GGBS is ground to manufacture a certain specific surface area powder, and X-ray fluorescence spectroscopy has been used pre- and post-grinding to determine whether this process would cause separation of chemical fractions. This separation could lead to the enrichment of certain components, but the outcome showed that grinding the product does not affect the chemical composition of the material [9, 36], which would suggest the change in performance is instead caused by the change in size or shape.

It is easier to determine the performance of finer and coarser cement powders once they are mixed with water to form cement pastes or grouts. The finer a powder is, the higher the specific surface area, which increases the water demand [37]. As the water content increases, a greater water to cement ratio is achieved and this can cause a bleed. Bleed is caused due to the settlement of solid particles, which forces an increase in the water/solids (w/s) ratio at the top of the sample and a decrease at the bottom, forming a thin layer of water at the surface [16]. The formation of additional water is not desirable in the nuclear industry because it becomes a secondary waste to have to control and will need to be treated, as the waste acceptance criteria for the GDF states no free liquids are permitted [38]. In terms of particle size, there has been no firm relationship determined between the bleed of a grout and the particle size distribution (PSD) of the powder [25].

The fluidity of cement grouts is significantly affected by the particle size of the precursors used. As mentioned above, an increased surface area causes an increase in water demand. This means that if the water content remains unchanged, as the fineness of the GGBS powder increases, the fluidity of the cement system decreases. If the alternative is considered, as the fineness of the GGBS powder decreases, it will reach a point where segregation of cement powder and water could be observed. This confirms the requirement to control the particle size of the cement powders used during encapsulation [9, 39]. Fluidity of the system is a crucial performance requirement for the encapsulation of nuclear waste [40].

A finer powder is favoured in terms of strength and durability as it has been found that a narrower PSD produces higher strength [36]. This is important in terms of nuclear waste encapsulation because the wasteforms are required to be durable for long term

storage and for handling purposes. Alongside this, the compressive strength of BFS cement is improved with increased fineness [36]. It is reported that to obtain an effect on strength up to 28 days, the slag must be ground to less than 40 μm as the finer particles contribute to the early development of the hardened cement resulting in increased strength [37]. The coarser fraction of BFS is significant because it affects the strength development after 28 days [36]. An optimum balance is required between coarser and finer particles so that voids are minimised to avoid a loosening effect because this could affect the particle packing density [41].

Overall, a lower fineness provides an improved performance according to the criteria needed by the nuclear industry, which is why the Sellafield specification GGBS has a lower fineness than the typical British standard [9].

2.2.2 Rheology

The rheology of cement pastes relates to the yield stress of the material and its workability in processes such as transporting, pumping, compaction and pouring [31]. Factors for consideration that affect rheology include flow, segregation, settlement and the water content requirement [42]. Measuring the rheology of fresh cement can help predict the properties and performance of the grout or paste produced.

The mixing procedure for cement has a significant impact on the rheological properties of cement. High shear rates during mixing can break down the cement powder agglomerates, increasing the surface area and therefore the water demand resulting in an increased water demand that changes the fluidity of the material [43]. The fluidity of cement grout can be measured using the slump test method [44]. This method is widely used in the construction industry and consists of filling an upturned cone of specific dimensions with a cement grout before lifting the cone up vertically. The distance the cement grout travels under gravity is recorded by measuring either the height or the area of the 'slump' [45]. The Bingham model is used as an analysis methodology to describe the flow of cement by defining two parameters which are yield stress and plastic viscosity [46]. The Bingham model, presented in Equation 2.1, is a simple tool where τ is the shear stress, μ is the plastic viscosity, $\dot{\gamma}$ is the shear rate and τ_0 is the yield stress.

$$\tau = \tau_0 + \mu\dot{\gamma} \tag{2.1}$$

The yield stress of cement is measured at very high viscosity and at low shear rate in order to determine the shear stress at which flow starts/stops. Yield stress can be measured by rotational rheometers where the shear stress to initiate flow is measured

[42]. The rheological behaviour of cement pastes is affected by the PSD of the initial powder due to changes in the packing density with variation in particle size. With improved particle packing, a more dense material is produced which has lower porosity, allowing increased water availability to act as a lubricant for better fluidity [37]. Therefore, it has been concluded that there is a positive relationship between the packing density of a cement system and its rheological properties [41].

A recent study considered the relationship between the width of a Rosin-Rammler PSD and yield stress in ternary and binary systems. The model published predicts the yield stress using the PSD width, the water/solid ratio and a series of assumptions. Over 90 mixes were investigated by comparing experimental and calculated data [47]. Details of this model are presented in Chapter 5, where the model was used to estimate an optimal PSD in order to see whether it can be used to achieve the best performance properties for the ternary system under investigation. Understanding the rheology of the cement system is essential in order to achieve successful pumping and encapsulation of nuclear waste without the segregation of water and cement.

2.3 Cement Encapsulation

Cement is used for encapsulation of intermediate level waste on the Sellafield Ltd. site. Cementitious matrices provide an inexpensive and readily available method of treating waste streams whilst providing radiation shielding [8].

2.3.1 Intermediate Level Waste

There is an estimated total volume of 290,000 m^3 of intermediate level waste in the UK [3]. The ILW is made up of different materials producing different waste streams which require different treatment methods [48]. The two waste streams of interest in this study are Magnox swarf and THermal Oxide Reprocessing Plant (THORP) hulls.

The Magnox name is derived from MAGnesium Non-OXidising and is an alloy consisting of 99.2 wt. % magnesium and 0.8 wt. % aluminium. The waste arises from Magnox clad uranium metal fuel rods (Figure 2.2) that were used in Magnox nuclear reactors. In order to reprocess the uranium fuel, the Magnox cladding must be removed by mechanical decanning, which strips the cladding away from the fuel rod, shown in Figure 2.2. The decanning process produces the Magnox swarf which is then encapsulated in cement for final storage [40].

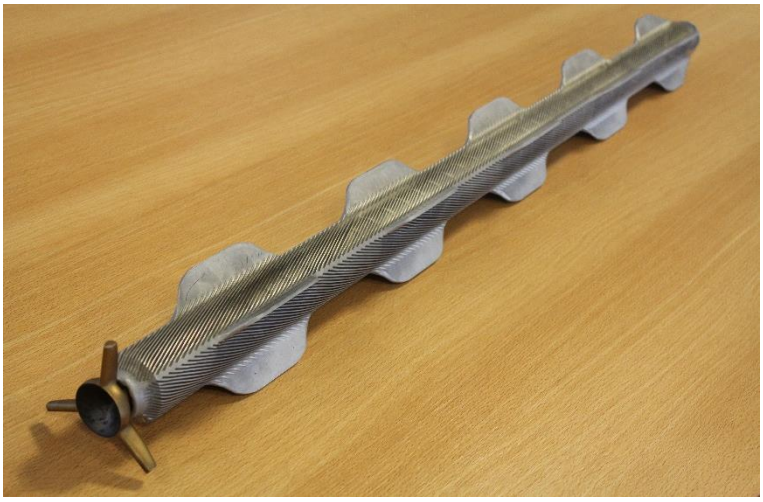

Figure 2.2. Dummy Magnox clad uranium metal fuel rod used in Magnox reactors.

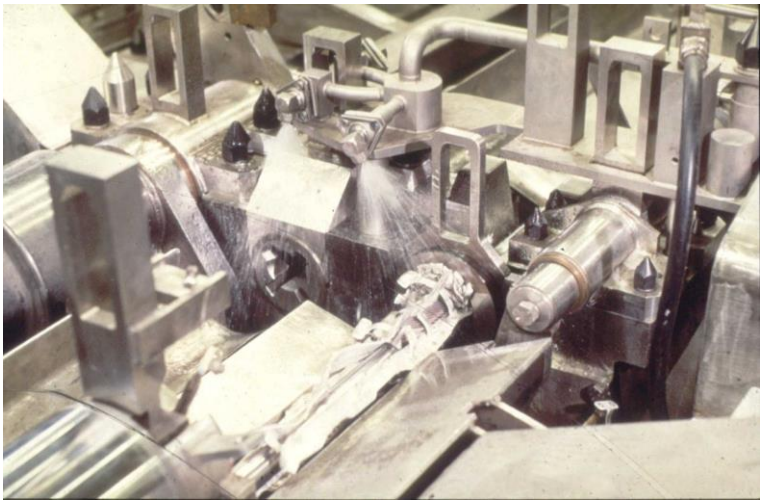

Figure 2.3. Image of the decanning process carried out in the Magnox Encapsulation Plant [49].

The waste stream containing THORP hulls arises from reprocessing of nuclear fuel assemblies used in both Light Water reactors (LWR) and Advanced Gas-Cooled reactors (AGR). The fuel assemblies consist of fuel pellets or pins enclosed within tubing made from either stainless steel or zircaloy. During reprocessing, the fuel is dissolved out of the tubing leaving it hollow before it is chopped up into smaller pieces of approximately 50-75 mm long. These sheared fuel pin cases are known as THORP hulls.

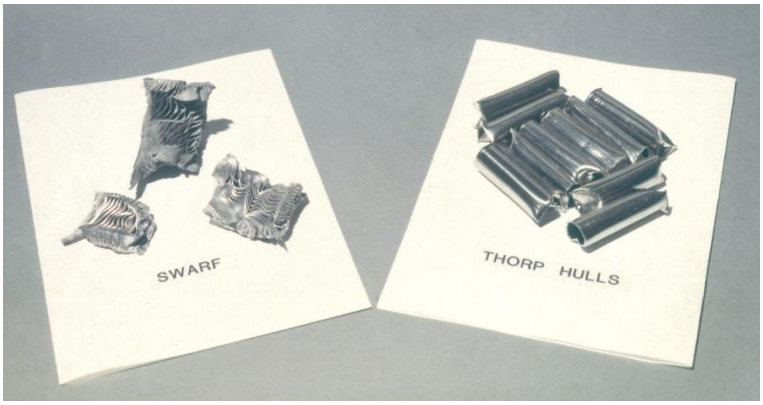

Figure 2.4. Images of typical Magnox swarf and THORP hulls; the wastes that are encapsulated at Sellafield [50].

2.3.2 Encapsulation Plants

In the 1980's, the main UK storage option for ILW was reaching capacity and as such, alternative options were investigated. The store had already been extended and it was decided that an additional expansion was not a long term solution. This is when the need for onsite encapsulation plants was considered. The initial design was to construct a single plant to encapsulate all ILW, including the inventory in storage and that produced from future processing. However, the lead-time for the construction and operation of this plant was not a suitable option as it would have meant that processing of Magnox swarf would have to cease temporarily, which was not desirable. An alternative option was presented where the concept for the single plant would be divided into three encapsulation plants [40]. These were:

- EP1: for Magnox swarf
- EP2: for THORP hulls and slurries, and enhanced actinide removal plant (EARP) flocs
- EP3: for in-store ILWs

The development for EP1 would be the priority in order to maintain the processing of Magnox swarf. The design originally proposed that EP2 would have two encapsulation lines capable of meeting needs for processing THORP hulls, THORP slurry wastes and EARP flocs, and it was also intended to encapsulate Magnox swarf as a back-up line to EP1. After a series of discussions and considerations, the final conclusion was that EP2 would have one encapsulation line. The feeds for consideration for EP2 were THORP hulls, slurry wastes, and retrieved ILW sludge wastes. EP1 remained the plant that would encapsulate Magnox swarf while the EARP flocs would be treated in a separate plant called the Waste Packaging and Encapsulation Plant (WPEP) [51].

Once the strategy for the different plants was decided, it was necessary to develop the encapsulation technique. As a result, the Product Evaluation Task Force (PETF) was set up to develop the encapsulation techniques for ILW streams. They had three objectives which were to determine the characteristics of the ILW waste streams, to optimise the matrix used for encapsulation, and to produce a database that included this information, i.e. the waste stream and the selected suitable matrix [40, 51]. The PETF were responsible for the development of the 'acceptance test' and the performance specification that the cement systems have to adhere to (to be discussed in section 2.4.3). The PETF also took into consideration what would happen to the cement system if there was a delay before it was used. As such the cement grout must still conform to specification after a 150 minute 'hold-up', where essentially the material will be kept agitated in the cement mixer until plant is ready to use the cement grout. This extended mixing time was incorporated into the acceptance test, and monitored during small scale testing.

EP1 was named the Magnox Encapsulation Plant (MEP) and was commissioned in 1990 [40]. EP2 became the Wastes Encapsulation Plant (WEP) and was commissioned in 1994 [52]. Both of these plants use the cement system under investigation in this project during the encapsulation process. The two plants have small differences in the grout formulation needed for the different types of waste, but the cementitious system is the same and the powders supplied for both originate from the same sources.

2.3.3 Wasteform Production

A significant amount of development was carried out over a number of years by the PETF team to develop the optimum method and process for the production of ILW wasteforms. In the nuclear industry the wasteform is defined as the waste and cement grout, whereas a waste package consists of both the wasteform and outer container. The final wasteform produced from both MEP and WEP consists of a 500 L stainless steel drum that is filled with the respective waste streams. The cement grout is then pumped into the drum and the product is then vibrated. This process is called vibrogrouting and is to enable the cement grout to flow freely during the infill process. Vibrogrouting encourages the displacement of air with grout to achieve minimal voidage in the product. The wasteform is then cured for approx. 24 hrs to allow the cement to set and develop strength before a lid is added and transported for storage [4, 40, 53, 54]. One of the biggest challenges during the whole process is that it is necessary for the whole encapsulation method to be carried out under remote handling conditions. This is necessary to maintain containment of radioactive material.

2.4 The Sellafield Ltd BFS Story

2.4.1 History of Supply

Over the past 20 years Sellafield have been faced with a number of difficulties and challenges in regard to the supply of cement powders for the encapsulation of radioactive waste. Although cement has been used in other industries for over two hundred years in various forms [31], it is still a relatively new technology for the nuclear industry. Using cement powders for the encapsulation of nuclear waste has been successful, and proved to be the favoured route for disposal [8]. However, due to changes in the cement industry such as plant closures, the supply of cement powder has not been consistent to the nuclear industry. This has caused additional and continual development of the cement powders used for encapsulation due to the unique specification needed for the encapsulation grouts [9].

A significant amount of research and development has gone into future proofing and decreasing the risk to cement powder supply in the UK nuclear industry [24]. The original BFS used at Sellafield was manufactured by Castle Cement at Ravenscraig steelworks and at their Coatbridge works. However, the steel works closed in 1992, causing the granulate supply to originate from the Redcar steelworks, but the material was still processed (ground) at the Coatbridge works. When the Coatbridge works finally closed, the grinding of the Redcar BFS was transferred to Castle Cement's Ribblesdale works based in Clitheroe [55]. The supply was changed again in 2003 after development work confirmed the viability of using Redcar BFS supplied by the North East Slag Cement works located in Redcar. The testing programme found that the Redcar BFS achieved the Sellafield specification in both small and full-scale trials. This was advantageous as it removed the need for transport between plants and the potential for contamination with PC because Ribblesdale is a Portland cement works [56]. In 2008, the availability of supply by Redcar Steelworks was promised for 10 years, but due to mothballing of the steelworks, production was ceased in February 2010 with notice of only three months [55].

It was decided between NNL, SL and Hanson Cement that, due to the significant risk to the supply and considering the very short timescale available to identify a suitable replacement, Hanson's Scunthorpe Cement works BFS would be the best option [12]. This conclusion was made based on research which demonstrated the GGBS had the properties required for the encapsulation of ILW [39]. Following the initial investigation into the suitability of Hanson's Scunthorpe supply, further development work was carried out. NNL reported a series of experimental trials which discovered that the

Scunthorpe BFS was finer, i.e. fell out of the desired 210-310 m^2/kg of the Sellafield Ltd. specification [39], causing low fluidity. To address the increased fineness, Hanson Cement had to modify their production process to incorporate a coarse fraction of partially ground BFS. This coarser BFS fraction was known as 'grits' and this was blended with their construction industry grade (BSEN 15167-1 [57]) product known as Ground Granulated Blastfurnace Slag (GGBS). This blended material was compared to the previous Redcar supply by assessing the performance of BFS/OPC grouts over a 10-week sampling period. Although the performance criteria were achieved by the blended material, a number of observations were raised such as variability within the 'grit' granulate, and that it seemed to hydrate quicker than the Redcar equivalent. One benefit from using the Scunthorpe GGBS/'grit' blend was the facility to change the blend, giving the ability to change the performance of the material such as bleed and flow relatively easily [12]. The Scunthorpe GGBS is a finished product that Hanson supply to the construction industry but the modification in their production process required in order to produce the 'grit' was quite significant. It soon became apparent that it was not a viable option for Hanson to continue to produce the 'grit' and it became unavailable after February 2010 [12]. As a result of this development, a second coarser fraction known as Calumite was proposed by Hanson Cement as an alternative and is currently used on the Sellafield Ltd site.

2.4.2 Development Work on Current Supply

Once Calumite was identified as a possible alternative to the 'grits' previously tested, NNL carried out work to determine how it would perform as part of the BFS fraction within the encapsulation grouts. A similar development programme to that of the GGBS/'grits' assessment was carried out on the alternative GGBS/Calumite system [28]. This programme again consisted of a 10-week sampling period of both the GGBS and Calumite and was carried out in two stages. In stage one, each sample of GGBS (i.e. week 1-10) was mixed and tested with each Calumite sample to monitor their properties. The performance of each grout (i.e. water and cement with no added aggregate) was measured using designated product quality tests such as; compressive strength and dimensional stability. Stage two of the testing was designed to investigate the sensitivity of the blended powder ratio by mixing both materials in increments of 10 wt. %. Grout acceptance tests were carried out on each of the blends including fluidity, bleed and setting times. It was found that the GGBS/Calumite blend ratio should be between 60/40 – 50/50 wt. % because these grouts gave the most favoured results and closest consistency with previous data. While the previous programme had focused on achieving the required fineness, this series of trials concentrated on the grout

performance such as; fluidity, bleed and setting times. It was considered that if the cementitious systems were achieving the required properties and the variety in fineness was within an 'acceptable envelope', the material was deemed satisfactory. This meant that any blended powder that had a fineness within the range of 260 ± 50 m^2/kg was considered to be suitable [58].

As expected, this development work showed that the finer a material is, the more reactive it will be, resulting in a faster setting time and quicker strength development [28]. It can also cause increased rates of hydration which reduces workability, but this can be a benefit because it decreases grout bleed. Bleed can be defined as the formation of a layer of water at the top surface of a cement sample as a result of the sedimentation of particles [31]. Some issues that surfaced during this programme involved the process of measuring the fineness of Calumite. It was found to be too difficult to produce a compact powder bed needed in the standard Blaine air permeability apparatus, therefore the Calumite fineness was only able to be assessed using stacks of sieves [28]. Useful information to consider in future trials would be that, as the BFS blend moved towards a high Calumite content, the samples without a hold up (after mixing for an initial 20 minutes and considered as t=0) experienced increased bleed up to >10 vol. %. Historic Redcar data [12] state that bleed values up to 5 vol. % at t=0 are acceptable but above this they are classified as non-conforming. This development work concluded that blends containing 10/90 and 20/80 wt. % GGBS:Calumite were declared to be non-conforming because they generated bleeds in excess of 5 vol. % at t=0. Equally, high GGBS content caused issues with fluidity and therefore a 90/10 wt. % GGBS/Calumite blend was also determined to be non-conforming. As a result of these findings defined the conforming blends to range from 80/20 – 40/60 wt. % GGBS/Calumite [28].

2.4.3 The Current Material and Specification

At the project start in 2013, the cement powders used on the Sellafield site was a blend ratio of 65:35 GGBS:Calumite wt. %, which was in operation since the end of 2012 [59]. These materials were used throughout this project as the baseline cement grout. However, by the end of the EngD project, the GGBS fraction of the BFS material was substituted for a very similar slag cement powder supplied by Hanson from their Port Talbot steelworks. This powder had been tested previously[13, 39] and showed promising results. Further development into the suitability of the Port Talbot cement powder as a replacement GGBS supply was carried out by NNL in 2016 [60]. The powder and performance of the materials used appeared in testing to be the same regardless of their source.

As previously mentioned, the PETF were responsible for producing a performance specification for the matrix intended for use during encapsulation and the requirements needed by the slag to make it a suitable option. The performance criteria consider fluidity, bleed, setting time and the heat of hydration. Optimisation of these criteria is crucial to achieve successful encapsulation. The fluidity of the matrix needs to be fluid enough to infill fully and flow through the plant, but not too much that it forms bleed or segregation and that it still sets efficiently. A low heat of hydration is important to prevent cracking within the waste form. In order to achieve the desired performance criteria, the powders have to conform to a specification defined by Sellafield that state limits for the chemical composition, density, fineness and glass content. The use of GGBS for encapsulation is beneficial because it lends itself to the specification requirements by containing a low alkali content to maintain a lower pH, whilst the chloride limits are defined in order to minimise Magnox and stainless steel corrosion and in turn the drum integrity.

Table 2.2.2. Additional requirements for the Sellafield Ltd specification [61] compared to the British Standard for construction.

Property	Sellafield Ltd Specification	British Standard
Fineness	There is no fineness limit.	The specific surface determined shall not be less than 275 m^2/kg.
Chemical composition	Shall have the following chemical limits (these are not controlled by the British and European Standard): $Fe_2O_3 \leq 1.0$ wt. % $Al_2O_3 \leq 15$ wt. % $Na_2O \leq 0.6$ wt. % $K_2O \leq 1.0$ wt. % Chloride ≤ 0.05 wt. %	The only exception is chloride as detailed below: Chloride ≤ 0.10 wt. %
Density	The material shall have a dry relative density of 2.80-3.00 g/cm^3.	Not specified
Glass Content	Shall comply with BS EN 15167-1 (≥67 wt. %).	

The Sellafield Ltd powder specifications for BFS comply with the British Standard BS EN 15167-1 [57] and BS EN 15167-2 [62]. There are a few additional limits/differences to the BS EN standard detailed that the SL specification BFS has to adhere to, as shown in Table 2.2.2.

Historically, the limits stated in the Sellafield Ltd specification for fineness were that the BFS powder should be within the range of 260 ± 50 m^2/kg, as determined using air permeability apparatus [58]. However, due to the changes in the material used for cement encapsulation, these limits were deemed not appropriate for a BFS produced by blending a coarser and finer material. As such, there is no current fineness limit and the acceptability of the powder is defined by the performance in the grout trials and development work. The additional chemical powder parameters are not absolute limits, but are used to identify any powders that should be monitored on plant for grout performance. The limits associated with the density were originally adopted to ensure consistency of the slag produced from the blast furnace, and that excessive iron was not carried over in the material [61].

The blend of BFS is then mixed with Sellafield specification ordinary Portland cement (OPC) at a ratio of 3:1 BFS:OPC with a water/solids ratio of 0.35. This is a baseline formulation used for acceptance testing and the grouts produced with this blend must conform to the Sellafield Ltd specification shown in Table 2.2.3. The laboratory scale acceptance tests have been designed to measure 'critical grout properties', but in reality and on plant the materials used will be more fluid, ensuring acceptable grouts [58].

When the acceptance test method was initially developed by the PETF, the plant set points were not established and they decided that a 75 wt. % replacement of Portland cement with BFS would be a reasonable starting point. A significant amount of development work was carried out at this BFS:PC ratio, which was found to produce promising and consistent data. As a result of this initial experimental programme, the acceptance test used today (20-30 years later) is still based on a 3:1 BFS:PC ratio. On-site, WEP operates at a target grout ratio of 4.5:1 BFS/OPC with a water/solids content of 0.35:1 [53], whereas MEP operates at a target grout ratio of 3.44:1 BFS/PC with a w/s content of 0.35:1 [40, 54]. This means that the grout used in WEP has a higher BFS content than MEP, this is due to the different types of waste processed in either plant and the different mixers used. At MEP a high shear, 250 L SD10 'off the shelf' mixer supplied by Colcrete [40] is used. The mixer used at WEP is a bespoke 500 L, mid-shear design produced specifically for BNFL [53].

Table 2.2.3. Sellafield Ltd specification for physical properties of the BFS/OPC grout [58].

Physical Properties	Test Method	Technical Requirement
Flow	Colflow test at 20 ± 5˚C *	To have minimum Colflow > 200 mm at 150 minutes after total initial high-shear mixing period.
Initial and Final Set	Vicat test	Grouts should not undergo initial set in less than 4 hours or final set in greater than 24 hours. (the time should be measured from the end of the initial high-shear mixing period)
Heat of Hydration	Approved method of Isothermal Conduction Calorimetry	Grouts should not have a cumulative heat output of greater than 180 kJ/kg of blended cement powder after 24 hours of hydration at 35˚C
Bleed	100 mL samples contained in a sealed 100 mL measuring cylinder cured at 20±5˚C	Grout should have bleed of less than 2 vol. % after 24 hrs

* The Colflow test developed by Colcrete Ltd where a specific amount of grout is released into a channel of specific dimensions and the distance the grout travels is recorded. This method has been used historically by Sellafield Ltd to measure the fluidity of cement grout.

2.4.4 Alternative Powder Sources

It has been established that the supply for cement powders to the nuclear industry is changeable. All of the suppliers considered so far have been from the UK, but there is scope to import cement powders from other countries if the supply is at risk from UK sources. Development work at NNL have considered some alternatives and identified that a Czech Republic Calumite could be a suitable replacement coarser fraction [13, 39].

2.5 Summary

The reported literature and industrial reports provided by the sponsors, indicate the importance of understanding the performance criteria of the cement grouts used during the encapsulation of intermediate level wastes. The literature highlights that the particle

size of the cement powders used has a significant effect on the resulting cement matrix and in turn on the wasteform produced. As such, investigation is needed into how the particle size distribution of the GGBS:Calumite:PC system affects the rheological behaviour, performance properties and the infill process during encapsulation. By varying the particle size of the formulation used, it should be possible to optimise the blend of BFS and PC to achieve the most desirable properties required for the encapsulation of nuclear waste.

3 Materials and Methods

3.1 Materials

All of the precursor materials used were supplied by Hanson Cement. The ground granulated blast furnace slag (GGBS) was sourced from Hanson's Scunthorpe works and complies with BS EN 15167-1:2006 [57]. The Calumite was produced by Calumite Ltd, also from the Scunthorpe works. The Portland cement (PC) used was a Sellafield Ltd. grade powder that conforms to the nuclear industry specification [58] as discussed in Chapter 2, from Hanson's Ribblesdale works.

3.1.1 Characterisation of Raw Materials

X-ray fluorescence (XRF) was used to determine the chemical composition of the cement powders. The XRF analysis was conducted externally by AMG Analytical Services using the fused-bead method, and the results are shown in Table 3.1.

Table 3.1. Oxide composition of the raw materials measured by XRF analysis.

Element/Compound	GGBS (wt. %)	Calumite (wt. %)	OPC (wt. %)
Na_2O	0.35	0.5	0.58
MgO	8.1	7.9	2.3
Al_2O_3	11.6	11.3	4.9
SiO_2	36.3	38.3	20.1
P_2O_5	<0.05	0.06	0.16
K_2O	0.64	0.78	0.77
CaO	39.0	38.9	63.4
Fe_2O_3	0.4	0.3	2.5
SO_3	0.53	0.31	3.6
Total	**96.97**	**98.35**	**98.31**

When the elemental compositions of the GGBS and Calumite materials are compared, it is possible to see that although the values are not identical, they are very similar. This is to be expected because they are sourced from the same blast furnace as noted above. It also suggests that both materials would react in a chemically similar manner, subject to particle size effects.

The density of the precursors was measured using a Micromeritics AccuPyc 1340 instrument. The samples were analysed after 200 purges, 30 cycles and with helium as the analysis gas, with a fill pressure of 44.8 kPa. Powder fineness of the raw materials was measured by using the Controls 62-L0041/A Blaine air-permeability apparatus in accordance to BS EN 196-6:2010 [63]. These results are presented in Table 3.2. There is no Blaine measurement for the Calumite material because it was not possible to form a compacted bed of powder, which is needed to carry out the test. This is due to the presence of very large particles (several hundred microns) and therefore the low surface area of the material. The Brunauer-Emmett-Teller (BET) method [64] was used to measure the surface area of the precursor materials using a Coulter SA 3100 instrument with nitrogen as the adsorptive on approximately 2 grams of sample.

Table 3.2. Characterisation of precursors using pycnometry, Blaine fineness and BET surface measurements.

	Density (g/cm^3)	**Blaine (cm^2/g)**	**BET (cm^2/g)**
GGBS	3.15	5978	34400
Calumite	2.87	-	27500
OPC	2.91	4359	27700

The particle size distribution (PSD) was measured via laser diffraction using a Malvern Mastersizer 3000 particle size analyser with a dry powder dispersion unit. A refractive index of 1.629 was used for the GGBS and Calumite materials and a value of 1.7 for the OPC powder [65]. The results are shown in Table 3.3 and Figure 3.1.

Table 3.3. Particle size parameters of raw materials as determined by PSD analysis.

	D_{10}	**D_{50}**	**D_{90}**
GGBS	1.5	10.4	32
Calumite	232	553	1003
OPC	2	16	51

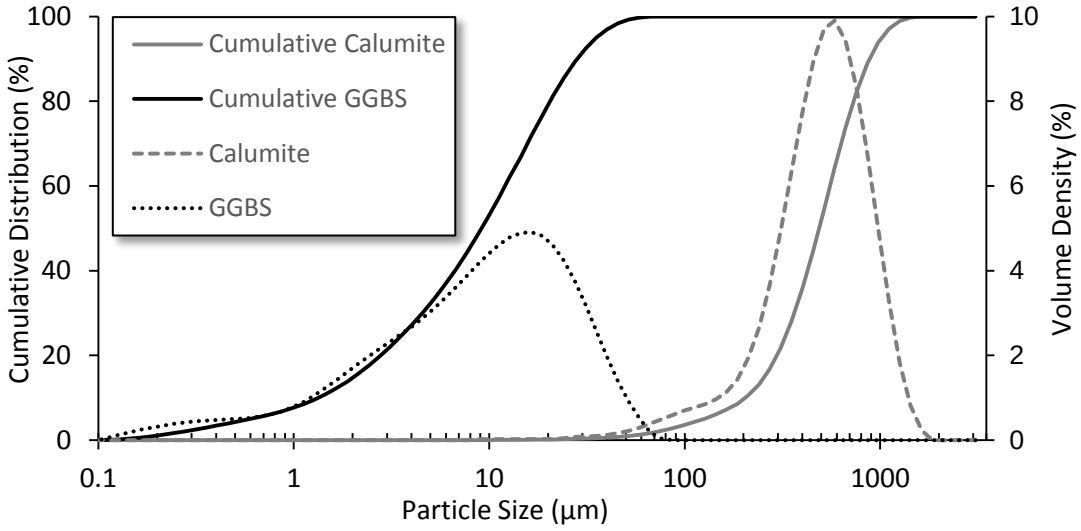

Figure 3.1. Particle size distribution data for GGBS and Calumite.

It is clear from Figure 3.1 that the GGBS and Calumite fractions have very different distributions: all of the GGBS material is sub-100 µm, but the majority of the Calumite particles are larger than 100 µm. Due to the broad distribution recorded for the Calumite material, and the limited reported literature (and therefore minimal knowledge) associated with this material, further investigation was carried out.

Figure 3.1 shows Calumite to have particles ranging from approximately 40 – 1800 µm which is a very broad range and possibly difficult to measure accurately with this instrument. Therefore, in order to understand how this is established, the Calumite powder was sectioned via sieve analysis into a series of fractions. A 200 g sample was separated into 6 sections (shown in Figure 3.2) and then each particle size range was analysed via laser diffraction once again. Fractionating the material highlighted that the particle size of the Calumite ranges from 67 to 1800 µm with nearly ¾ of the sample larger than 250 µm. The largest fraction by weight was the range from 425 – 710 µm.

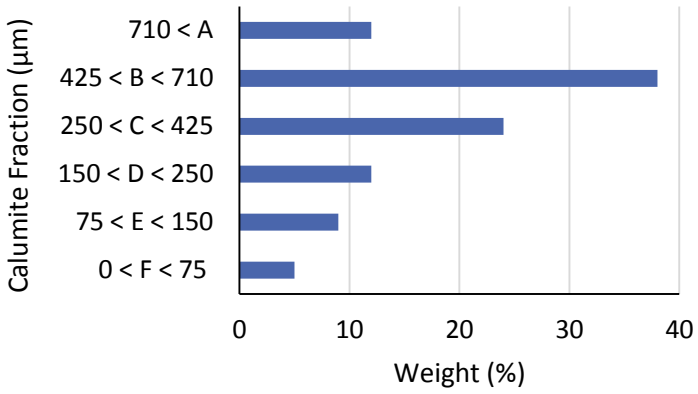

Figure 3.2. Weight percentage of the 6 Calumite fractions.

Thus, any blend of these two materials would create a bi-modal distribution with very few particles between 100 – 200 µm, which suggests the blast furnace slag (BFS) produced would be a gap graded powder.

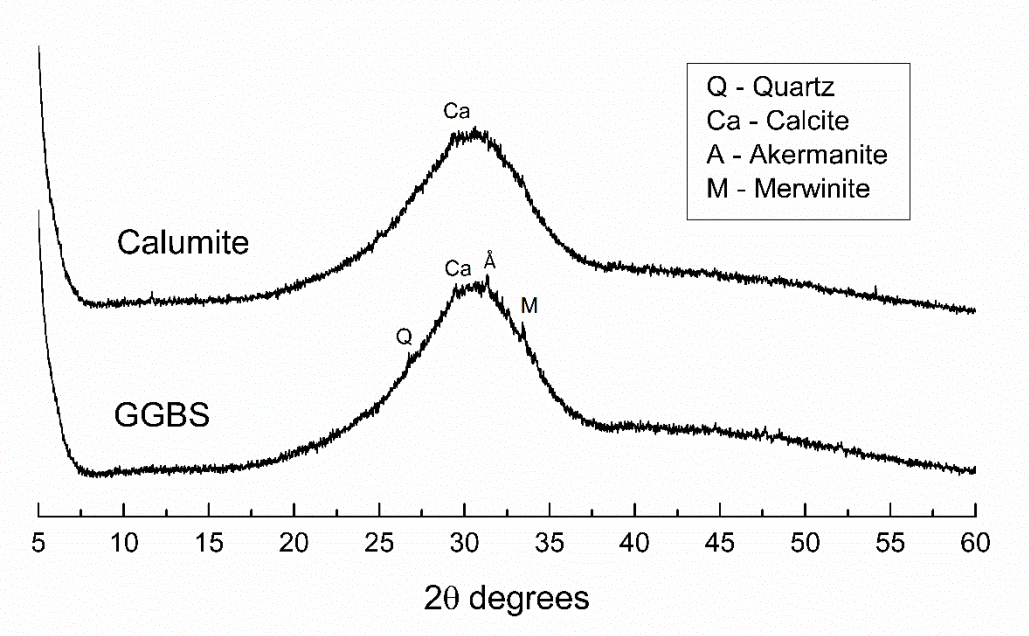

Figure 3.3. XRD data for the precursors GGBS and Calumite.

The X-ray diffraction patterns (method detailed in section 3.3.5) of the two BFS fraction are shown in Figure 3.3. Both materials produced almost identical diffuse scattering centered at 32° 2θ, which indicates that they are glassy materials, and a small amount of calcite ($CaCO_3$) at 29-30° 2θ, which is likely due to atmospheric carbonation of calcium oxide. Although additional minor crystalline phases (akermanite – $Ca_2Mg(Si_2O_7)$ and merwinite – $Ca_3Mg(SiO_4)_2$) can be observed for the GGBS, both diffraction patterns show

very similar results. The combination of XRD and XRF results validates the similarity between the two materials, suggesting their chemical reactivity would be the same.

3.2 Mix Design

The formulation used was designed to replicate those specified by the nuclear industry standard acceptance testing [58]. A blend of 3:1 BFS:PC by mass, at a water/solids (w/s) ratio of 0.35, was used as a baseline mix throughout this work as per the NNL standard [39]. The BFS fraction was made up of varying GGBS:Calumite ratios which ranged from 100 wt. % GGBS through to 100 wt. % Calumite. In total, ten different blends were used (see Table 3.4), including 65:35 GGBS:Calumite which was the original blend in use on plants MEP and WEP (previously described in Chapter 2). Two additional w/s ratios (0.33 and 0.37) were also analysed in order to monitor the effect of water content on the cement systems.

Table 3.4. Blend ratios of GGBS:Calumite comprising the BFS fraction of the system.

Mix	GGBS:Calumite Ratio (wt. % ratio)
P100	100-0
P80	80-20
P72	72.5-27.5
P65	65-35
P58	58.5-41.5
P52	52-48
P42	42.25-57.75
P32	32.5-67.5
P22	22.75-77.25
P0	0-100

3.3 Experimental Methods

3.3.1 Mini-slump

The mini-slump method was used to measure the workability of the cement grouts and is based on work reported by Kantro [66]. The technique is based on a scaled-down Abrams slump test, which is widely used in the construction industry [67], and consists

of filling an upturned cone (poly(tetrafluoroethylene) with cement paste. The cone, with a height of 57 mm, a 19 mm top diameter and a 38 mm base diameter [66], is then lifted vertically from a base plate (poly(methylmethacrylate)) and the cement paste is left to flow. The distance the sample travels under gravity is measured by recording the area covered by the grout using a 2x2 cm grid marked on the base plate. This was achieved by taking a photograph of the final slumped pat from directly above the sample (Figure 3.4), and the area was then calculated using the ImageJ software [68]. The flow areas reported are based on the average of 3 measurements of the samples, which were conducted in triplicate.

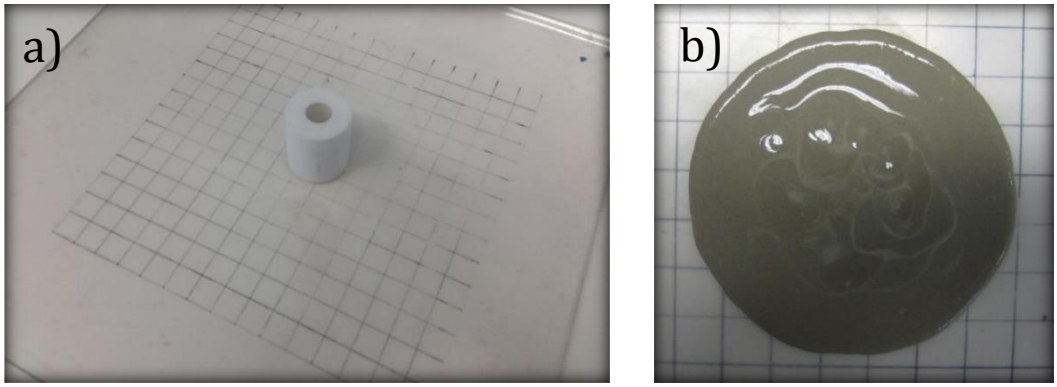

Figure 3.4. Mini slump - a) equipment set up b) example of sample slump pat for analysis.

Sample Preparation

The dry components were combined before the addition of water, and were hand mixed for two minutes. When the water was added, the pastes were subjected to a further 10 minutes of mixing on a high shear Heidolph RZR2020 bench top mixer at 1650 rpm to achieve a homogeneous paste.

3.3.2 Particle Packing Density

Centrifugation of the grout formulations was used to measure the maximum particle packing density achievable for the different cement pastes. The equipment used was a Heraeus Biofuge Primo Centrifuge (Thermo Scientific, UK). The cement paste (prepared with water) was poured into a centrifuge tube (15 mL) and then subjected to 30 minutes of centrifugation at 4000 rpm [69, 70]. The volume of supernatant above the centrifuged bed of solids within each sample was calculated by taking a photograph and analysing the image using ImageJ [68], and thus the maximum particle packing density obtained.

Sample Preparation

Samples were prepared as described in section 3.3.1 and the tests were conducted in triplicate.

3.3.3 Isothermal Calorimetry

Isothermal conduction calorimetry analysis is used to measure heat evolution from cement samples [71]. The principle of this technique is to measure the heat released from a sample that is held at a constant temperature. It is compared to a reference sample, which has a similar heat capacity to the measured sample, so that any heat flow external to the reaction can be subtracted, and the temperature associated with each sample is recorded.

Isothermal calorimetry was conducted using an isothermal calorimeter (TAM Air, TA Instruments) on the cement formulations stated in Table 3.4. The instrument was re-equilibrated for each temperature for 24 hours prior to running the analysis.

Sample Preparation

The dry components were combined together in a sealed plastic container before the addition of the required amount of water required and were hand mixed for two minutes. Each sample, of approximately 20 g, was poured into a plastic ampoule and placed into the instrument for 14 days. An amount of water equivalent to the total water content of each sample was used as a reference. The same experimental procedure was used for cement samples hydrated at 25, 35 and 60 ˚C.

In addition to the standard formulations, calorimetry was carried out for additional samples with quartz as a substitute for the Calumite fraction. For these samples, all of the formulations were renamed whereby P was replaced by Q (i.e. P100 became Q100). The material used was a standard quartz sand supplied in individual 1 kg bags. The quartz was ground and sieved into fractions, before blending the correct contributions from each PSD range to mimic the Calumite particle size distribution.

3.3.4 Semi-Adiabatic Calorimetry

The main principle of semi-adiabatic calorimetry is to determine the adiabatic temperature profile of a cement sample through achieving minimal heat loss by surrounding the specimen with insulation [72]. The insulated calorimeter is maintained at room temperature externally, but this is not necessarily the temperature inside, and can be calibrated for heat loss [73]. Semi-adiabatic calorimetry was carried out on the formulations described in Table 3.4, using 500 g batch sizes. Each mix was poured into

one of a series of identical 500 mL vacuum flasks with a T type thermocouple inserted in the centre of each sample, as shown in Figure 3.5. The temperature change was monitored using the thermocouple via a Pico Technology USB TC-08 data logger, which was set to record data points at 1 minute intervals for 14 days.

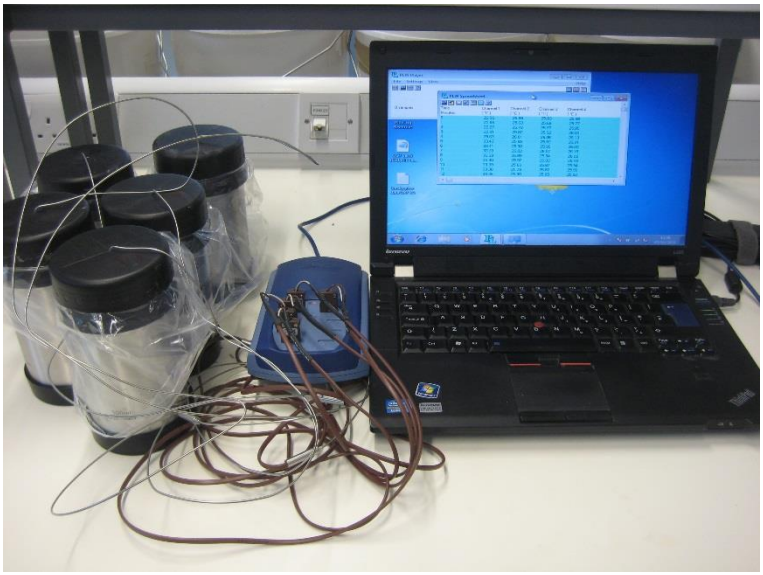

Figure 3.5. Semi-adiabatic experimental set up.

Sample Preparation

The dry components were combined before the addition of water and were hand mixed for two minutes. The samples were mixed for a further 10 minutes using a high shear Silverson L4RT mixer at 3500 rpm. A 500 g batch was used due to the need for a larger sample size for the method and is also a better replication of larger plant mixes.

3.3.5 X-ray Diffraction

X-ray diffraction (XRD) is a technique that can be used for identification of crystalline phases within materials. X-rays, referred to as monochromatic X-rays, are generated by bombarding a metal target with high energy electrons and as the electrons come into contact with the metal they generate radiation. Within the metal, the incident beam collides with electrons in the inner shells of the atom causing an electron of higher energy to drop into the vacancy and the excess energy is emitted as an X-ray photon [74]. When the X-ray is exposed to the sample, the incident X-ray interacts with the crystal structure in planes, known as crystallographic planes which are characterised as the Miller indices (hkl) [75]. The parallel planes are regarded as semi-transparent mirrors

and the distance between them is defined as d spacing. The Bragg's Law ($n\lambda = 2d \sin \theta$) models crystals as stacks of reflecting lattice planes which makes it easy to calculate the angle at which the crystal must make to the incoming incident X-ray. The path length differs and depends on the glancing angle (θ) and to satisfy Bragg's Law, the reflected X-rays must be in phase and interfere constructively. For constructive interference to occur the distance between two incident X-rays (i.e. on two different planes) is a whole integer. High intensity peaks form a diffraction pattern by detecting the diffracted X-rays, which is then plotted against the diffraction angle (2θ) and this can be used to gain structural information about the crystalline phases [74].

Sample Preparation and Analysis

Samples were cured for 28 days when the on-going hydration was stopped using acetone, the hardened material was dried, crushed and ground using an agate mortar and pestle and passed through a 63 μm brass sieve prior to XRD analysis. Data were collected between $5° < 2\theta < 60°$ using a Bruker D2 PHASER desktop diffractometer with a Ni filtered Cu Kα (1.5418 Å) source operating in reflection mode, using a step size of 0.02° and time per step of 4 s. The reflections were analysed using DIFFRAC.EVA V3.1 software provided by Bruker.

3.3.6 Rheology

The rheology of the cement systems was measured at two different stages of the experimental program using two different instruments.

3.3.6.1 Haake Viscometer

During the small laboratory scale trials (approx. 500 g), a Haake Viscotester 550 supplied by Thermo Scientific was used with a FL100 6 blade vane tool attached. The sample was subjected to a 60 second ramp up from a shear rate of 0 to 100 s^{-1}, 5 second rest time and finally followed by a 60 seconds ramp down. These trials were conducted at The University of Sheffield.

Sample Preparation

Samples were prepared as described in section 3.3.1 and the tests were conducted in triplicate.

3.3.6.2 Lamy Rheometer

During the 3 litre mixes, a Lamy Rheology RM200 rheometer supplied by Meritics was used. Two different blades were used, the first was a FL100MB3 6 blade vane tool and the second was a MS-R2 anchor shaped paddle. The sample was subjected to a 60 second ramp up from a shear rate of 0 to 100 s^{-1} followed by a 60 seconds ramp down. The

samples were measured using both the vane tool and the paddle attachment and were conducted at NNL's Workington facility.

Sample Preparation

The cement grouts were prepared according to the method described in section 3.3.7.

3.3.7 3 Litre Acceptance Mix

Mixes of 3 litres of grout were conducted for the blend ratios stated in Table 3.4. The PC was added to the water, followed by the BFS fraction, and mixed in a standard 5 L Hobart mixer for 5 mins before stopping the mixing to scrape down the edges of the bowl. The grout was then mixed for a further 5 minutes using the Hobart mixer before transferring to a Silverson high shear mixer for 10 minutes at 6000 rpm. Performance properties of the grouts were measured after the conclusion of mixing.

3.3.7.1 Setting

The time it takes for a cement paste to set was measured using two methods; one is a manual check according to BS EN 196-3:2016 [76] and one is an automated system. A Vicat needle (1.13 mm diameter) is used to measure the initial set of a sample, and the Gillmore needle is used to assess the final set [77]. For the manual Vicat, the sample was prepared by pouring the mixed cement paste into a container to a depth of 40 mm, and penetration measurements were taken for samples with no holdup time and with 150 minutes hold up time (i.e. t=0 and t=150). The samples were placed in a humidity cell at 20 ˚C for overnight and checked using both needles. The setting time was also recorded automatically using an ELE Vicotronic instrument, where a Vicat needle free falls under gravity onto the sample at 30 minute intervals. For this test, the cement paste was poured into a 70 mm sample holder mounted onto a Perspex plate and tested repeatedly over a 24 hour period under ambient conditions.

3.3.7.2 Bleed Measurement

The formation of a water layer on the top of a hardened cement paste is known as 'bleed', and can be caused by the settlement of solid particles. This forces an increase in w/s ratio at the top of the sample and a decrease at the bottom forming a thin layer of water at the surface [16]. UK nuclear industry specifications require that grouts show very minimal bleed. In order to determine the surface bleed of grout samples, a plastic measuring cylinder was filled with 100 mL of grout and sealed for 24 hours in a humidity cell at 20 ± 1 ˚C and >90 vol. % RH. After 24 hours, the amount of water that had settled at the top of the sample was measured and calculated as a percentage of the total sample mass. Aliquots of sample were collected on the conclusion of mixing and at 30 minute

intervals, i.e. t=0, 30, 60, 90, 120 and 150 minutes, in order to analyse the bleed measurement at 24 hours respective of when the sample was taken.

3.3.7.3 Dimensional Stability

The chemical shrinkage of cement can be measured by analysing the dimensional stability. This is achieved by casting prisms of cement grouts, curing the products and finally de-moulding each prism before individually wrapping each sample in polythene to minimise drying. The change in length is then monitored using the method and apparatus stated in ASTM C490 [78] and an Invar reference bar as a starting point. Standard prism moulds were prepared according to ASTM C490 [78] and pre-coated with Febstrike (a chemical release agent for moulds). The moulds were infilled with cement grout and tapped/shaken in order to remove entrapped air. The cast prisms were stored in a humidity cure cell at 20 ˚C for 2 days before de-moulding and analysis was carried out at 2, 7, 14, 21, 28, 42, 56, 70 and 90 days.

3.3.7.4 Colflow

The Colflow test was developed by Colcrete Ltd. and is routinely used by the nuclear industry in order to measure the flow character of cement grouts, due to its simplicity and the ability to execute the test with ease on plant. The principle of the test is that 1 quart (1.14 L) of grout is allowed to fall under gravity from a cone into a channel with specific dimensions (Figure 3.6). The distance the grout travels along the channel is measured.

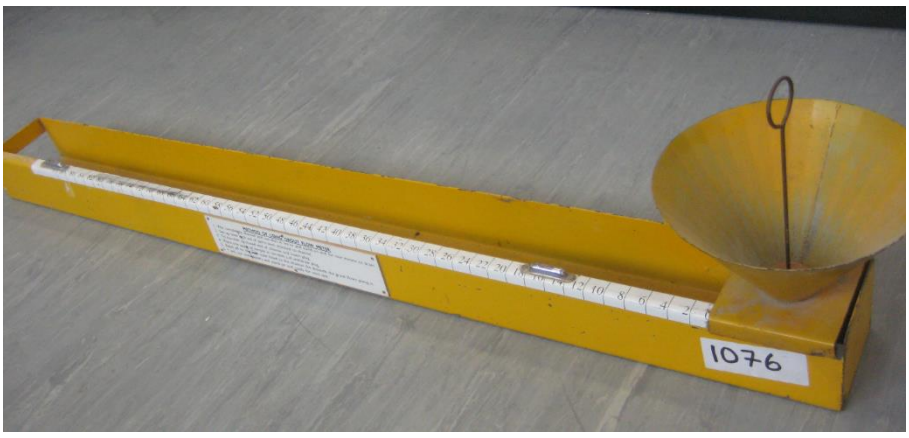

Figure 3.6. Colflow test apparatus.

In order to carry out the test method, the cone (tundish), Colflow channel and quart jug are thoroughly coated with water for 60 seconds before leaving to drain for an additional

60 seconds. The Colflow channel is set up on a flat designated area before placing the tundish, containing a plug, on one end of the channel. The quart jug is filled with grout and the sample is poured into the tundish before withdrawing the plug in a smooth motion. The grout is allowed to stop flowing before measuring the distance and therefore the flow of the material. If an uneven grout 'front' is produced, and average of the distance is recorded and measured using the method shown in Figure 3.7. The Colflow was measured at the conclusion of mixing, and after a hold up time of 2.5 hours, i.e. t=0 and t=150 minutes.

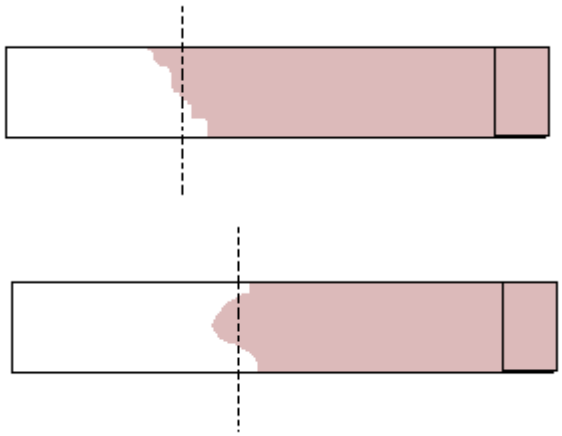

Figure 3.7. Method of obtaining an average measurement for an uneven grout flow during the Colflow method.

3.3.8 Plant Scale Trials

Two large scale trials were carried out to mimic wasteforms produced on plant. A 500 L mix was prepared using a mixer specifically developed by British Nuclear Fuels Ltd (BNFL) for use in encapsulation processes as used at WEP. The dry components were weighed out into a large Solibin container and lifted into place ready for mixing. Prior to the addition of the powders, the correct amount of chilled water (ca. 9 ˚C) was poured into the mixer. Once the water was added, the powders were vibrated and transferred into the mixer via a screwfeed system at a rate of 55 kg/min. The grout was mixed for a total of 20 minutes at an impeller speed of 460 rpm. After the mixing time elapsed, the speed of mixing was lowered to an impeller speed of 180 rpm in order to maintain agitation during infill. The grout was pumped in situ into the 500 L stainless steel drums, containing THORP hulls simulant, at an infill rate of 30 litres/min. The simulant waste used consisted of stainless steel tubing that was cut and partially crimped into 50 mm sections. Thermocouples were inserted into the drum at various points prior to infill, to enable monitoring of the temperature profile of the sample. The bleed, setting times and

Colflow of the samples were tested using the methods stated in 3.3.7. The samples were cured at 25 ˚C for 7 days. The compressive strength of the grout used was also monitored at 2, 7, 28 and 90 days.

4 Fresh State Properties and Measuring Yield Stress

4.1 Introduction

It is important to understand the rheological behaviour of the cement system in its fresh state to underpin the science behind how different formulations can affect the performance of the material. More specifically, it is essential to understand how the PSD of the system changes the physical properties, and in fact controls how the cementitious matrices perform in a practical sense. The rheology of fresh cement systems can be analysed by using a variety of methods such as the slump test, flow tests and viscosity measurements [79]. In the majority of these tests the shear rate is the variable parameter, which can impose different shear stresses depending on time and the mass and geometry of the sample [80]. Associated with shear stress is the yield stress; the yield stress of cement is defined as the minimum amount of stress required in order to initiate flow [45, 81]. There are two types of yield stress that can be measured. The first is known as static yield stress, and describes the viscoelasticity of a material, so is the stress required to initiate flow. The second yield stress is referred to as dynamic yield stress, and is the stress that occurs as the viscous flow stops, taken on the downwards ramp [82, 83]. This is the yield stress measured here during the rheology and slump tests. Yield stress is historically very difficult to measure in a fully reproducible way, and therefore results are generally only compared when they are collected from the same method.

In this chapter, the results of a series of tests carried out on fresh state cement pastes are presented. The first test method reported is the mini-slump test. The slump test was originally developed for use in the mining and construction industries using large samples, but it has been developed into a much smaller benchtop format for use on the laboratory scale [66, 84, 85]. The full-sized slump test has become a widely accepted method, but this is not necessarily the case with the mini-slump test. However, it is being utilised more and more within the cement research field, as a method of measuring the rheological features of a material [45, 67, 86]. The connection between slump testing and yield stress works on the assumption that the material will flow until the shear rate is equal or smaller to the yield stress, and consequently the spread achieved by the material is linked to the yield value. It is possible to calculate the yield stress of the cement pastes using the results from the mini slump tests, by Equation 4.1. Originally reported by a group in Japan[87] this equation has been reported to be used for estimating yield stress with success [67, 81, 88].

$$\tau_0 = \frac{225 g \rho V_c^2}{4\pi^2 D_f^5} \tag{4.1}$$

Where ρ is paste density, g is the acceleration due to gravity, V_c is the conical volume, and D_f is the final slump diameter. The equation relates the yield stress to the cone volume and the paste slump diameter. The equation was developed based on a few assumptions such that only the material's own weight is considered, the sample must be representative of the mixture, the thickness of the material must be five times the size of the largest particle, and the inertial and surface tension effects must be minimal [81, 87-89].

Understanding the rheology of the cement system is essential in order to achieve successful pumping and encapsulation of nuclear waste. The plastic viscosity and yield stress of the different cement systems were measured here using the vane method, which is reported to be the most reliable form of rheological analysis for cement systems as it enables the operator to minimise slip [90]. The rheology of a specific material can also be affected by the agglomeration of particles, either previous to mixing or during that process, which is why high shear mixing is essential. Conventional laboratory viscometer test methods, that use a cup and bob attachment or where the material is sheared in a narrow space, are not suitable for the materials investigated here such as the coarse Calumite because the larger particles can get stuck in the narrow gap [79].

It is well established that particles within BFS materials are not spherical, and this will affect how the particles pack together. Figure 4.1b illustrates a cross-section of a tomographic reconstruction of a sample of dry Calumite powder, and it is very clear that the particles are irregularly shaped and variable in size, and this is also true for the GGBS material (Figure 4.1a). The images demonstrate the significant difference in particle size between the two powders. They also highlight some internal porosity within the Calumite particle and although this may not influence the reactivity of the powder, because the external surface area remains the same, it will affect the density of the material. The data were collected by the National Nuclear User Facility at NNL's central laboratory using a Bruker Skyscan 1172 high resolution desk-top micro-CT. A detailed discussion of tomography methodology in general will be given in Chapter 7.

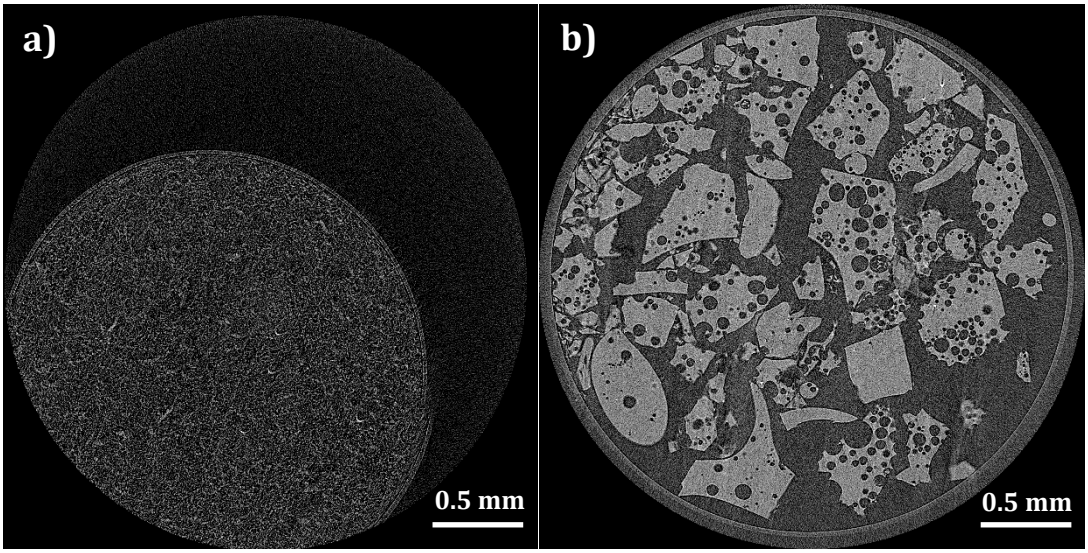

Figure 4.1. Image of one slice from a tomography scan of anhydrous a) GGBS and b) Calumite powder.

It is fair to say that a blend of these two materials could be unpredictable in terms of packing due to the wide particle size distribution. In order to gain some insight into the effect of PSD on the system, a series of particle packing tests were carried out on the various blends. The method used is very similar to that reported in the literature as being used for monitoring consolidation of materials [69, 91]. Centrifugation was used as described in Chapter 3, to consolidate the solid material within the cement paste, which allows re-arrangement and compaction of a bed of particles to achieve maximal packing densities.

4.2 Results and Discussion

4.2.1 Mini-slump

The fluidity and workability of the cement grout used on plant for waste encapsulation are crucial. Due to the nature of the encapsulation plants, the cement pastes require a long enough working time and high enough flow to be processed via remote handling without causing any issues in the production of wasteforms. The mini-slump test that was used is a simple but useful method of measuring workability of the cement formulations at benchtop scale. It also highlights the effect of water on the properties of the system at each blend ratio. Figure 4.2 show the results for all 10 blends at 3 different water/solids ratios.

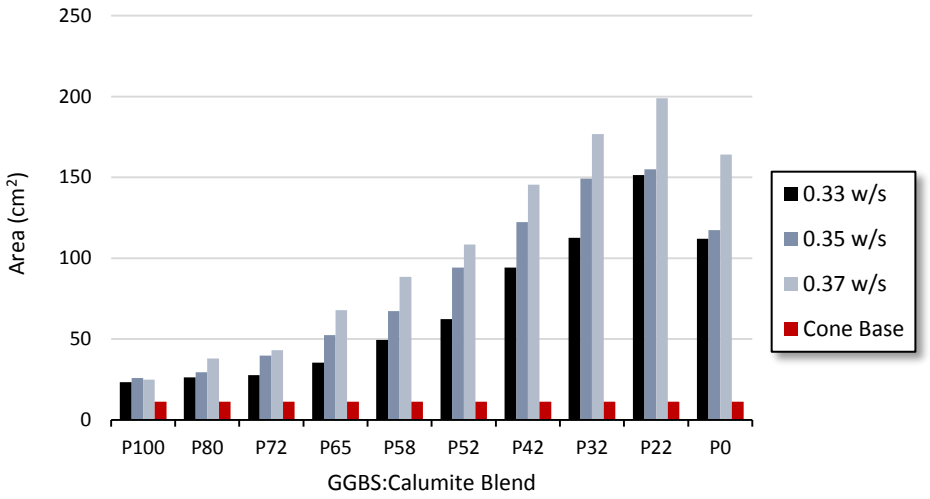

Figure 4.2. Slump areas for the 10 GGBS:Calumite blend ratios at 3:1 BFS:PC ratio and at 0.33, 0.35 and 0.37 w/s ratios.

As expected, a higher w/s ratio creates a larger area slump for each blend. However, simply increasing the water content is not a suitable solution to improve flow characteristics because it can cause the formation of a bleed water layer on the top of the hardened cement paste and also results in detrimental effects on physical properties such as strength and stability. Any bleed water released, in the context of nuclear waste disposal, would then become an unwanted secondary waste which would need additional processing, as free liquids are not permitted in wasteforms for disposal [38].

An interesting observation from this series of experiments is that as the surface area of the material decreases the slump area increases, but only up to a point. The P32 and P22 blends evidently reach the point where the balance between large and small particles is no longer favourable for increasing fluidity because the P0 blend falls out of trend. Another consideration is that gap graded powders are known to present a low water requirement [92, 93], and the results here suggest that the bimodal PSD of the blend of BFS powders also reaches an optimum with regards to water content. This suggests that there needs to be an optimum contribution from both the GGBS and Calumite materials to enable good flow, and also verifies the basis of the powder fineness requirement in the Sellafield specification [58].

The yield stress of the cement pastes was calculated from the spread of each respective mini-slump test, and the results are detailed in Table 4.1. Overall, the tests achieved the required conditions for Equation 4.1 to be applied correctly and the results show that as the Calumite content increases the yield stress decreases. This is reasonable result

because as the Calumite content increases the fluidity of the systems increases (as shown in Figure 4.2), and therefore a lower yield stress would be expected. This is also true if the w/s content of the systems are compared. With the exception of the extremities of the blend ratio, as the water content increases the yield stress decreases.

Table 4.1. Yield stress values obtained from the mini-slump areas, for the ten blends of GGBS:Calumite in Table 3.4, at 0.33, 0.35 and 0.37 w/s ratios.

Mix	Yield Stress (Pa)		
	0.33	**0.35**	**0.37**
P100	344	188	286
P80	256	189	93
P72	180	85	66
P65	100	44	21
P58	40	17	10
P52	18	10	7
P42	10	6	3
P32	6	4	2
P22	3	3	1
P0	4	6	3

The P100 sample does not follow the trend shown by the others, which could be due to the increased water demand caused by a high surface area of GGBS producing a very stiff material with a firm consistency making it difficult to take a reliable measurement. The P0 blend also falls out of trend which could be because of segregation of materials prior to release of the cement paste from the cone. This is likely due to the low surface area resulting in excess water, which has caused saturation of the Calumite particles, and has resulted in a higher yield stress than the previous blend. These attributes suggest that the P100 and P0 systems do not fulfill the assumptions needed to apply Equation 4.1 to obtain the yield stress of the systems.

4.2.2 Vane Rheometry

Shear rate-shear stress measurements were recorded using a Thermo scientific Haake Viscotester 550 viscometer for each of the 10 formulations at 3:1 BFS/OPC and 0.35 w/s; pastes were tested in triplicate using a fresh batch for each measurement, and the results are presented in Figure 4.3.

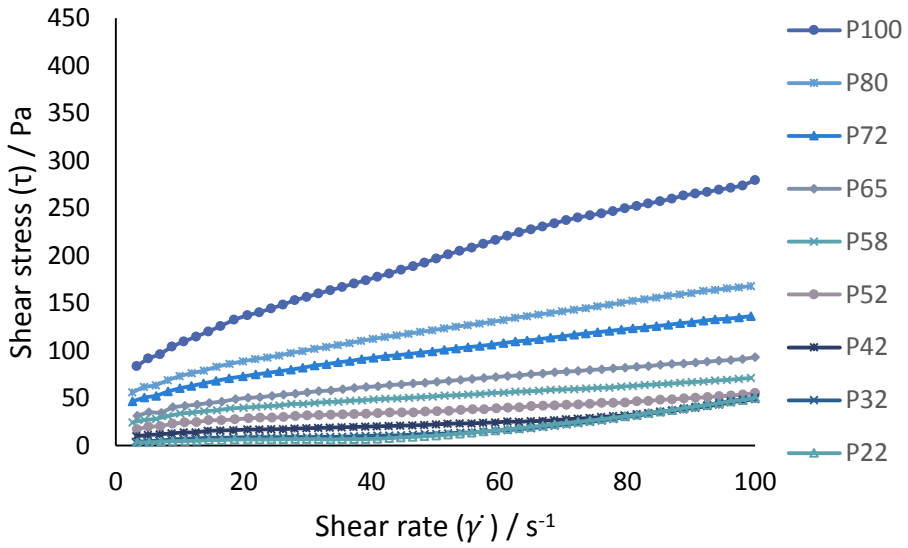

Figure 4.3. Viscometry data for all 10 GGBS:Calumite blends at a 3:1 BFS:PC ratio and a 0.35 w/s content.

From Figure 4.3, the results show that all 10 blends follow the Bingham model fairly well. However, as the Calumite content increases the results tend to deviate from the linear part of the model, this is especially obvious in the P0 blend. The measurement of the P0 system failed due to the centrifugation of particles and segregation within the material, and as such the data for this formulation are not included in Figure 4.3. This formulation also falls out of the trend of decreasing yield stress with increasing Calumite content; this is likely due to centrifugation of the larger particles within the material caused by the paddle of the instrument. Measurements were also tested at 0.33 and 0.37 w/s in order to understand the effects of water content (Figures 4.4 and 4.5); these results show very similar trends to the 0.35 w/s content data.

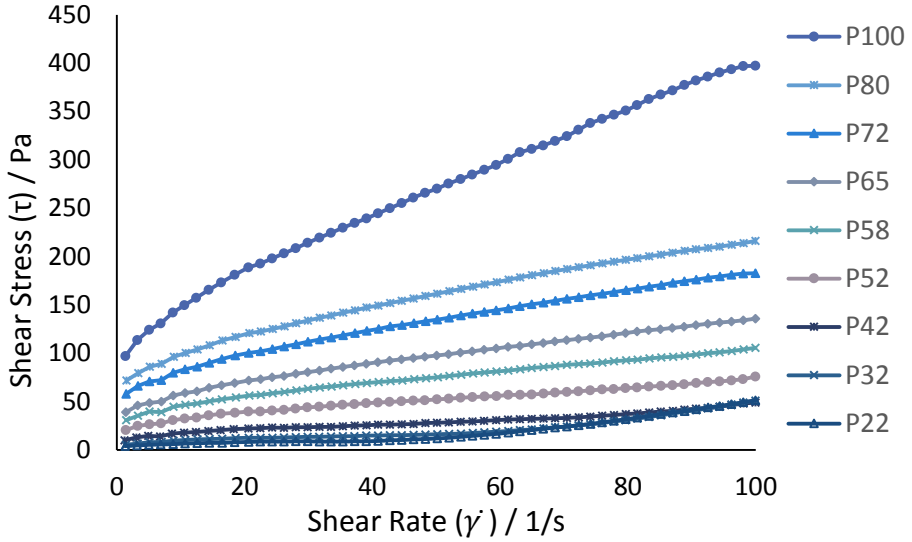

Figure 4.4. Viscometry data for all 10 GGBS:Calumite blends at a 3:1 BFS:PC ratio and a 0.33 w/s content.

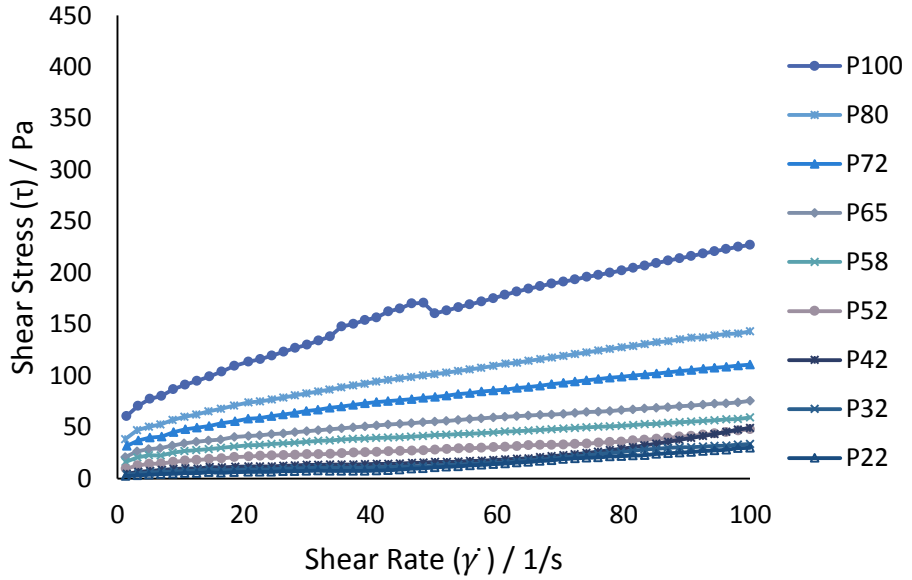

Figure 4.5. Viscometry data for all 10 GGBS:Calumite blends at a 3:1 BFS:PC ratio and a 0.37 w/s content.

The yield stress for each of the ten pastes was calculated at three w/s ratios (0.33, 0.35 and 0.37) by fitting of the Bingham model, shown in Table 4.2. Blends P32 and P22 start to achieve apparent negative yield stress values, and the P0 system completely falls out of trend as discussed above. These unusual results confirm the yield stress data obtained from Figure 4.2 in Table 4.1; as the Calumite content increases the yield stress decreases. However, the cement pastes start to diverge from the Bingham model, which means that these unphysical negative yield stress values are a result of the model being inappropriate. It is also widely reported that low yield stresses are inherently difficult to

measure [90], and it is possible due to the increased fluidity of the cement pastes containing higher volumes of Calumite, that the yield stresses of these systems are just too low to obtain data for them using the vane rheometry method that was used here.

Table 4.2. Yield stress values measured by extrapolation of the Bingham model for the ten GGBS:Calumite blends (Table 3.4) at 3:1 BFS:PC and a 0.33, 0.35 and 0.37 w/s ratios. Values in italics are considered unphysical or unreliable.

Mix	Yield Stress (Pa)		
	0.33	**0.35**	**0.37**
P100	121.9	94.9	80.6
P80	89.2	65.2	51.2
P72	73.2	54.5	41.1
P65	51.2	37.1	30.1
P58	40.5	30.2	23.1
P52	28.1	20.4	13.2
P42	13.5	8.2	1.99
P32	2.04	*-3.03*	1.49
P22	*-3.28*	*-5.94*	*-0.21*
P0	*112.9*	*161.3*	*33.6*

Yield stress is historically very difficult to measure and generally results can only be compared within the experimental method being used. Here, although the numbers do not exactly match, a comparison can be made between the yield stress values obtained during the mini-slump tests and the rheology tests, shown in Figure 4.6.

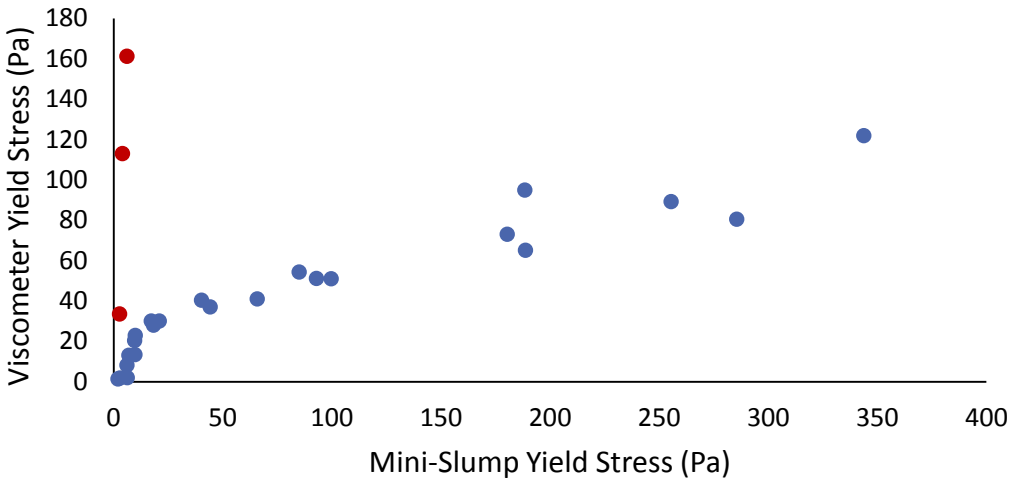

Figure 4.6. Comparison between yield stress values obtained via the mini-slump and viscometry methods.

Considering the simplicity of the mini slump test versus the sophistication of the rheology lab equipment used, it is significant that the values obtained are within the same order of magnitude of each other and have a positive correlation if the 'failed' tests are ignored. The 'failed' data points are due to the P0 blend, highlighted in red in Figure 4.6, showing that this mix consistently displays anomalous behaviour across various test methods. As previously reported [88], when comparing values for yield stress obtained via the mini-slump method and from vane rheometry, the lower yield stress values appear to be more accurate. At higher yield stress values the correlation starts to deviate but still shows a comparable relationship.

4.2.3 Particle Packing

Centrifugation of the 10 blends (Table 3.4) produced a compact material with a supernatant that collects above the compacted material as shown in Figure 4.7.

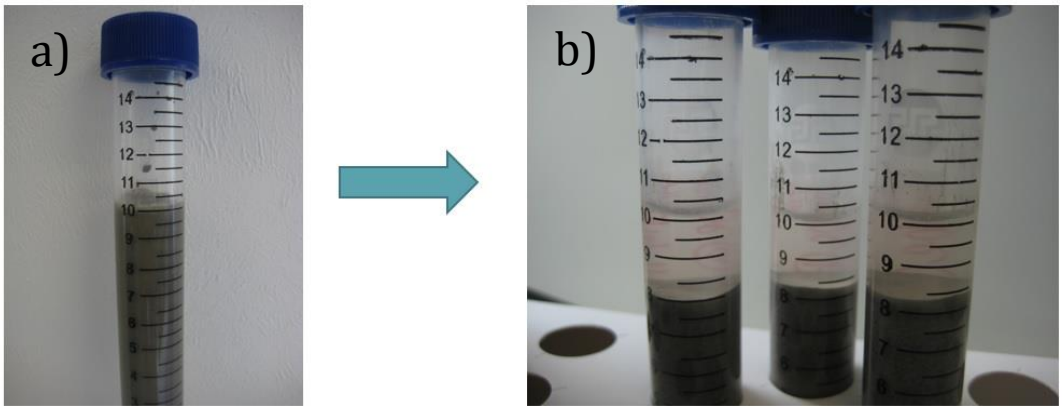

Figure 4.7. Cement paste before (a) and after (b) centrifugation.

The particle packing density of each cement system was calculated by monitoring the volume of supernatant produced above the bed of solids within each sample following centrifugation, and the results for the 0.33, 0.35 and 0.37 w/s content ratios are shown in Figure 4.8. The P100 blend has the highest packing density and this is due to the PSD of the GGBS. If the GGBS is considered as an individual material, the PSD of the cement powder ranges between 0.1 – 100 μm and the data illustrate that this distribution contains a sufficient amount of smaller and larger particles in order to compact well together. However, the use of GGBS as an individual powder is not possible, because it does not achieve the fluidity specifications required for waste encapsulation. As the PSD of the cement changes, i.e. the GGBS content is altered, the particle packing density is affected. In general, as the Calumite content increases the packing density decreases, and this caused by the larger Calumite particles. It is also likely that the porosity of the Calumite particles visible in Figure 4.1, will make this powder less dense than the GGBS material and will in turn affect the packing density of the blended BFS systems.

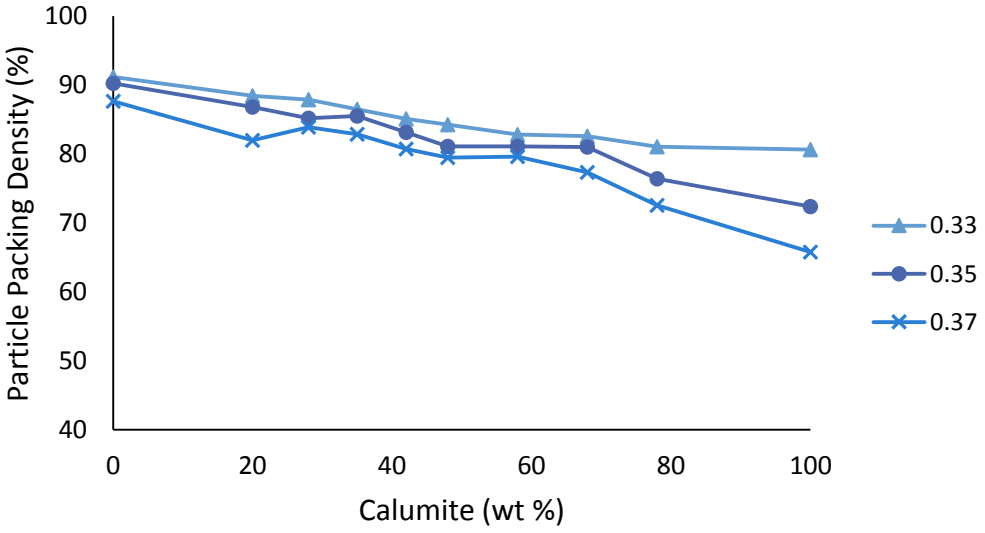

Figure 4.8. Particle packing density of the 10 blends at a 3:1 BFS:PC ratio at three w/s ratios (0.33, 0.35 and 0.37).

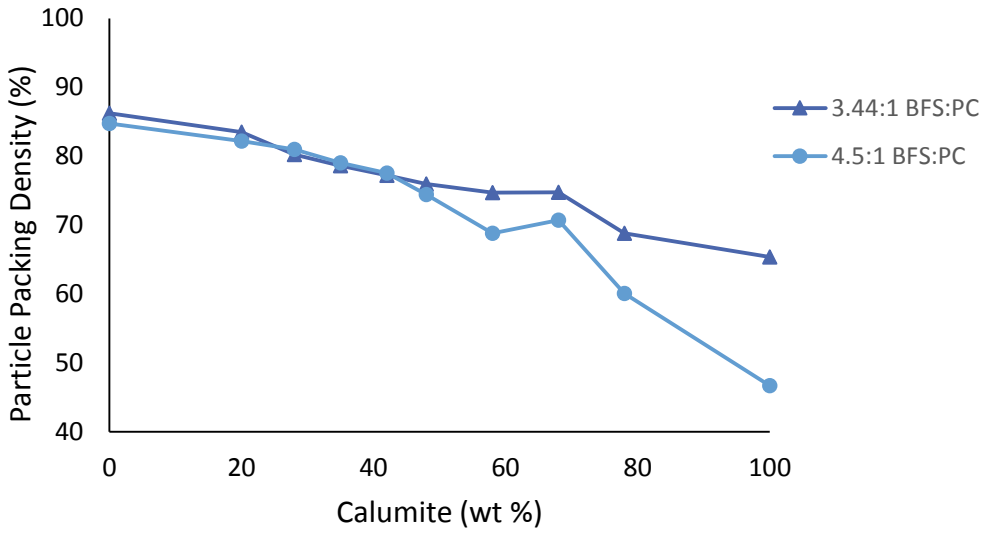

Figure 4.9. Particle packing density of the 10 blends at 3.44:1 and 4.5:1 BFS:PC ratios, at a w/s ratio of 0.35.

Figure 4.8 shows the data for the 3:1 BFS:PC blends at 3 water ratios, these results were also collected for the two other BFS:PC ratios (3.44:1 and 4.5:1 shown in Figure 4.9) at a 0.35 w/s ratio. Although there were minor differences, very similar trends were seen for the two additional BFS:PC blend ratios. The effect of w/s ratio on the cement systems can be seen from the data collected, which show that with additional water the particle packing density decreases. This suggests that the water in the system creates greater voids and therefore reduces the compaction of the material. This is particularly problematic in the P22 and P0 systems, with over 15 vol. % difference between the packing density observed for the 100 wt. % Calumite samples when comparing w/s ratios of 0.33 and 0.37. In terms of waste encapsulation, high particle packing density is desirable in order to minimise the formation of voids within the wasteform, because this will reduce porosity.

4.3 Conclusions

Overall, across all three fresh state test methods, there is a recurring pattern where the majority of the 10 GGBS:Calumite blends follow a clear trend, both from a PSD perspective and in terms of w/s content ratios. As the GGBS content increases the yield stress and the packing density of the blend systems increased, whilst the fluidity decreased. The exception to this is the P0 (i.e. 100 wt. % Calumite) blend, which consistently falls out of trend and is unpredictable or under performs. This is because of

the high proportion of large particles in the material, and strongly highlights the importance of incorporating the finer GGBS powder to achieve a balanced PSD. As the w/s ratio was increased the yield stress and particle packing density decreased, whilst the fluidity increased.

The mini-slump results highlight the influence that finer particles have on the workability of the cement pastes. This is also true for the coarser fraction, and therefore it is important to have a balanced mix of particle sizes in order to achieve the optimum flow. The slump area results provide the values required to predict the yield stress of that material and the method used was in general very reliable. When the yield stress values are compared to those obtained using the vane method, there is a positive correlation. However, the P0 system falls completely out of trend causing a very unusual result, because the material does not fulfill the requirements for the yield stress equation. It is also possible that the vane method is not suitable for measuring this coarse material because it causes centrifugation of the larger particles.

With regard to the centrifugation tests, it is possible to achieve reasonable particle packing with the addition of the Calumite, but it is more favourable to maintain a higher GGBS content within the BFS fraction. As the Calumite content increases, it causes an unfavourable balance between small and large particles. These experiments also provided information on the maximum packing volume fraction of each of the cement formulations. These data will be used in Chapter 5 as part of a modelling study carried out in parallel to complement the results found in this chapter.

5 Modelling Yield Stress

5.1 Introduction

As discussed in Chapter 4, measuring the yield stress of a material can be particularly problematic. Once experimental yield stress measurements are obtained via methods such as the mini-slump or viscometry tests, it is necessary to use equations or models to extrapolate the data in order to obtain the yield values. However, previous studies have reported models that are capable of predicting the yield stress of a material based on the particle size distribution of the precursor powder. In this chapter, to complement the experimental data collected during the mini-slump tests and rheology work, mathematical modelling has been used to attempt to predict the yield stress of the systems. Two different models have been applied to the formulations used in this project, and all of the values will be compared to conclude whether the prediction tools are reliable for these cementitious blends. The aim of the study is that irrespective of the cement powder used, as long as the chemical composition is similar, it is hoped that it will be possible to predict the yield stress and therefore optimum performance behaviour based solely on the PSD of the cement system.

The first model applied to the GGBS:Calumite:PC system in this chapter was presented by Kashani et al. [47] and was based on the ability to predict yield stress of ternary cement-slag-fly ash pastes from particle size distribution (PSD) parameters. Although the ternary system in this project does not contain fly ash, there are still three components (PC, GGBS and Calumite) with varying PSD contributions. The model of Kashani et al. [47] was developed to relate the paste yield stress to the width parameter of the Rosin-Rammler PSD and water/solid mass ratio (w/s). Their study applied the model to 30 mixtures and assumed that PSD and w/s were the most important parameters determining yield stress at early age. The PSDs of the main precursors were quantitatively compared using the Rosin-Rammler function [94, 95]. The Rosin-Rammler model uses a plot of $\log_{10}[\log_{10}(100/R_{Dp})]$ vs $\log D_p$, where R_{Dp} is the cumulative percentage of particles with diameter greater than D_p (μm), to calculate n which is the slope of the plot and describes the width of the distribution. In the original implementation of the Kashani model, this was calculated for each of the precursors, and scaled in a ratio for each mix proportional to the mix design. It was found that some of the PSDs of their materials did not follow the Rosin-Rammler relationship [47], so to resolve this issue the smallest 5 wt. % of the particles were removed from the plot for all mixtures in this chapter. The n values were plotted against experimentally measured

yield stress values for each of the 30 mixes at 3 different w/s ratios. The lines for each w/s ratios converged to a single point of n = 0.68, suggesting that if the PSD is broad enough ($n \leq 0.68$) the yield stress can approach zero, and that its value can be predicted from the PSD of a mixture.

This can be used to predict the linear relationship between 'n' and the paste yield stress through Equation 5.1.

$$\tau_y = \frac{n-b}{a}, n > b \quad (5.1)$$

$$\tau_y \approx 0, n \leq b$$

Based on the point of convergence where n = 0.68 and τ_0 = 0, b was determined to be 0.68 and it was found that $1/a$ is related to the w/s ratio. The slope obtained as a result of plotting these values provided the relationship between $1/a$ and w/s. This was incorporated into Equation 5.1 to produce Equation 5.2, which can be used to predict the yield stress of mixtures based on the PSD width parameter n and the w/s of the paste.

$$\tau_y = (n - 0.68)[1470 - 3141(w/s)], n > 0.68 \quad (5.2)$$

The calculated yield stresses were then compared to the previously measured yield stress values and this paper found the two match fairly well [47]. In this model the PSD and w/s mass ratio are taken to be the only parameters that contribute to the determination of yield stress at an early age. This is a simplified view of the system, because as described in other models, other parameters can contribute to the flow properties such as: particle shape, particle surface charge, and inter-particle forces. However, this simplified approach was not meant to be a truly universal expression and has produced effective outcomes across the ternary system investigated in the reported study.

In this chapter, this model has been applied to the GGBS:Calumite:PC system under investigation, to analyse if this could be used as a viable method of predicting the performance of the cement paste from the PSD.

The second model utilised in this chapter is based on the Yield Stress model (YODEL) for concentrated particulate suspensions, which incorporates microstructural parameters such as: particle size distribution, volume fraction of solids and inter-particle forces, and was developed by Flatt and Bowen [96]. The motivation for developing this model was the ability to predict the rheological behaviour of cement based systems, therefore once the model was developed for concentrated suspensions it was then applied to cementitious materials. Understanding the contribution of inter-particle forces is

important because the dispersion of the powder within the cement system produces increased flow with a minimum water requirement. This model discusses the particle size distribution and the interparticle forces between spherical particles and was validated by experimental data published by Zhou *et al.* [97] which were fitted very well. However, the model does not fully agree with experimental results with regards to particle diameter reported by Zhou *et al.* [97]. The model shows that the variation of yield stress for a suspension is inversely proportional to the particle diameter, but the experimental data do not show this dependency. Therefore, the dependence of yield stress on the particle size is described in terms of radius of curvature and the volume fraction of solids [96]. Bowen and Flatt went on to extend the application of the YODEL model to multimodal distributions [98] which, as established from the PSD data presented in Chapter 3, would be required to describe the materials used within this study. The key parameters needed to develop the model for multimodal systems are the PSD and the maximum packing fraction of the precursor powder mixtures provided by using the de Larrard compressive packing model [99]. The physical parameters used in the YODEL model incorporate geometrical considerations which allow the model to account for agglomeration within the particle packing of the material.

The model uses a yield stress function, Equation 5.3, to predict the yield stress of a material [98].

$$\tau_0 = m_1 \frac{\phi(\phi - \phi_0)^2}{\phi_{max}(\phi_{max} - \phi)} \tag{5.3}$$

Where ϕ_{max} is the maximum packing fraction of the powders, ϕ_0 is the percolation threshold and m_1 is a pre-factor that accounts for inter-particle forces, particle size and particle size distribution. The pre-factor m_1 is dependent on inter-particle forces, and the authors who developed the model assumed that contact points between particles have a fixed average radius of curvature, a^* [98]. This implies that the radius does not change or scale with different particle size, such as with smooth spherical particles. Therefore, m_1 can be presented as Equation 5.4.

$$m_1 = \frac{1.8}{\pi^4} G_{max}\, a^*\, u_{k,k} \left(\frac{f^*_{\sigma,\Delta}}{R^2_{v,50}}\right) \tag{5.4}$$

Where, $R^2_{v,50}$ is the volume mean radius, and G_{max} is the maximum attractive inter-particle force and is calculated using Equation 5.5.

$$G_{max} \cong \frac{A_0}{12H^2} \tag{5.5}$$

Where H is the minimum separation distance and A_0 is the Hamaker constant of the particles. Zhou *et al*. showed that the minimum separation distance can be treated as equal for all powders [97]. The particle size distribution is taken into account by the function $f^*_{\sigma,\Delta}$ and is derived using Equations 5.6 – 5.10 as part of the YODEL model [98].

$$f^*_{\sigma,\Delta} = \frac{1}{u_{k,k}} \sum_{k=1}^{m} \phi_k \sum_{l=1}^{m} S_{a,l} \frac{A_s}{A_c} \frac{\Delta v_{k,l}}{b_k^3} \frac{1}{(b_k^2 + b_l^2)} \tag{5.6}$$

Where b_i is the particle radius (a_i) normalised by the mean volume radius $R_{v,50}$, and ϕ_k is the volume fraction of particles of size b_k in the size interval k.

$$\frac{A_s}{A_c} = \frac{2(b_l + b_k)}{b_k + b_l - \sqrt{b_k\,(b_k + 2b_l)}} \tag{5.7}$$

$$S_{a,l} = \frac{\phi_l / b_l}{\sum_{i=l}^{m} \phi_i / b_i} \tag{5.8}$$

$$\Delta v_{k,l} = 4\pi(b_k b_l)(b_k + b_l) \tag{5.9}$$

$$u_{k,k} = \frac{16\pi}{2 - \sqrt{3}} \tag{5.10}$$

Both the Kashani and YODEL models were applied to the GGBS:Calumite:PC cement systems and the results are presented here.

5.2 Model Implementation

5.2.1 Kashani Model

The Kashani model was applied to the ternary grout systems studied in this project. In the original model implementation, *n* was calculated for each precursor and then scaled with the ratio of the precursors in each blend. However, in this study *n* values were calculated for each mix from individual PSD data to eliminate the requirement for scaling. The *n* values obtained from the PSDs here are plotted in Figure 5.1 against the yield stress determined from the mini-slump tests, in section 4.2.1 for the ten blends of GGBS:Calumite:PC at 3:1, 3.44:1 and 4.5:1 BFS:PC formulation with 0.33, 0.35 and 0.37 w/s ratios (90 mixes in total). The data points with an *n* value between 0.9 and 1, represent the P100 blend mixes. The other blends all achieve an *n* value of between 0.5 and 0.7. This is due to the unimodal nature of the P100 system which produces a much better slope fit. The *n* value describes the width of the PSD and as the ratio of GGBS/Calumite changes, it causes the slope fit to deviate suggesting that the model is not suited to materials with a bimodal distribution.

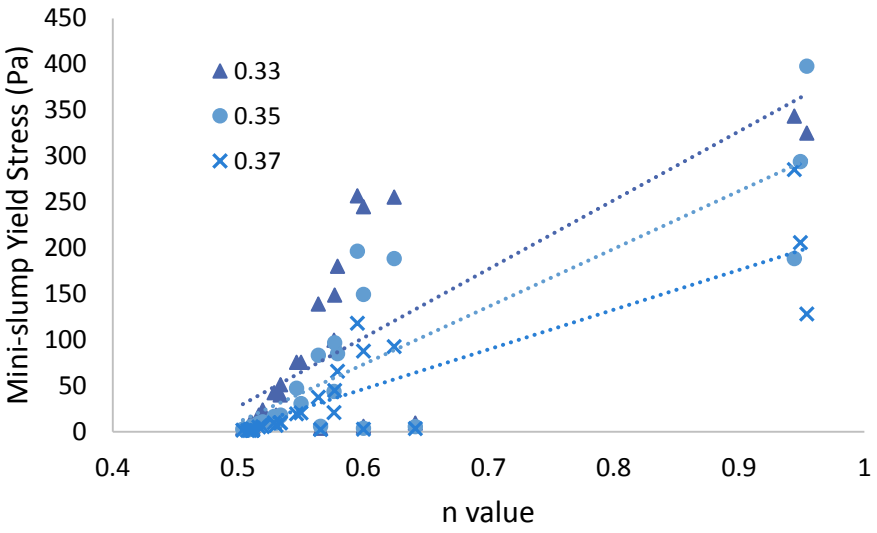

Figure 5.1. Yield stress values of the 30 mixes at 0.33, 0.35 and 0.37 w/s ratios and their corresponding *n* values. Dashed lines are linear trendlines fitted to the data at each w/s ratio.

For these ternary mixes, the point of convergence of the trendlines in Figure 5.1 was found to be 0.46. Therefore for this system, $b = 0.46$ in Equation 5.1 and is used in the final equation. The slope (1/a) for the data set at each w/s ratio (Figure 5.1) depends on the w/s mass ratio. By plotting these two values (Figure 5.2), the linear relationship provides the Kashani yield stress equation parameters.

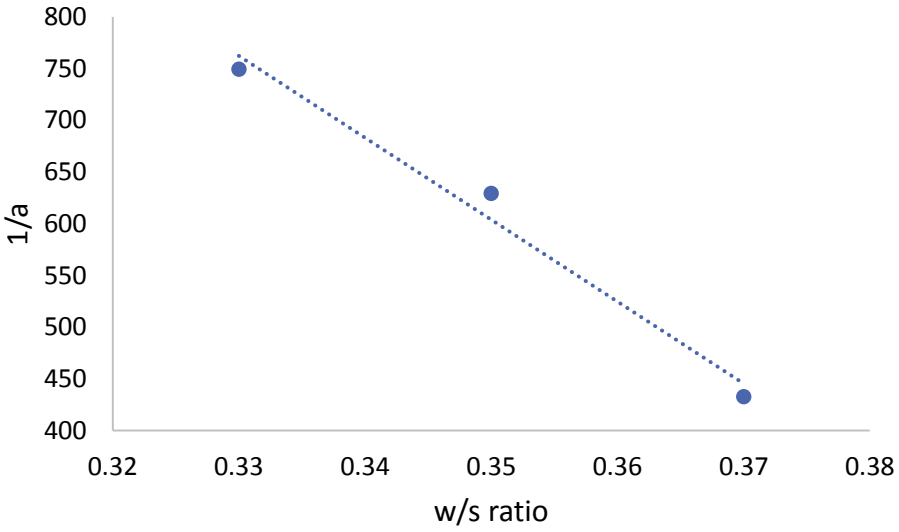

Figure 5.2. Values of 1/a (calculated for each line in Figure 5.1) against w/s mass ratio.

The yield stress equation for the mixes in this project therefore becomes equation 5.11.

$$\tau_y = (n - 0.46)[3378.5 - 7927.5(w/s)], n > 0.46 \quad (5.11)$$

Equation 5.3 was used to calculate the predicted yield stress values for the 90 formulations from Chapter 4, and compared against the values calculated from the mini-slump tests, Figure 5.3. A general trend is observed whereby as the surface area becomes larger, and therefore water demand increases, the yield stress values increase, which is to be expected. Unfortunately, although some of the data points have a reasonable relationship to the equation, some of the values deviate too far from the X=Y line (dashed diagonal line in Figure 5.3) to consider this a viable model to use with the GGBS-Calumite-PC ternary system. The calculated values were also validated by working the model backwards for the yield stress calculation. Using the 'smallest predicted' value of yield stress, the model calculated that the slump spread would need to be over a metre in diameter to produce the predicted yield stress. This spread was not replicable in the lab and as such, these results are considered to be unreliable.

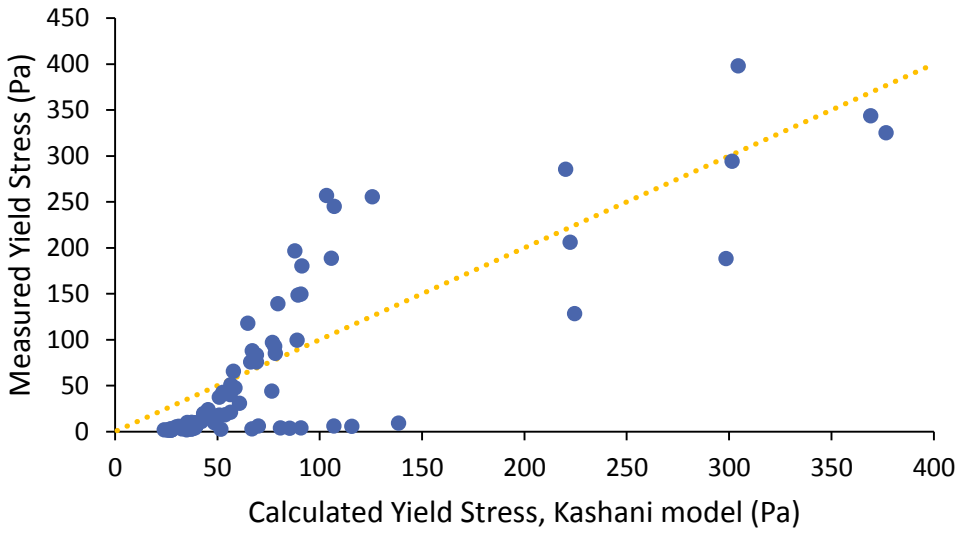

Figure 5.3. Relationship between calculated (Kashani model) and measured yield stress values for the 30 cement paste mixtures at 0.33, 0.35 and 0.37 w/s ratios. The orange dashed line indicates equivalence of the model and measurements.

If the Kashani model had been applicable to these systems, it should have been possible to predict the optimum PSD of the GGBS:Calumite:PC mix that would produce the best workability. The optimum *n* value for the GGBS:Calumite:PC cement system was calculated to be 0.46, and by using this value in the model it should in theory predict

mixes with the optimum PSD. The optimum PSD for the best workability was predicted, this was determined by varying the PSD contributions from the GGBS, Calumite and PC materials. The workability of the grouts produced using the predicted PSD values were tested via the mini-slump test method to obtain experimental yield stress data. The actual PSD values were also applied in the yield stress model to obtain theoretical values. The correlation between the measured and calculated values did not show a reliable relationship, suggesting that the model cannot be used in this manner. Although they predict similar *n* values, the model does not take into consideration the actual flow of the slump. This statement was validated by inputting the calculated yield stress values back into Equation 4.1 discussed in Chapter 4. The slump was predicted to have a diameter of over 1 metre, which would be physically impossible with the quantity of material used.

It is reasonable to conclude that the Kashani model does not work well for the gap graded powder, and that the Rosin-Rammler distribution width parameter is not sensitive enough to use as the sole characteristic value for these materials in predicting yield stress.

5.2.2 Validation of the YODEL Model implementation

To validate the correct implementation of the YODEL model and confirm full understanding, before applying it to powders in this project, the model was applied to published data [100]. A PSD extracted by hand from a printed version of the paper by Stuer and Bowen (because the exact figures were not available) was input into the developed interpretation of the YODEL model. The parameter values stated in the publication were used to validate the implementation of the model by reproducing their data, as shown in Figure 5.4.

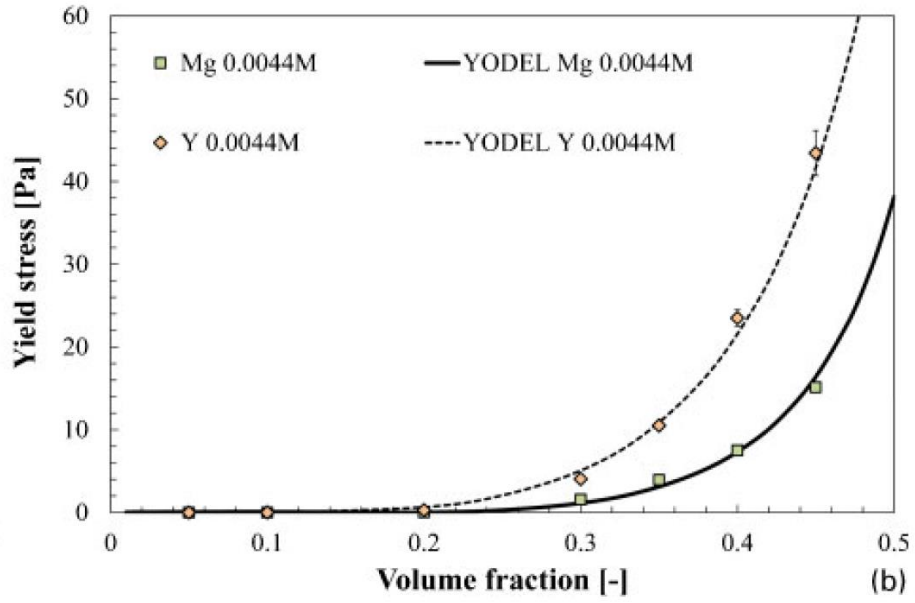

Figure 5.4. Experimental and modelled yield stress curves as a function of volume fraction for Mg^{+} and Y^{3+} at 0.0044 M. Results reported by Stuer and Bowen comparing experimental values and YODEL model calculated data [100].

By setting the percolation threshold and minimum separation according to the two dopants in the model calculations here, it was then possible to produce yield stress values for a series of volume fractions. The validation data are shown in Figure 5.5.

Considering that the PSD values used in Figure 5.5 were obtained manually from a published graphic, the results achieved were in very close agreement to those reported by Stuer and Bowen. This confirmed and validated that the YODEL model implementation was correct and could be applied with confidence to the powders in this project.

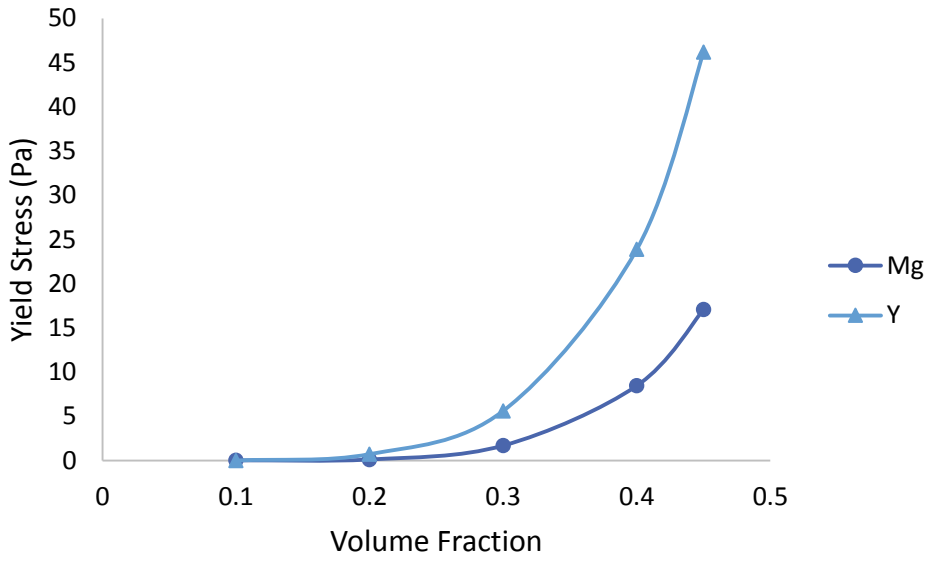

Figure 5.5. Reproduction of data reported by Stuer and Bowen to validate the YODEL model implementation.

5.2.3 Application of the YODEL Model

The YODEL model was therefore applied to the ten blends of GGBS:Calumite:PC system at 3:1 BFS:PC formulation with 0.33, 0.35 and 0.37 w/s ratios (30 mixes in total), by producing a PSD for each formulation. These individual PSDs and corresponding volume fractions were then translated into the YODEL model in order to calculate $f^*_{\sigma,\Delta}$ for each powder blend. G_{max} was calculated using a Hamaker constant of 7.8 x10^{-21}, reported by Lomboy [101] which was specific to slag materials and therefore was a reasonable fit for use in this study. The minimum separation distance *H* was calculated using an equation from the original YODEL paper, H = h_0 (9.5exp (-4.5ϕ)) [96]. A value of 24 Å was used for the surface separation (h_0) which was originally used for oxide particles and taken from the paper by Zhou *et al.* [97]. Although the GGBS:Calumite:PC particles will differ in chemistry and surface charge to those used by Zhou *et al*., more specific data was not available and so this value was adopted. The $f^*_{\sigma,\Delta}$ function and G_{max} values were used to calculate m_1, using an a^* value of 50 nm, which was chosen as a reasonable estimate based on information provided from the original YODEL model that states that it should be between 20 and 80 nm [96]. Finally, the m_1 value was used to determine the yield stress in Equation 5.3. However, the results reported during the development of the YODEL model, were obtained using maximum packing values theoretically calculated using a packing model. This was not necessary for the GGBS:Calumite:PC system, because experimental maximum packing values for each individual formulation were obtained using the particle packing density method reported in Chapter 4. Consequently,

these values were used directly in the model. As with the Kashani model, the calculated values gained from the YODEL model were plotted against the measured yield stress values from the mini slump and rheometer tests, shown in Figure 5.6.

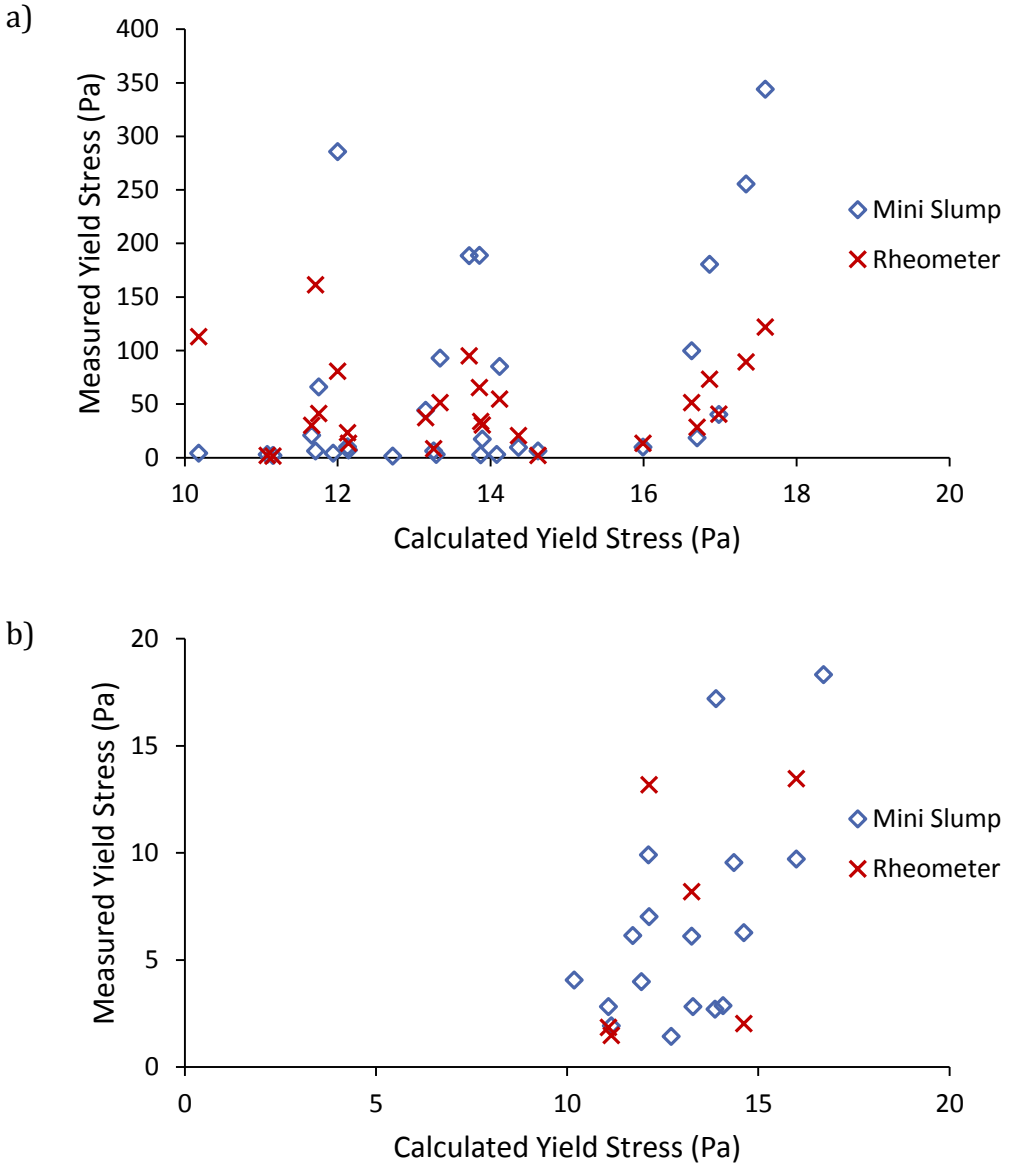

Figure 5.6. Relationship between calculated (YODEL model) and measured yield stress values for the 30 cement paste mixtures at 0.33, 0.35 and 0.37 w/s ratios. Note the differences in axis scaling to highlight a) the full data set and b) the lower yield stress values.

Figure 5.6 illustrates the biggest difference between these results, is that the calculated values all sit within a narrow range of 10 to 20 Pa compared to the broad distribution of data for the measured yield stress. Although there is a general trend with the YODEL data, that as the Calumite content increases, the yield stress values decrease slightly. The output values from the model were dissimilar to yield stress values that the

experimental results show. The data also highlighted the difference between the two experimental methods, mini-slump and rheometer. The yield stress values obtained from the mini-slump method range from 0 to 400 Pa, compared to the rheometer results which peak just below 200 Pa.

The sensitivity of the model was explored by altering some of the parameters such as: the surface separation, the radius curvature and the maximum packing one at a time. This was achieved by changing the values by ± 10 % for the P65 system at a 0.35 w/s. This showed that with a 10 % increase in the surface separation (h_0) the yield stress decreased by 17 %. However, a 10 % decrease in h_0 produced a 24 % increase in yield stress. A similar trend was seen regarding the maximum packing value, where a 10 % increase produced a 26 % decrease in yield stress and an increase of 45 % was observed with a 10 % decrease in max packing fraction. The initial range considered for the radius curvature (a^*) was stated as 20 – 80 nm [96], and a value of 50 nm was used for the GGBS:Calumite:PC. However, when the extremes of the suggested range (20 and 80 nm) were considered, the model predicts that as a^* increases, the yield stress increases by ± 60 %. The variation of results found by altering the parameter input values highlight the sensitivity of the model and the errors that are likely to be due to some of the assumptions made for the application of YODEL.

The range of predicted yield stress values gained from the YODEL model is far too narrow to feel confident that the model is producing reasonable results for the GGBS:Calumite:PC system, especially considering the wide range of fluidities observed in Chapter 4.

5.3 Summary

The aim of this chapter was to determine if it was possible to predict the yield stress and in turn the workability of the GGBS:Calumite:PC system using previously published models. These results were then compared to yield stress values that were collected experimentally in Chapter 4.

The Kashani model produced values that followed the same trend and in the same order of magnitude when compared to the experimental data. However, some of the data points were varied, suggesting that the model is not reliable enough to predict the yield stress of the gap graded powder used in this study. A reasonable assumption is that the Rosin-Rammler distribution is not a sensitive enough sole parameter to use for characterising this material.

The YODEL model was then applied, following some validation trials of the method, to the GGBS:Calumite:PC powder system due to its published claims of suitability for multimodal systems. However, the model predicted a very low and narrow range of yield stress values for the formulations. Working with the cement pastes during the experimental testing in Chapter 4, it is clear that some of the formulations were very fluid and others were very stiff, suggesting that they would have wide ranging yield stress values. Therefore, the results predicted by YODEL would contradict the experimental results. The YODEL was designed to describe suspensions of a single type of non-reacting material, whereas the systems investigated here have particles with two types of chemistry, and reactivity, and an extremely broad PSD. The YODEL is, unfortunately, not suitable for these cements.

Neither of the two models applied to the powder system under investigation provided consistent and reliable results. The Kashani model predicted the most comparable results to the experimental values, but unfortunately the results do not correlate well enough to use it further as a predictive tool for this project.

6 Heat of Hydration

This chapter is adapted from the two following published papers authored by R. A. Sanderson et al.:

- R. A. Sanderson, G. M. Cann, J. L. Provis, The effect of blast-furnace slag particle size on the hydration of slag-Portland cement grouts at elevated temperatures, *Advances in Cement Research,* **2018***, 30*: 337-344.
- R. A. Sanderson, G. M. Cann, J. L. Provis, Comparison of calorimetric methods for the assessment of slag cement hydration, *Advances in Applied Ceramics,* **2017***, 116*: 186-192.

6.1 Introduction

One of the key performance parameters required by the nuclear industry is the capability to control the heat evolution of cement wasteforms. The waste packages produced are required to be durable and safe, therefore a need for low heat evolution from the cement is essential to minimise cracking and reduce problems with the waste packages during storage and emplacement, as well as in situ in the GDF. The semi-adiabatic temperature rise during cement hydration is thus a key performance parameter, and must be monitored and predicted accurately.

This requirement to be able to measure the heat release during hydration of blended cementitious materials straightforwardly and with consistent, reliable results was one of the main drivers of this chapter. Currently, there are two standard methods in the UK for measuring the heat of hydration of cement: solution calorimetry at 7 days (BS EN 196-8), and semi-adiabatic calorimetry measured at 41 hours (BS EN 196-9), which are claimed to give equivalent results [102, 103]. In solution calorimetry, the cement is hydrated at a constant temperature and this is therefore essentially an isothermal test. However, the measurement involves dissolving the hydrated cement into a highly corrosive and hazardous mixture of nitric and hydrofluoric acids, making it an unattractive method to use routinely in a laboratory or field setting. Semi-adiabatic calorimetry consists of preparing a freshly made sample and measuring the heat emitted [104]. This method requires insulated flasks in order to have the lowest heat loss possible, calibrated against a reference flask and with known rates of heat loss to the environment to enable calculation of heat evolution rates from the temperature history in the sample flask, and uses quite a large sample (1575 g of fresh mortar in BS EN 196-9). The British and European Standards (BS EN 197-1) classify a low heat cement as a

cement that '*shall not exceed the characteristic value of 270J/g*' determined using either of the above methods [17].

Isothermal conduction calorimetry can also be used to measure the heat production rate of small cement samples and would be a useful method to classify 'low heat cements'. This method has been extensively used and reported, and is being considered at pre-standardisation levels across Europe [105] but is still not a standard technique for the measurement of heat of hydration in Europe. Isothermal calorimetry is used as a standard method in other parts of the world as stated in ASTM C1679 and C1702 [106, 107]. Wadsö and Arndt [71] reported a study carried out in 2003 to evaluate the use of isothermal conduction calorimetry as an appropriate method for the determination of the heat of hydration of cement at 3 days. They concluded that it is more precise than traditional methods for Portland cement, but did not perform as well for slag-based cement. In this chapter the method is applied to slag based cements which are used by the nuclear industry.

The thermal behaviour of the cement grout used during nuclear waste encapsulation impacts on the stability and durability of the wasteform produced. It is reported that in mass concrete structures, the heat produced during the cement hydration reaction can result in a large rise in temperature in the first few days after casting. This is due to exothermic hydration reactions, and can result in cracking as the concrete cools to ambient temperature [108]. Any thermal gradients within the wasteform could also cause microcracking, altering the microstructure and porosity. Thermal stresses could be controlled by releasing any excess pressure in the system. However, this could be hindered by the presence of the metallic wastes [6, 109], therefore it is important to understand how the cement pastes behave at higher temperatures.

In this chapter, isothermal and semi-adiabatic calorimetric methods for measuring the heat evolution from cement grouts that contain a high slag content were analysed and compared. The semi-adiabatic method was used to determine the maximum temperature rise during hydration rather than as a method of directly quantifying the heat evolution. Isothermal calorimetry was also used to evaluate the contribution of Calumite to the hydration reaction, and how these pastes perform at higher temperatures. The formulations were varied by changing the PSD of the slag component of the blended cement powder, and mixing at different water to solids (w/s) ratios, as in the preceding chapters.

6.2 Results and Discussion

6.2.1 Isothermal Calorimetry at 25 ˚C

Isothermal calorimetry was carried out to determine the heat production rate of the samples and to obtain the total heat evolution of each cement paste. The 10 formulations with the BFS fractions stated in Table 3.4 were analysed at a 3:1 BFS:PC blend ratio and at 0.33, 0.35 and 0.37 w/s ratios. The IC data (Figures 6.1 - 6.3) shows that as the GGBS content increases, the total heat evolution increases from approximately 60 J/g in P0 to 140 J/g in the P100 system. This suggests that the total heat evolution reduces by 50 % when the GGBS is replaced with Calumite, and that a high percentage of the heat is due to hydration of cement clinker. All of the pastes considered here conform to the European standard classification whereby the heat of hydration does not exceed 220 J/g, and therefore can be described as very low heat cements [110].

From the data shown in Figures 6.1, 6.2, and 6.3, it is clear that the peak heat of reaction decreases as the Calumite fraction increases, and this is likely due to reduced reactivity caused by the larger particles present in this fraction. An initial heat release peak was observed in all 10 blends between 3-9 hours (inset on Figures 6.1 a, 6.2 a and 6.3 a), which was assigned mainly to alite hydration [30]. The time at which the alite peak occurs shifts to the left, demonstrating a shorter reaction time, as the GGBS content increases. This behaviour agrees with observations reported in literature and is due to the increased surface area of the GGBS material providing more nucleation sites for C-S-H [111, 112]. The GGBS also packs well together resulting in closer particles which also promotes acceleration of the reaction. Calcium hydroxide reacts with GGBS causing the alite to diminish and the formation of C-S-H is observed. This reaction is accelerated with increasing slag content which causes a higher peak heat and results in the shift of peaks because the rate of reaction in the system occurs more rapidly. The formation of a secondary ettringite peak between 7-8 hours is due to aluminate hydration caused by the depletion of sulfate species present and reducing conditions. At 16 hours, and AFm phase was identified with increasing intensity as the GGBS content rises [30]. Hydrotalcite will also be forming during this early stage and will also be contributing to the curve area. These observations are visible at all three w/s ratios, suggesting that the difference in water content has minimal effect on the reactivity of the system.

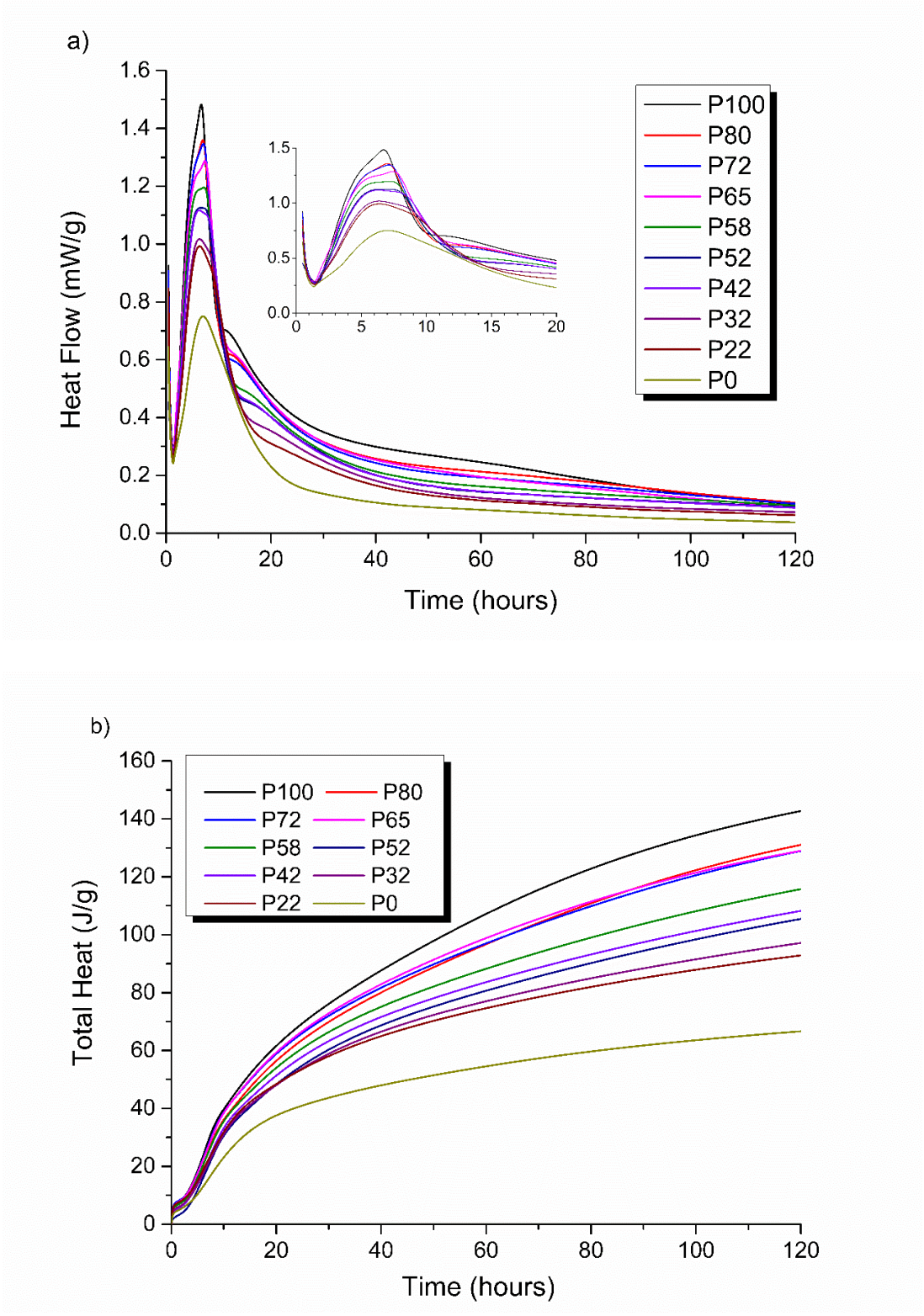

Figure 6.1. Isothermal calorimetry (a) and total heat evolution (b) curves measured at 25 °C for 120 hours for the ten GGBS:Calumite blend ratios (Table 3.4), at w/s = 0.33.

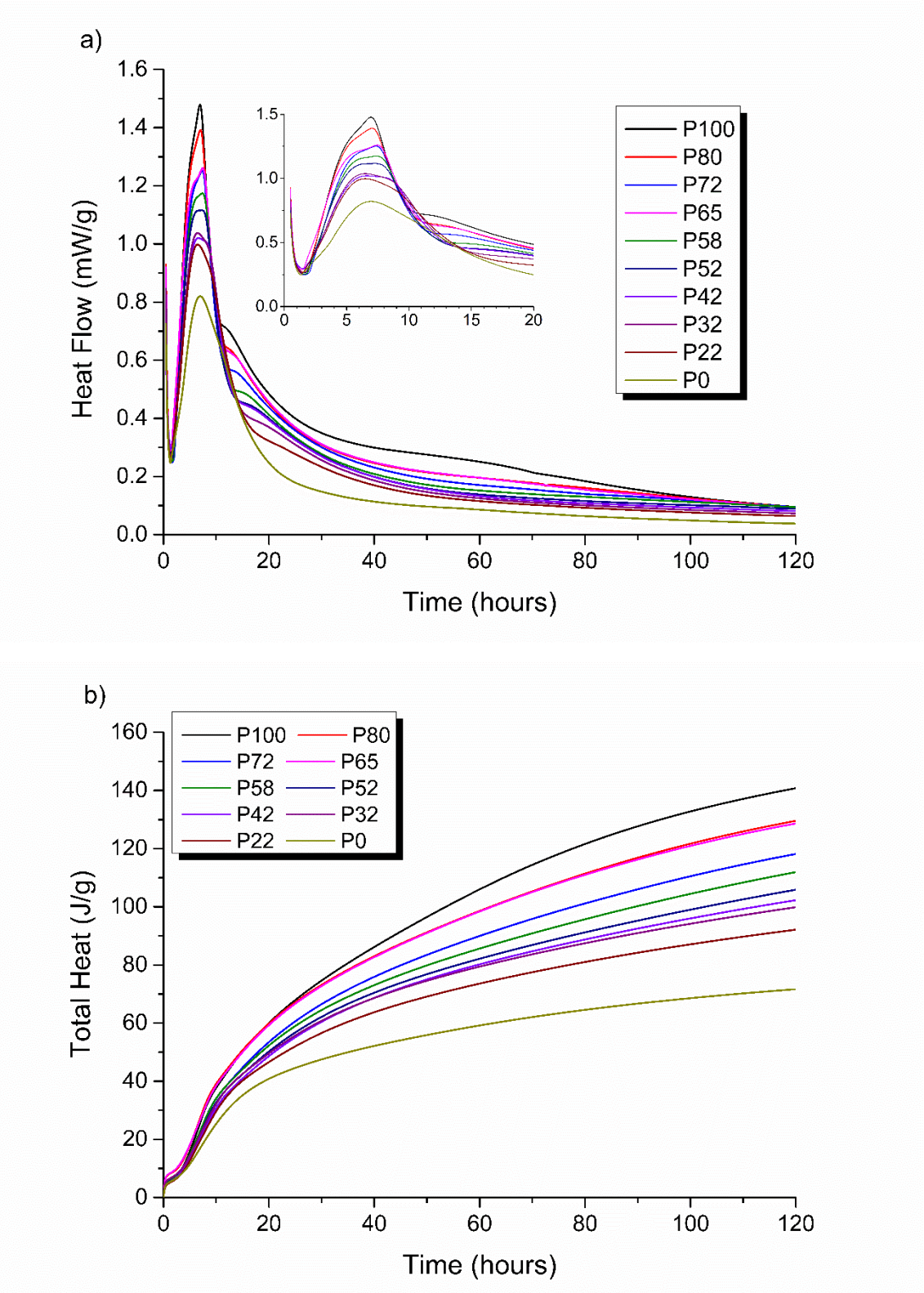

Figure 6.2. Isothermal calorimetry (a) and total heat evolution (b) curves measured at 25 ˚C for 120 hours for the ten GGBS:Calumite blend ratios (Table 3.4), at w/s = 0.35.

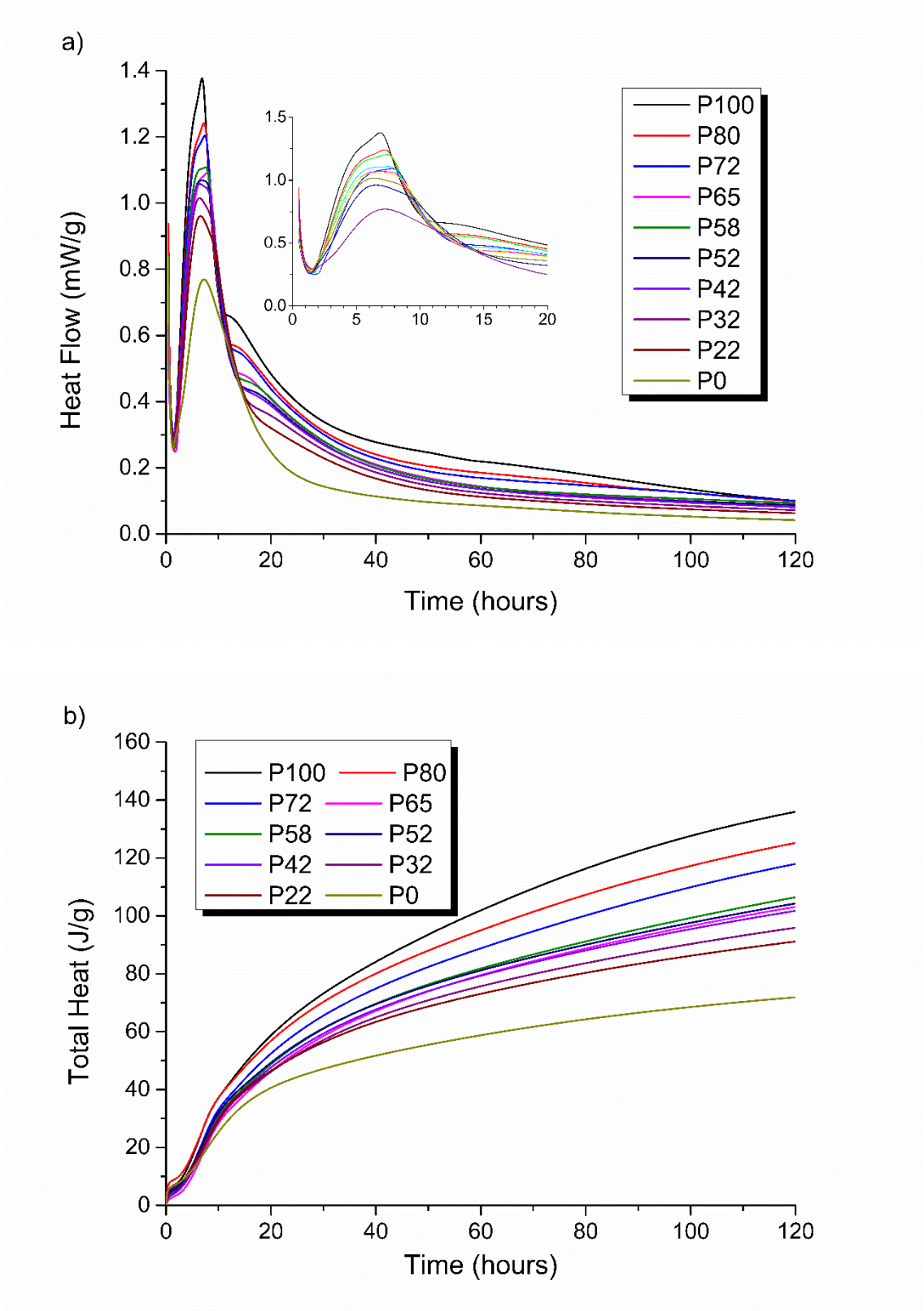

Figure 6.3. Isothermal calorimetry (a) and total heat evolution (b) curves measured at 25 °C for 120 hours for the ten GGBS:Calumite blend ratios (Table 3.4), at w/s = 0.37.

In order to further understand the early stages of the hydration reaction, some short term (approx. first 20 hours) tests were carried out on the P100 mix (i.e. 100 wt. % GGBS was used for the BFS fraction at a 3:1 BFS:PC blend with a 0.35 w/s ratio), shown in Figure 6.4. The samples were prepared and heated to 25 ˚C to mimic the isothermal calorimetry method environment. In situ XRD was taken of samples at 5, 10 and 15 hours (shown in Figure 6.5).

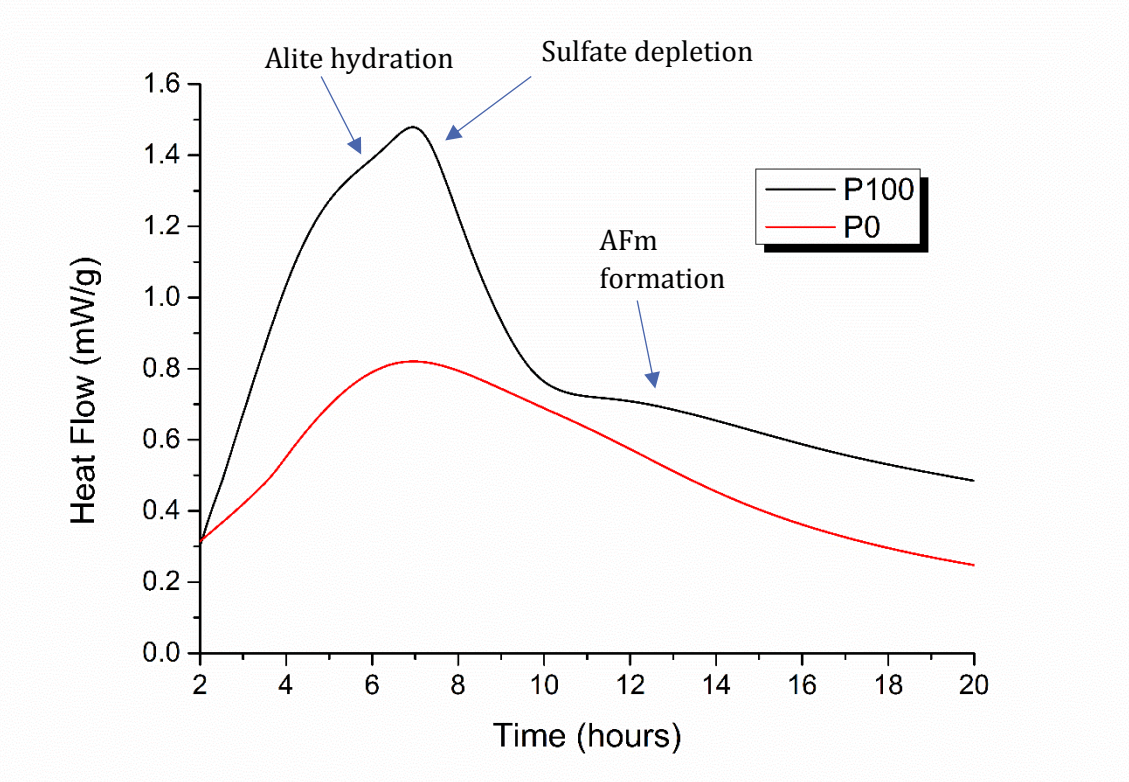

Figure 6.4. Calorimetry data up to 20 hours for P100 and P0 at 25 ˚C.

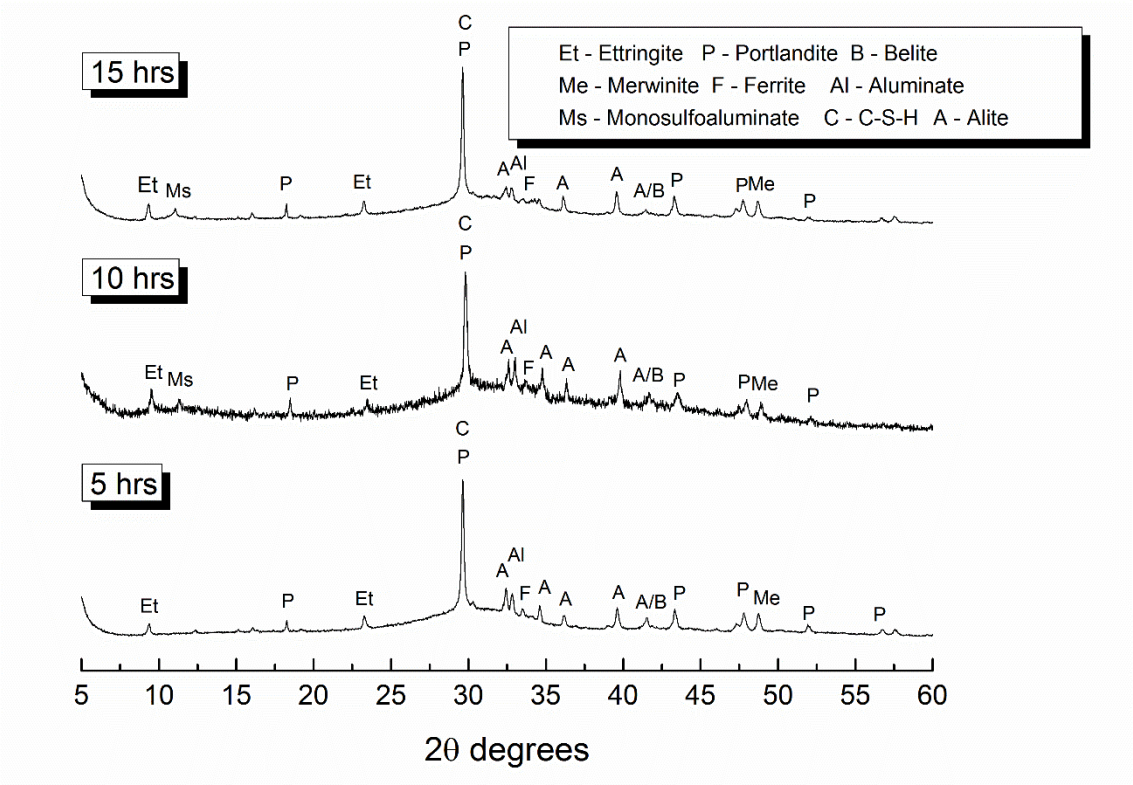

Figure 6.5. In situ XRD data for mix P100 at 5, 10 and 15 hours.

By comparing the XRD data to the calorimetry analysis it is possible to identify phase formation during early hydration. The XRD data show a strong portlandite presence which is likely due to the alite hydration peak seen in the calorimetry curve at around 5 hours. The monosulfate reflection that appears at 12° 2θ degrees in the 10 hour XRD scan correlates nicely with the AFm peak in the calorimetry data. The formation of ettringite is observed in the XRD data which is the cause of sulfate depletion i.e. typical hydration of cement blends containing BFS [109].

It is important to notice that when the BFS component was made up purely of the coarse-ground Calumite, these additional peaks are of lower intensity in the ICC data. This indicates that over the first 24 hours, the PSD of the slag component is influencing the rate of the cement hydration reaction and the chemical properties of the system, even when the early-age hydration is dominated by the PC fraction.

6.2.2 Isothermal Calorimetry at Elevated Temperatures: 35 °C and 60 °C

Isothermal conduction calorimetry was used to analyse the heat output of the cement pastes at elevated temperatures, which may be more representative of the conditions inside a large waste container undergoing cementation.

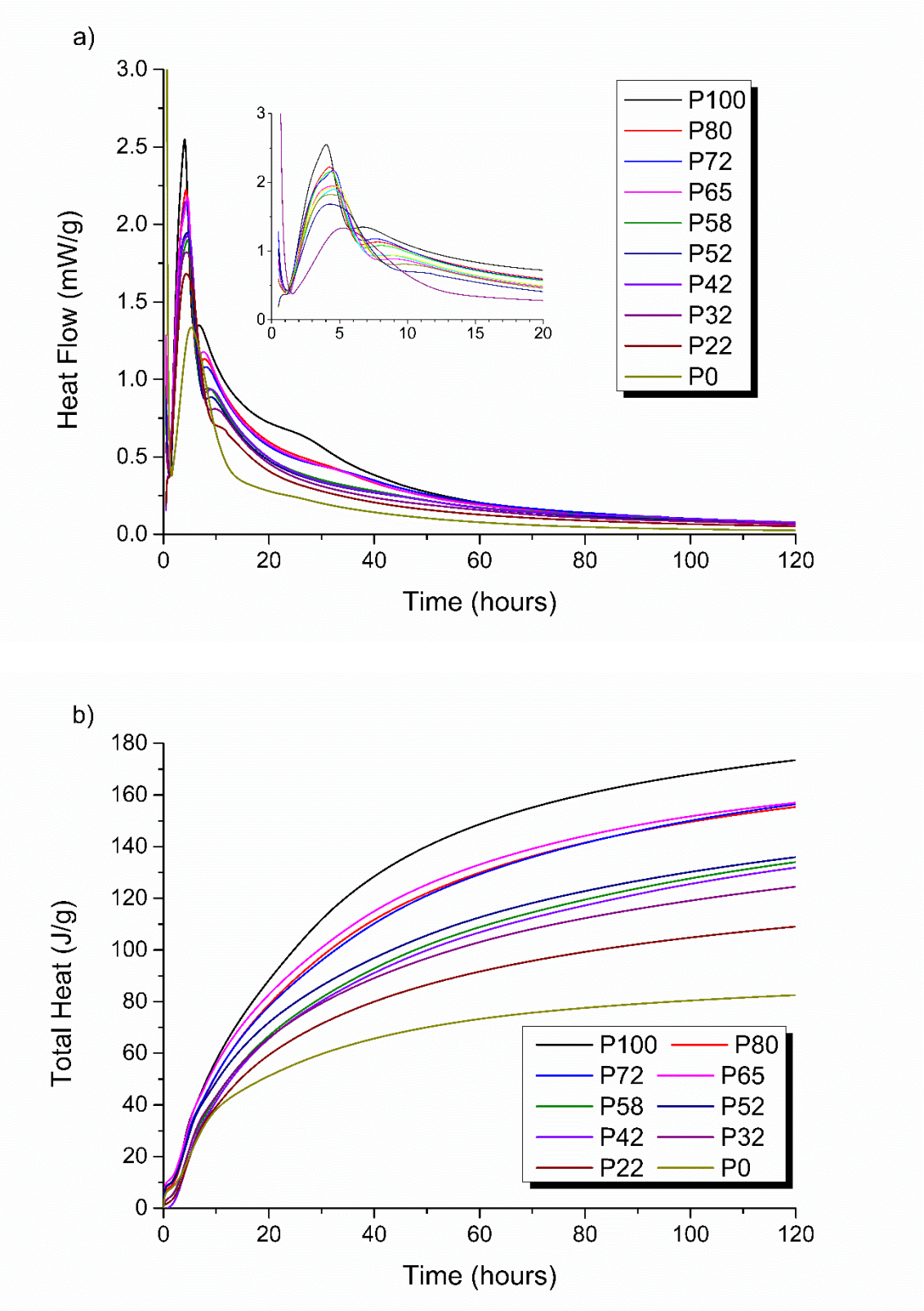

Figure 6.6. Isothermal calorimetry (a) and total heat evolution (b) curves measured at 35 ˚C for 120 hours for the ten GGBS:Calumite blend ratios (Table 3.4), at w/s = 0.35.

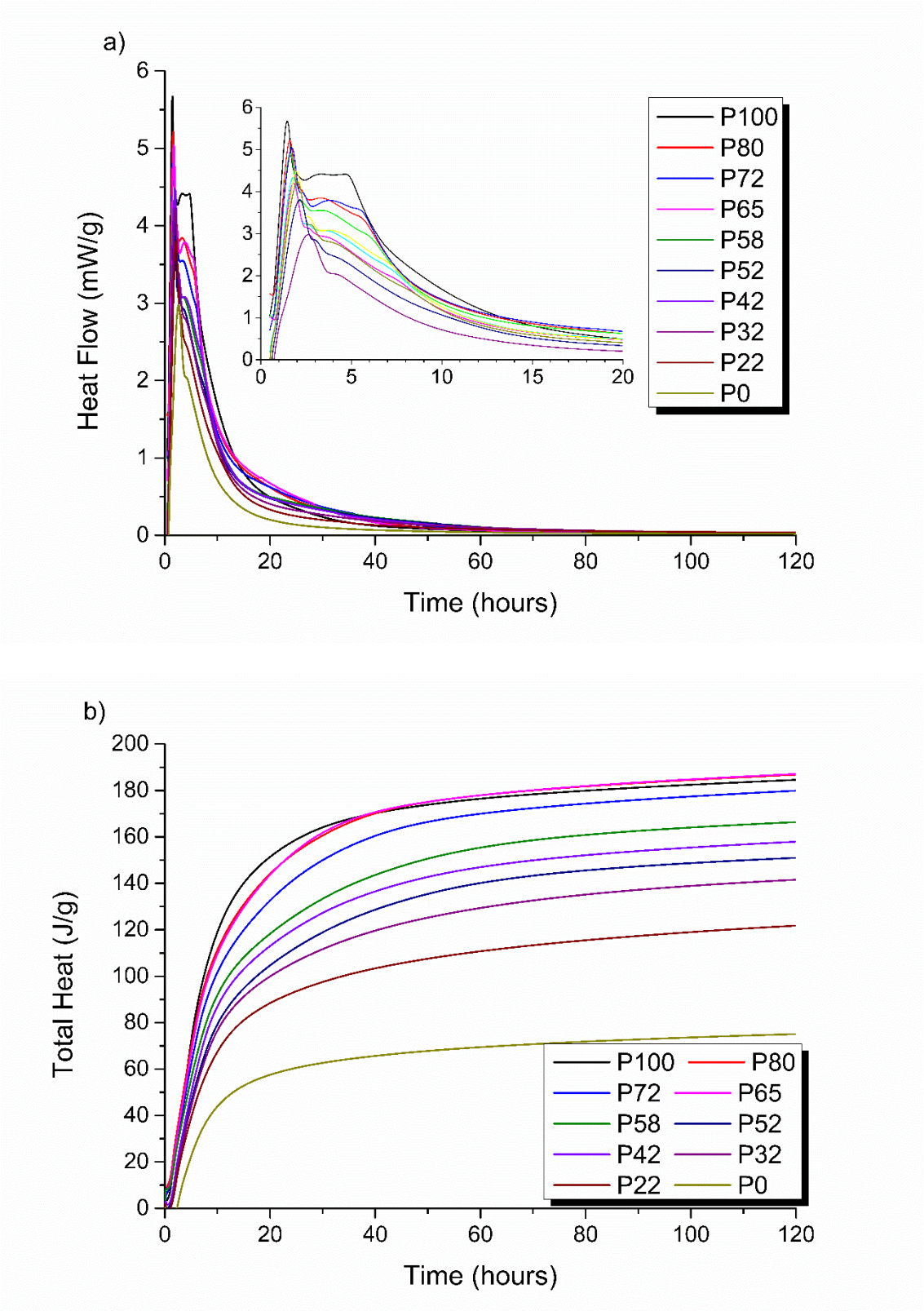

Figure 6.7. Isothermal calorimetry (a) and total heat evolution (b) curves measured at 60 °C for 120 hours for the ten GGBS:Calumite blend ratios (Table 3.4), at w/s = 0.35.

The samples were initially measured at 25 ˚C, as mentioned previously, and then to analyse the heat output of the cement pastes at elevated temperatures, further testing was carried out at 35 and 60 ˚C. A temperature of 60 ˚C was chosen to monitor the cement pastes under extreme conditions. However, the NNL acceptance test specifies a constant heat of 35 ˚C for their calorimetry data, this temperature is chosen to challenge the 'worst case' scenario that could occur on plant i.e. the maximum curing temperature. Therefore, it was logical to also carry out the experiments at this temperature. The 10 formulations for the BFS fraction stated in Table 3.4 were analysed as a 3:1 BFS:PC blend at a 0.35 w/s ratio. The full data sets are shown in Figures 6.6 and 6.7.

Similar heat evolution profiles were observed at 25 ˚C, 35 ˚C and 60 ˚C. The results show that the peak heat flow rate and the total heat evolution both increase as the GGBS content increases, at a constant BFS/PC ratio. This is to be expected due to the higher fineness of the GGBS than the Calumite, causing greater reactivity in the P100 system compared to the coarser P0 mix. The total heat evolution data collected at 60 ˚C plateaus much sooner compared to other conditions. However, the total heat evolution for the Calumite system is very similar across all temperatures and w/s ratios, this confirms the low reactivity of the Calumite material. Another observation to note is that the peak attributed to sulfate depletion is affected much more by varying temperature compared to the alite peak. This is caused by the slag hydration reaction which is accelerated at higher temperatures.

Previous studies that investigated the particle size of BFS/PC systems have reported that finer slags have shown a higher heat of hydration than coarser ones [113], consistent with the effect of greater available reactive surface area. To determine the effect of temperature on these cement systems, a direct comparison between the extreme cases

of the blends under investigation (P100 and P0) at all three temperatures is illustrated in Figure 6.8.

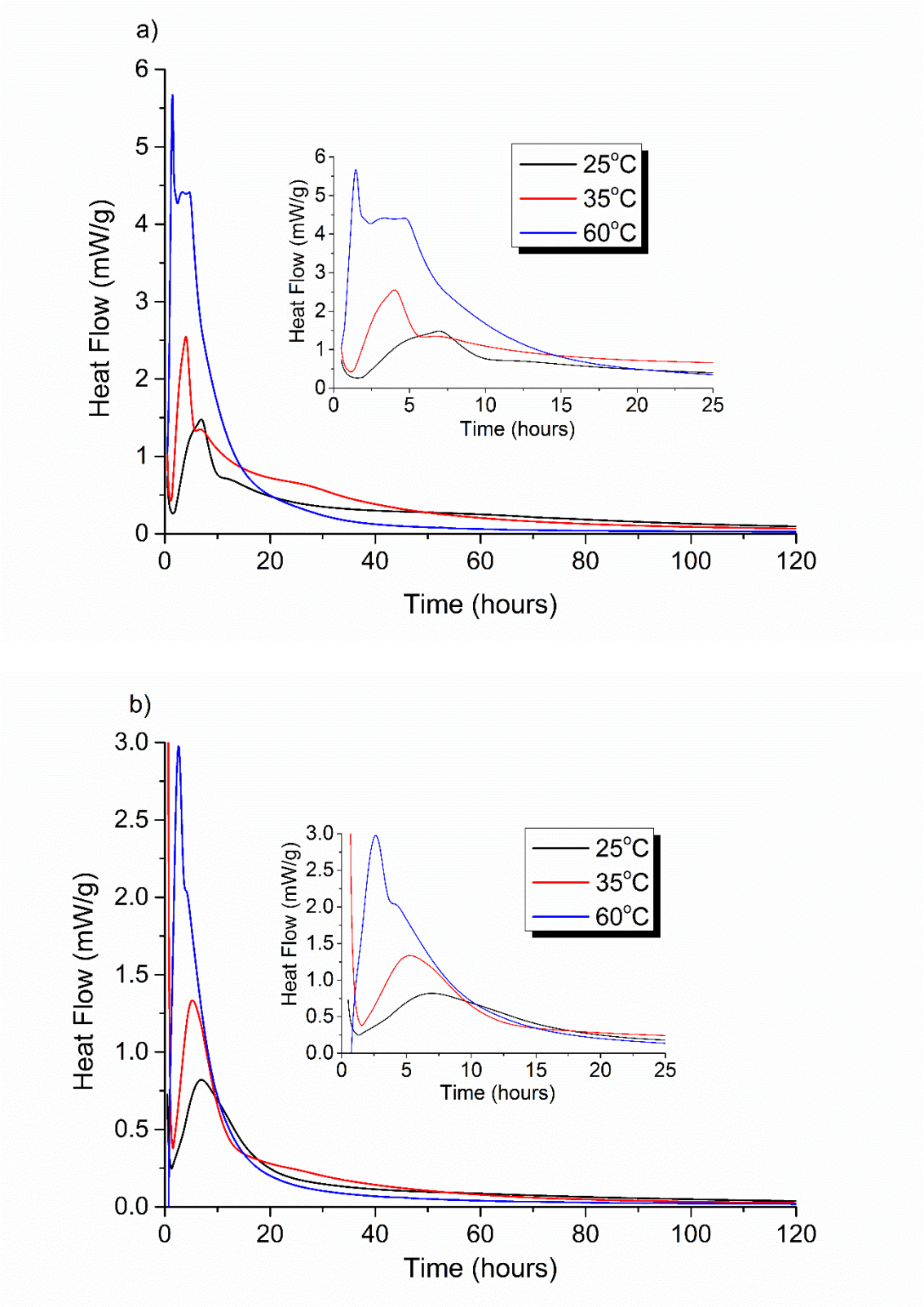

Figure 6.8. Isothermal calorimetry curves for the mix P100 (a) and P0 (b) measured at 25 ˚C, 35 ˚C and 60 ˚C for 120 hours, at w/s = 0.35.

The results in Figure 6.8 show a difference in heat output between the P100 and P0 cement pastes, which is again to be expected due to greater reactivity caused by increased fineness in the P100 sample (GGBS) compared to P0 (Calumite). The peak heat flow of P100 is approximately twice the value of the P0 equivalent. This is consistent across all three temperatures, suggesting that the main contributing factor is the PSD of the BFS blend, and providing insight into the contribution of the GGBS component to the reaction of the blended cement. Numerous studies have shown that enhanced clinker hydration can be achieved by blending filler materials into cement systems, and the particle size of the filler has a significant impact on the rate of reaction, commonly referred to as the 'filler effect' [114-116]. The cement system considered here has a very high volume fraction of PC replacement by slag, and therefore the limited early-age reactivity of the BFS component of the blend (particularly the coarse Calumite particles) causes such an effect, allowing extra space for hydration of the clinker phase, and is conducive to enhanced nucleation.

Although the BFS fraction can contribute to the filler effect here, it is also common to overlook the reactivity of the filler itself [115]. Due to the chemical effect seen when reducing the GGBS content, a series of filler tests with the Calumite replaced by quartz were carried out to investigate what, if anything, the Calumite is actually contributing to the reaction process. The quartz was ground down and sieved into fractions, which were then re-combined to replicate the measured particle size distribution of the Calumite. The samples were analysed by isothermal calorimetry, and the data collected (Figure 6.9) show a very similar result to the original GGBS:Calumite blends including the formation of peaks within the first 20 hours.

Figure 6.10 shows a comparison between the temperature profile of the P72 grout, and its quartz-substituted equivalent (Q72). When the results are compared, the Calumite blend has a very similar (if not practically identical) heat of hydration to the 'inert' quartz. Quartz has been used as an inert replacement during many studies reported in literature and was therefore assumed to contribute very little to the early hydration reaction [111, 116-118]. By the replacement of Calumite with the inert filler, it is evident that there is very little impact on the cement hydration reaction curve, which confirms the minimal contribution of Calumite to the reaction process over the first 24 hours.

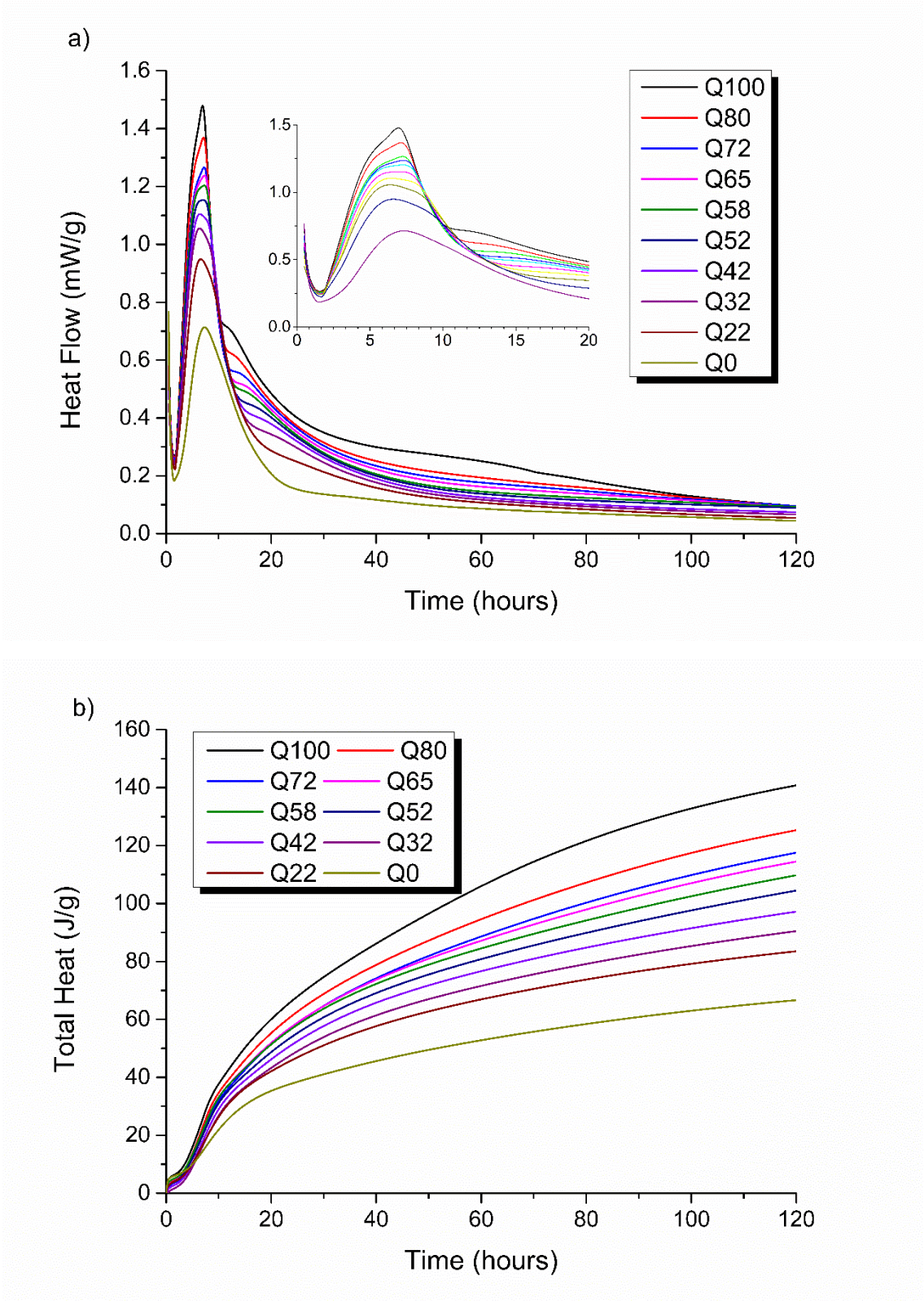

Figure 6.9. Isothermal calorimetry (a) and total heat evolution (b) curves measured at 25 ˚C for 120 hours for the ten GGBS:quartz blend ratios (Table 3.4), at 0.35 = w/s.

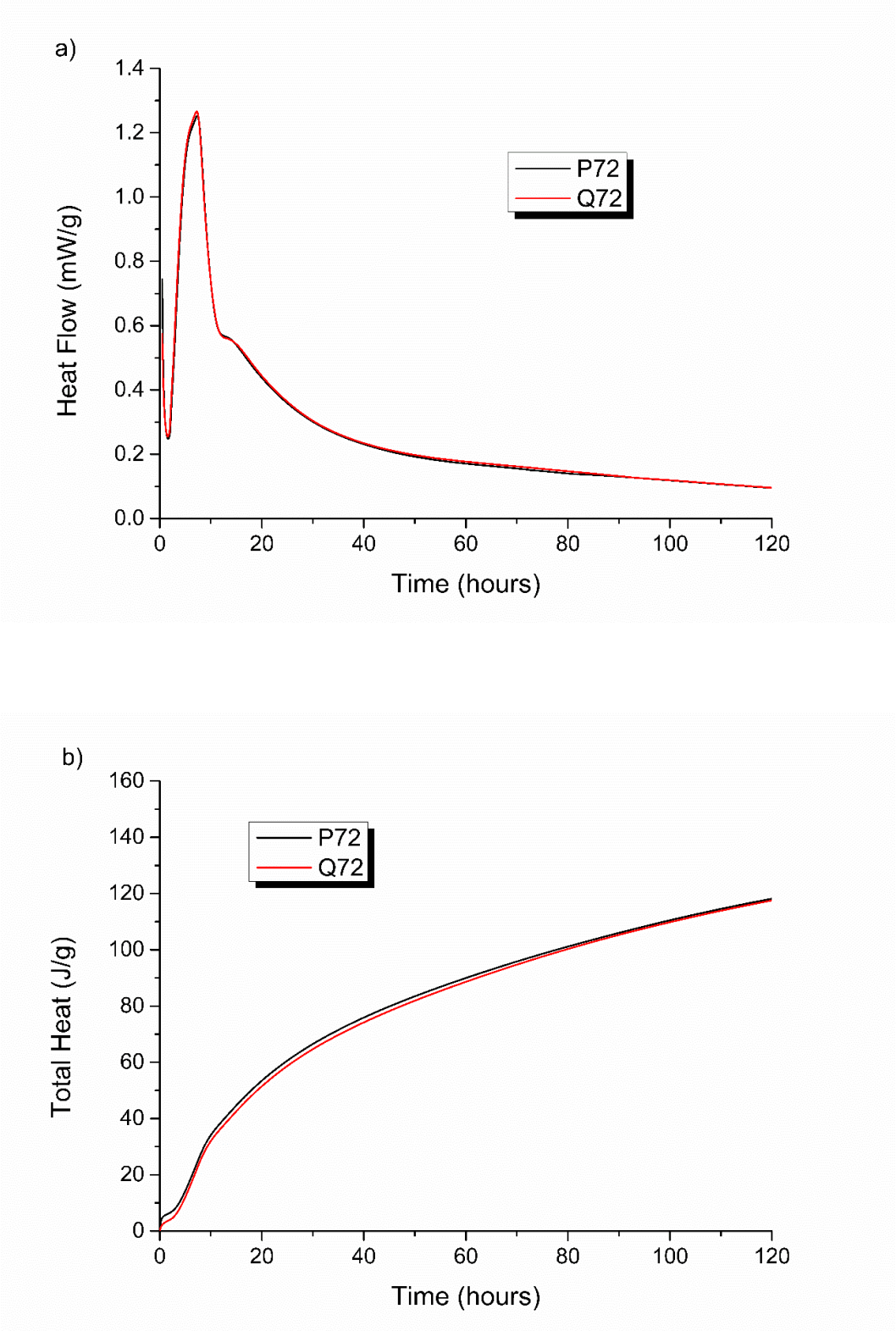

Figure 6.10. Isothermal calorimetry (a) and total heat evolution (b) curves for the Q72 GGBS:Quartz and P72 GGBS:Calumite blend measured at 25 ˚C for 120, hours at w/s = 0.35.

To further understand the Calumite contribution to the hydration reaction, Figure 6.11 illustrates the direct comparison of the P0 and Q0 blends, i.e. the blend where all the BFS

is Calumite, and where it is replaced wholly by quartz. There is a little change in the heat output observed where the P0 system is slightly greater, but not a significant amount. It can therefore be assumed that the Portland cement present in the matrix is responsible for the majority of the recorded heat output.

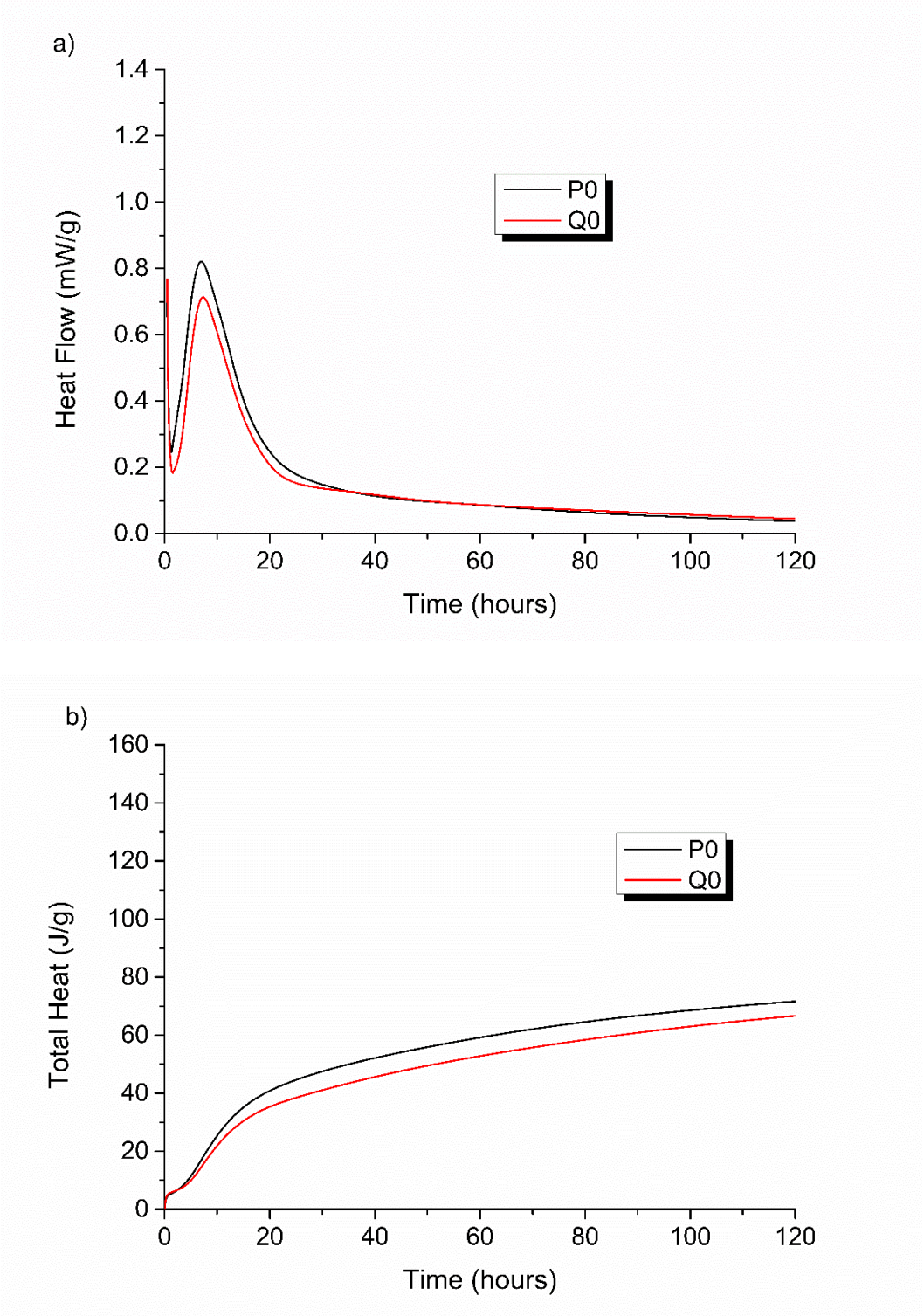

Figure 6.11. Isothermal calorimetric data for the P0 and Q0 systems measured at 25 ˚C for 120 hours, at w/s = 0.35. (a) differential curves, (b) cumulative curves.

To give an indication of how much the GGBS is reacting, under the assumption that the Calumite contributes very little at this early stage, the data for P0 was subtracted from the corresponding data for the P100 system [119-121]. Figure 6.12 shows the resultant heat evolution profiles, which can be identified as the contribution of the GGBS to the reaction process, at each of the three experimental temperatures.

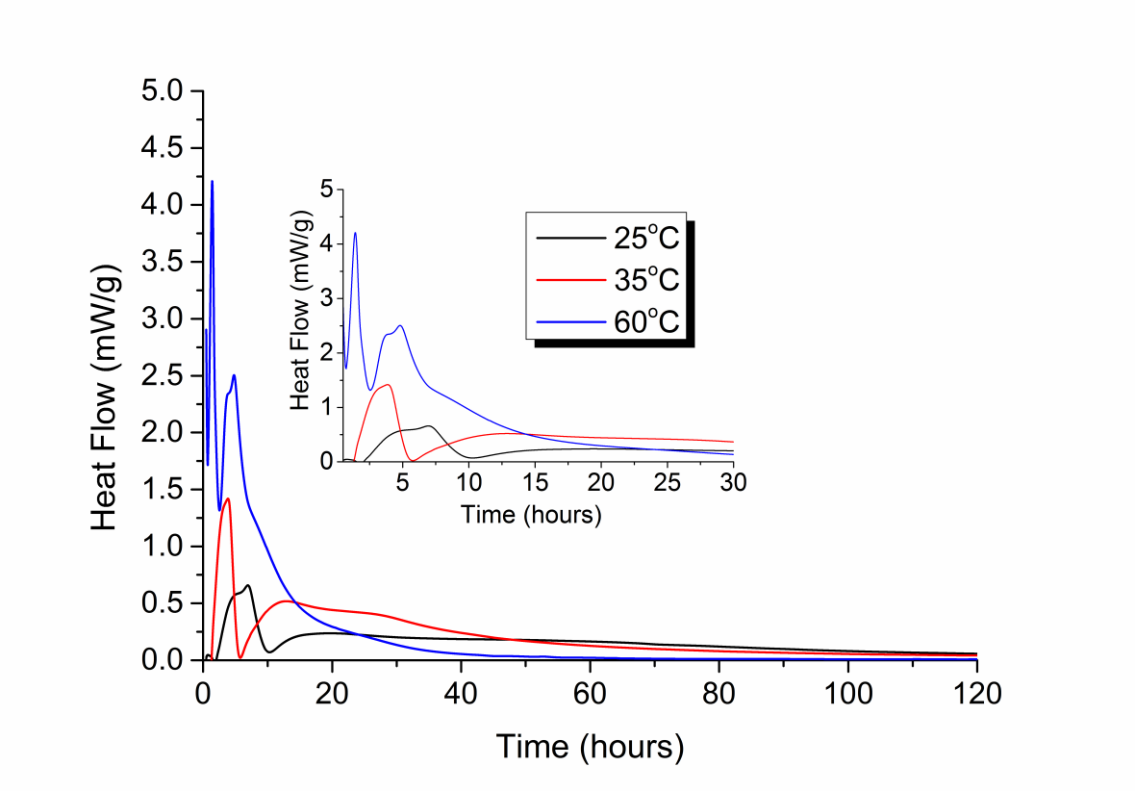

Figure 6.12. Isothermal calorimetry difference curves (where data for P0 are subtracted from data for P100), measured at 25 ˚C, 35 ˚C and 60 ˚C for 120 hours, at w/s = 0.35.

These results show that in addition to the filler effect contribution and the increase in nucleation sites, the fine GGBS fraction is also altering the rate of reaction. The GGBS contributed significantly to the heat of hydration at all three temperatures. There is also a shift in the time at which the peak heat evolution (i.e. the most rapid period of reaction of the GGBS) occurs between the different experimental temperatures; this lengthens with decreasing temperature. This agrees with previous studies that show a similar pattern when different experimental temperatures are used during isothermal calorimetry [29, 122].

The peak in the heat evolution which is attributed to the GGBS contribution also changes in intensity between the P100 and P0 systems, and thus it is also possible that there is a difference in activation energies between the GGBS and the Calumite. This means that

the increased temperature accelerates the reaction to different extents for each material and contributes to the variation in peak heat evolution. The hydration of the Calumite is slower than that of the GGBS, and therefore requires more clinker to drive the reaction [32]. It is reported that the substitution of Portland cement with GGBS at varying increments affects the activation energy [123]. The overall activation energy of the P0 system is defined by the Portland cement, as the Calumite contribution is minimal and reacts only to a limited extent at early age, whereas the GGBS-containing system shows contributions from both BFS and PC components.

The total heat output from both GGBS:Calumite systems can be seen in Figure 6.13 for all three temperatures. By comparison of the P100 blend with P0, is it clear that the GGBS system generates a cumulative heat output approximately double that of the Calumite mix during the first 120 hours. Again, this can be expected due to the increased reactivity caused by a higher surface area within the slag powder, therefore providing more nucleation sites for the hydration of clinker phases [115]. For the P0 blend, the 35°C sample also starts to generate more heat than the 60 ˚C sample at around 40 hours. The likely reason for this is due to the slow reaction rate of the Calumite. At a higher temperature of 60 ˚C, the PC reacts too quickly and does not allow enough time for portlandite generation to activate the Calumite before the material stiffens, particle surfaces are blocked by hydration products, and mass transport becomes very hindered, which causes the Calumite reaction to be even slower than would otherwise be the case. Conversely, 35 ˚C gives better control for the Calumite:PC system, allowing increased energy for the reaction to occur but on a longer timescale, which in turn allows the Calumite to contribute to the reaction, causing a higher overall total heat output.

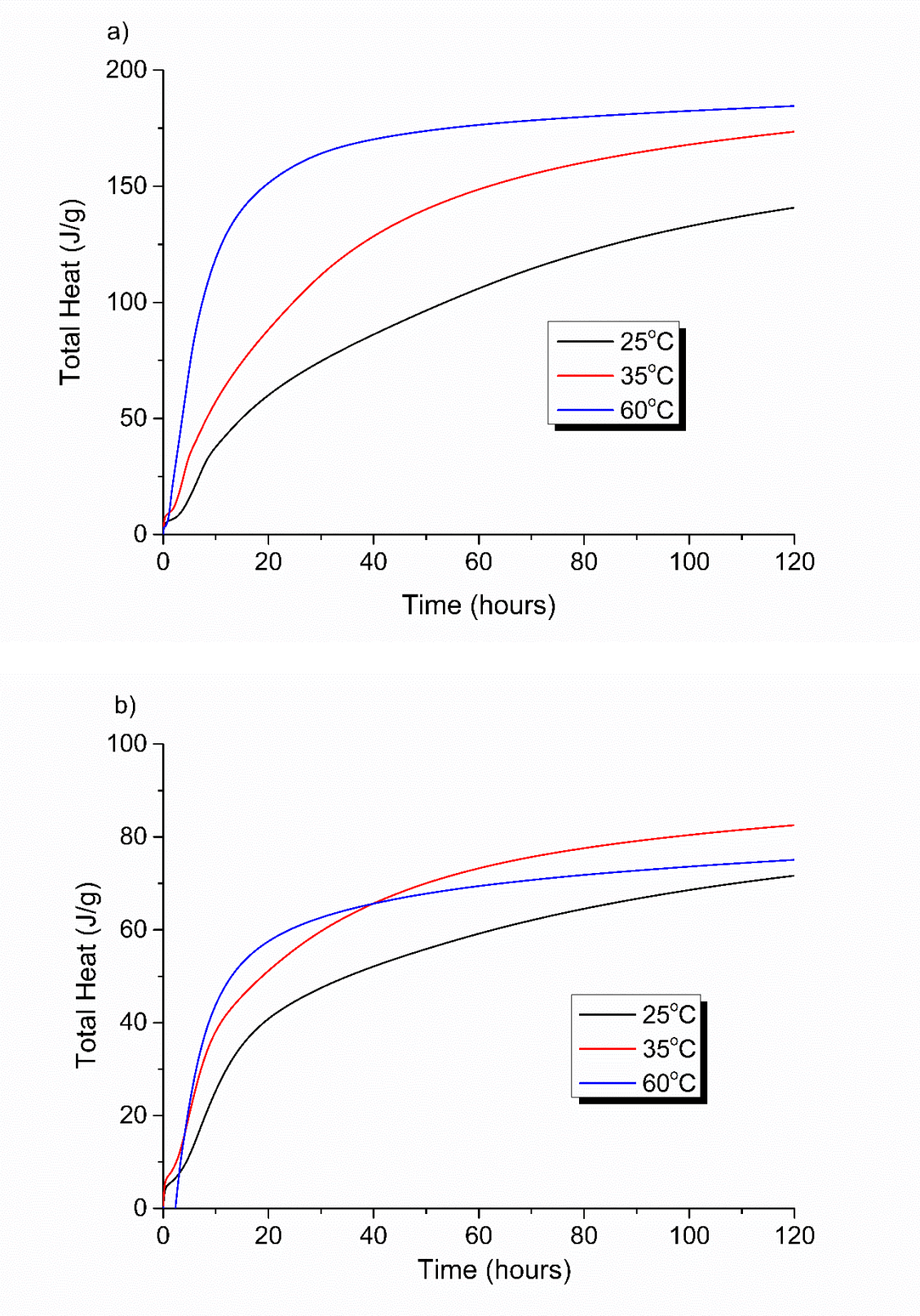

Figure 6.13. Cumulative heat evolution curves for the mix P100 (a) and P0 (b) measured at 25 ˚C, 35 ˚C and 60 ˚C for 120 hours, at w/s = 0.35.

Within the Sellafield Ltd. specification, a low total heat evolution is one of the main criteria required by the nuclear industry when considering different grout formulations. Although (as previously mentioned) the European Standard states a value of 270 J/g, the Sellafield Ltd. specification requires that the grout should not have a cumulative heat output greater than 180 kJ per kg of blended cement powder after 24 hours of hydration at 35 ˚C. Therefore, this is what the cement systems under investigation in this study have to conform to. All of the cement systems investigated during this work conform to this specification, even at the increased temperature of 60 ˚C.

6.2.3 Semi-adiabatic Calorimetry

The semi-adiabatic calorimetry data (Figure 6.14) illustrate a more representative temperature profile of the cement grouts compared to small samples held under strict isothermal conditions (Figure 6.2). The flasks used in these experiments are moderately well-insulated and although the exact temperature rise for a larger sample is not captured, it does provide a closer representation of how the materials would perform within a full-scale wasteform. These results show a different trend from the data obtained through isothermal calorimetry; there was more variation in the maximum heat of reaction peak obtained for the combination mixes. Therefore, there was not a fully consistent trend in maximum peak temperature observed with respect to the GGBS content. A similar result was observed at all three w/s ratios (0.33, 0.35 and 0.37).

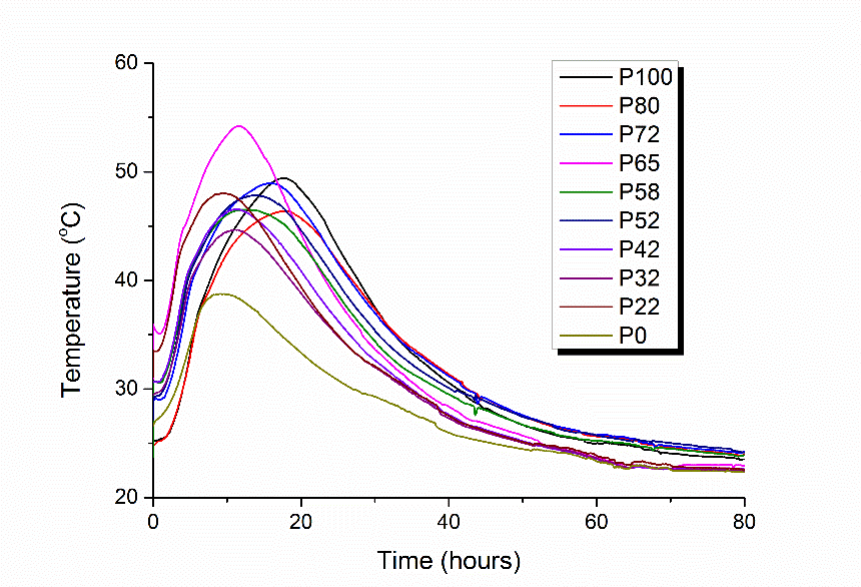

Figure 6.14. Semi adiabatic calorimetry curves for the ten GGBS:Calumite blend ratios measured at room temperature for 80 hrs, at w/s = 0.35.

The initial temperature rise observed in the semi-adiabatic calorimetry for each of the ten blends was recorded, as shown in Table 6.1. Some of the blends fall out of trend at all three w/s ratios, with a peak temperature higher than would be expected. This suggests that at each of those blends, the mix ratio may have a more optimal PSD for reaction. The wider PSD introduced by blending the GGBS and Calumite has created more space for hydrates of the clinker phase to form, which has enhanced the reaction causing a higher temperature, comparable to the 'filler effect' [112]. However, a greater amount of finer GGBS is required to maintain the reactivity of the system and induce nucleation on the larger surface area of the fine particles. The lack of fine particles in the P0 (0:100 GGBS:Calumite) blend results in fewer nucleation sites producing a lower peak heat. These results highlight the importance of reaching the optimum blend of GGBS:Calumite, but also ensuring that the correct w/s ratio is used in order to achieve the required heat output and fluidity specifications.

Table 6.1. Initial temperature rise observed in semi-adiabatic calorimetry for the ten GGBS:Calumite blends at three w/s ratios.

GGBS:Calumite Wt. ratio	0.33 w/s ratio (˚C)	0.35 w/s ratio (˚C)	0.37 w/s ratio (˚C)
P100	31.1	28.5	25.2
P80	27.1	24.7	21.9
P72	24.6	27.3	26.0
P65	29.5	31.8	24.9
P58	24.9	24.7	22.1
P52	24.4	26.2	20.7
P42	24.2	24.1	23.5
P32	23.2	21.4	19.7
P22	23.7	24.7	19.6
P0	16.4	15.5	18.7

If the three w/s ratios are compared against one another, the results show that the highest w/s ratio (0.37) generally has a lower peak temperature compared to the lower two w/s ratios. However, the P0 blend does not follow the observation; in this case, the 0.37 w/s has a higher peak temperature of 18.7 ˚C. It has been well reported and

discussed that the rate determining step in the acceleration period is the growth of C-S-H as reviewed by Scrivener *et al.* [112]. Due to the low surface area of the Calumite there is an increase in the water/PC ratio and seemingly results in faster hydration of PC, enhancing the growth of C-S-H. This potentially means that more portlandite is produced to react with the BFS, causing a higher peak heat temperature in the P0 blend at a 0.37 w/s ratio.

During the isothermal calorimetry tests, changing the w/s ratio did not affect the general behaviour of the results significantly and produced very similar trends in the data across the three ratios. Throughout the semi-adiabatic experiments there is less consistency in temperature rise as a function of w/s, suggesting that the w/s ratio has more influence on the heat evolution of the cement grouts. The semi-adiabatic method is more representative of plant conditions where a significant temperature rise is expected in the 500 L waste drums, and therefore, may be a more indicative method of testing the cement grouts, as there are differences in the activation energies of the cement and slag which change their relative reactivities as a function of reaction temperature [104]. However, both calorimetry methods do show similar results across the different w/s ratios, which suggest that for this BFS:PC system, the water content can be considered an insignificant contributing factor for temperature rise.

6.2.4 Comparison of Calorimetric Methods

The results of the two calorimetric methods were analysed in order to compare a series of characteristics of the techniques and determine the relationship between them. The relationships compared were the semi-adiabatic temperature rise against different parameters from the isothermal calorimetry tests: the isothermal total heat evolution at 24 hours, the isothermal peak heat flow, and the slope of the isothermal peak (i.e. the rate). The isothermal rate was also compared to the slope (i.e. rate) of the semi-adiabatic peak.

The comparison between the rates of both calorimetry methods produced rather a poor correlation, as shown in Figure 6.15. It is clear from the wide scatter of data points that the rates of the two techniques do not correlate well. It may be expected, due to the similarities between the chemical processes which drive both the temperature and heat flow profiles, which these two measures of the rate of reaction would form a close correlation, but this does not seem to be the case here. These differences are likely to be caused because the semi-adiabatic method considers the thermal capacity of the hydration reaction. As shown previously, the blends containing higher GGBS content

exhibit a higher reactivity and therefore a higher temperature which drives the reaction at a different hydration rate between the two methods.

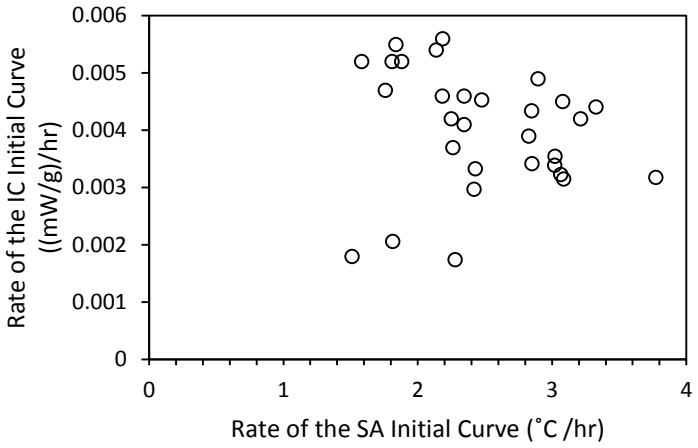

Figure 6.15. Relationship between the rate of the semi-adiabatic temperature curve and the rate of the isothermal heat flow curve measured for all of the formulations in Table 3.4.

However, the peak heat flow values for these blends measured using isothermal calorimetry do show a very good correlation to the initial semi-adiabatic temperature rise, shown in Figure 6.16. Here the maximum values obtained through both test methods are compared, and show a clear link to one another. This is a positive outcome for the reliability of the isothermal test method, regarding its use as a potential standard technique for measuring the heat evolution of cementitious material, and which requires significantly smaller volumes of material (and much less labour-intensive calibration protocols) than the semi-adiabatic calorimetry tests.

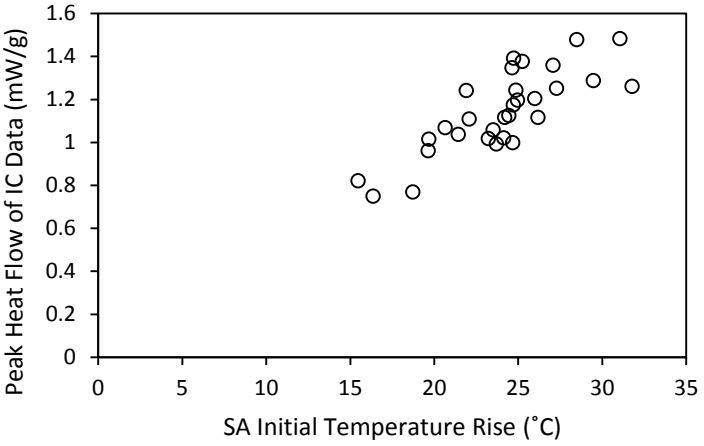

Figure 6.16. Correlation of the initial temperature rise in the semi-adiabatic calorimetry tests and the peak heat flow from the isothermal calorimetry tests of all of the mixes from Table 3.4.

Both sets of calorimetry results show that the main hydration peak of the reaction occurs within the first 24 hours of the test, consistent with widely reported data for Portland cement [30], and indicating that the early stages of reaction are dominated by cement hydration, with the slag only beginning to react during this timeframe once sufficient portlandite has been generated. However, at higher temperatures the slag contribution increases as shown in the data in Figure 6.16. The Sellafield Ltd. specification requires that the grout should not have a cumulative heat output greater than 180 kJ per kg of blended cement powder after 24 hours at 35 ˚C [124]. Therefore, the final correlation discussed in this chapter is shown in Figure 6.17, and describes the relationship between the total heat evolution of the isothermal calorimetry curve at 24 hours, and the initial temperature rise in the semi-adiabatic calorimetry data.

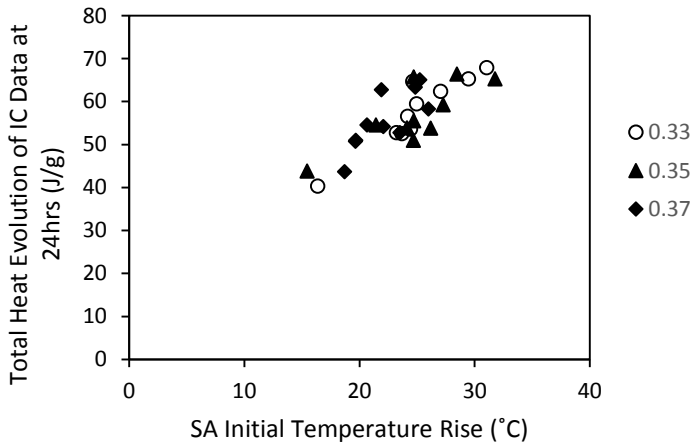

Figure 6.17. Relationship between the initial temperature rise in the semi-adiabatic calorimetry tests and the total heat evolution of the isothermal calorimetry data at 24 hrs, for all of the mixes in Table 3.4.

The correlation within this plot is quite close to linear suggesting a close relationship between the data sets, without any systematic error due to differences in the w/s ratios. This agrees with reported literature that investigate and compare the two methods [125]. From Figure 6.17, it may be noted that although the isothermal calorimetry testing used here was not carried out at 35 ˚C, all of the cement grouts produced in this study should conform appropriately to this aspect of the Sellafield Ltd. specification.

By comparing a series of characteristics of the two methods it was possible to determine how comparable the results of the two calorimetric techniques. The observations obtained during the comparison highlighted that the main difference between the two

techniques is that the semi-adiabatic method accounts of the thermal capacity and heat loss of the cement system and as such affects the rate of slag hydration [126]. Although this is possible more representative of practical situations, the minimal change in temperature maintained during isothermal conduction calorimetry provides a better understanding of the kinetics of the cement system [127]. Similarly to reported literature, the results in this section illustrate that the time taken to reach the peak heat is longer in semi-adiabatic calorimetry compared to the isothermal conduction calorimetry. Overall, there is a positive correlation between the two techniques, which confirms the ability to use isothermal calorimetry as a standard method to measure the heat of hydration of cementitious materials. This is in agreement with comparisons previously reported in literature [73, 125, 128]. However, there is significant potential practical advantages for the use of isothermal calorimetry over semi-adiabatic calorimetry regarding the sample size and instrument stability during measurement.

6.2.5 X-ray Diffraction

The X-ray diffraction patterns for hardened samples of the 10 blend formulations (stated in Table 3.4) cured for 28 days are shown in Figure 6.18. The main observation is that the diffuse scattering at around 30˚ 2θ degrees associated with the glassy fraction of GGBS becomes less prominent as the GGBS content decreases. It is clear the portlandite peak at about 34˚ 2θ grows more prominent as the GGBS content increases. This is caused by the increase in reaction, resulting in a greater consumption of portlandite during slag hydration. The peak at around 12˚ 2θ also becomes more prominent as the GGBS content increases due to increased slag hydration, which reflects the minimal contribution from the Calumite fraction to the reaction. The peak is attributed to both monocarbonate and hydrotalcite. This agrees with literature where the former is observed in Portlandite systems and the latter is predicted to form as the BFS content increases [115, 129]. More phases including alite and belite were observed in the P100 system compared to the P0 blend, confirming, that at this stage, the hydration reaction is affected more as the GGBS content increases.

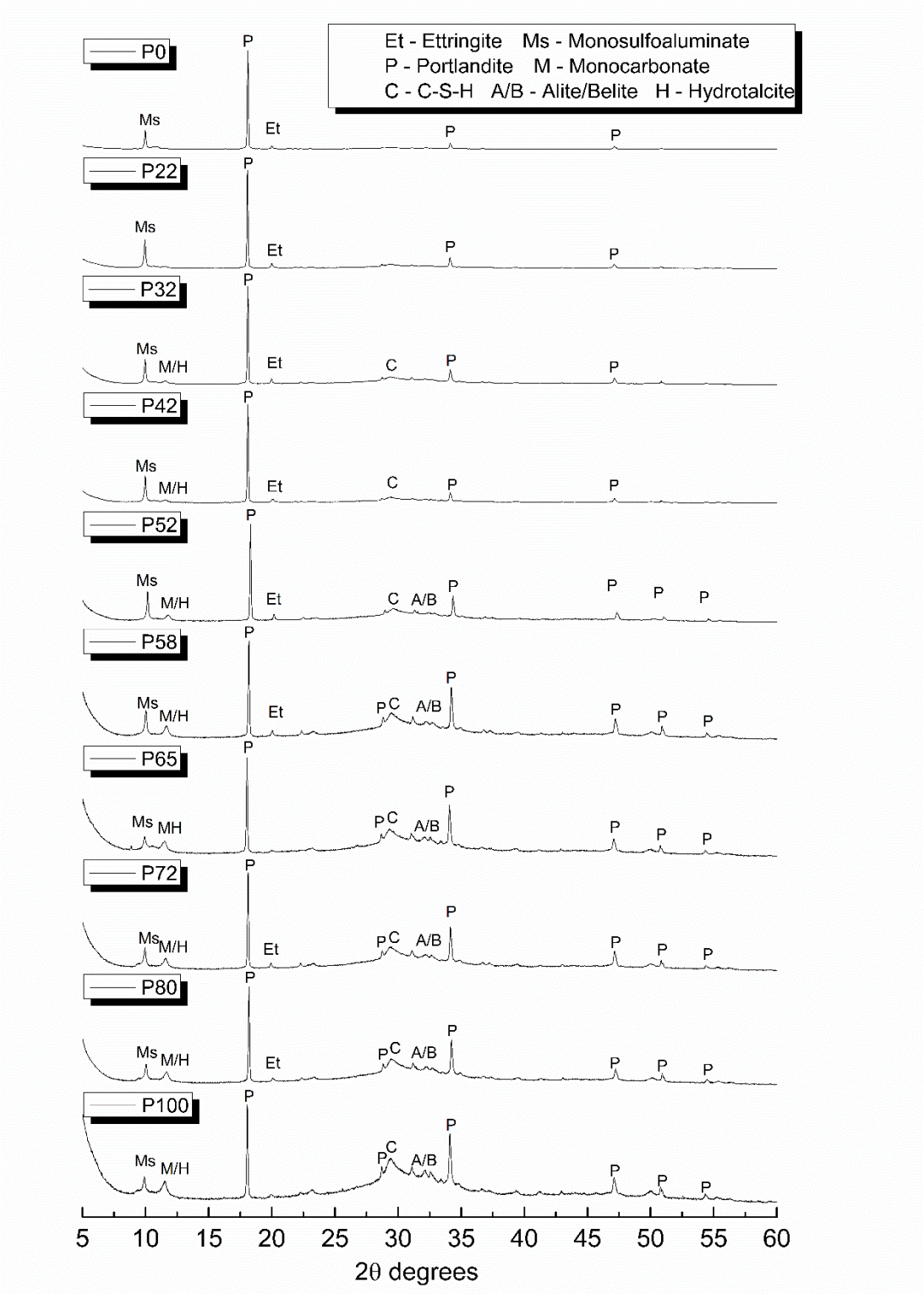

Figure 6.18. X-ray diffraction patterns of the 10 BFS:PC systems measured at 25 ˚C using isothermal conduction calorimetry, where the BFS fraction comprises the blends stated in Table 3.4, after 28 days of curing.

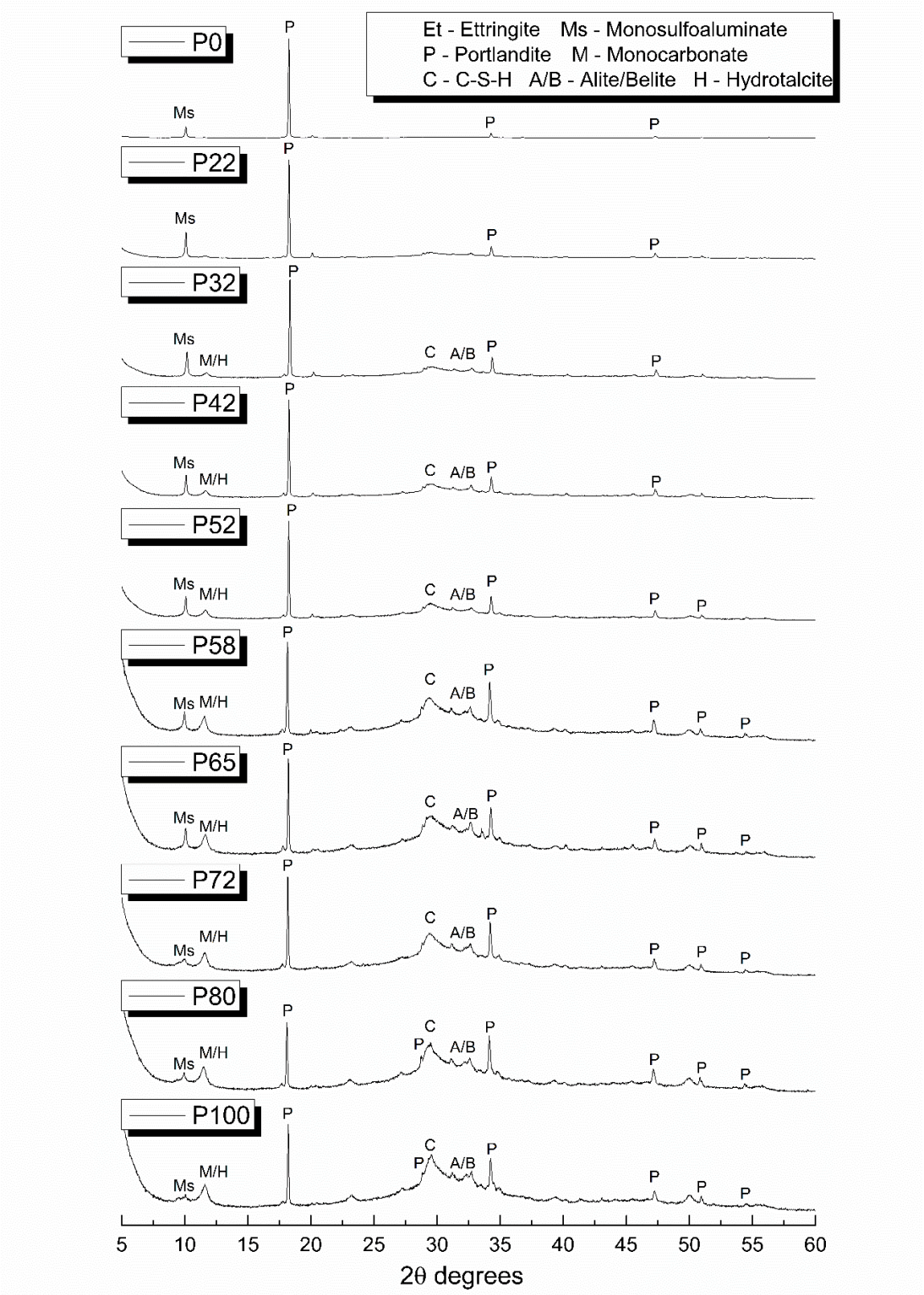

Figure 6.19. X-ray diffraction patterns of the 10 BFS:PC isothermal conduction calorimetry samples that were measured at 60 ˚C, where the BFS fraction comprises the blends stated in Table 3.4, after 28 days of curing.

The results shown in Figure 6.18 are for samples cured at 25 ˚C. The same analysis was carried out on the samples cured at 35 and 60 ˚C after extraction from the isothermal calorimeter. Very similar XRD patterns were observed at the elevated temperatures

(60 ˚C data shown in Figure 6.19 and the 35 ˚C data included in Appendix C), whereby the same phase assemblage was observed and again becomes less prominent as the GGBS content decreases. However, unlike the 25 ˚C data where the amorphous hump is not seen after the P52 system, the phases are still observed in the P32 sample. This validates the data observed during the isothermal calorimetry tests, where at 60 ˚C the hydration reaction is increased, suggesting that more of the BFS fraction is contributing. XRD data was also collected for semi-adiabatic calorimetry samples (Appendix C) and again, the results look very similar to those obtained for the isothermal conduction calorimetry samples.

6.3 Conclusions

This chapter has illustrated that changing the particle size distribution of the blast furnace slag in blended cement systems containing both coarse and fine slag fractions significantly affects the heat output from the cement during hardening. The hydration rate of the BFS:PC system is affected by a change in the GGBS:Calumite blend ratio, and therefore confirms that changing the PSD has a chemical effect on the cement grout. As the GGBS content increases, the rate of hydration is accelerated. The hydration reaction is also affected by elevated temperatures, whereby the peak heat of the reaction occurs much more rapidly as the temperature increases. The two extremes of the fine:coarse (GGBS:Calumite) blends were explored, and shown to behave differently at elevated temperatures. All of the cements considered, even at elevated temperatures, conform to the total heat evolution restrictions of the UK specifications and could therefore potentially be used for encapsulation according to this criterion.

Quartz substitution isothermal calorimetry provided a method of comparing the contribution of both BFS fractions. When the quartz substituted formulations were compared to the original cement pastes, the results illustrated that the systems behaved very similar to one another. This suggests that by replacement of the Calumite with an inert filler, there is very little impact on the hydration reaction, confirming very minimal contribution of the Calumite to the overall process. It was possible to calculate the contribution of the GGBS by subtracting the P0 data from the P100 system, which showed that the fine GGBS fraction alters the rate of reaction and contributes significantly to the heat of hydration at all three temperatures.

The semi-adiabatic calorimetry results provide good temperature profiles, and give an indication of how the cement paste would perform within the wasteform. However, some of the results are inconsistent, and the required sample volumes are large in

comparison to the isothermal calorimetry. In general, as the w/s content increases the temperature rise decreases with the exception of the P0 blend at 0.37 w/s. This is due to the low surface area of the Calumite resulting in faster hydration of the PC, enhancing the growth of C-S-H and therefore increases portlandite production causing a higher peak heat temperature. The isothermal calorimetry provides a much more apparently reliable set of results using a method that is sensible and much more straightforward to standardise once a suitable instrument is purchased.

By comparing a series of characteristics of the semi-adiabatic and isothermal calorimetry methods, it was possible to determine comparisons between the results of the two calorimetric techniques. Overall, there is a positive correlation between the two techniques, which supports confidence in the use of isothermal calorimetry as a future standard method to measure the heat of hydration of cementitious materials for the nuclear industry.

7 Tomography and Radiography Experiments

7.1 Introduction

A significant amount of research and development has been invested into cement grout used for nuclear waste encapsulation. Specifically, the optimum chemical and physical properties of the material needed for successful encapsulation have been discussed and refined. Although the compressive strength and dimensional stability test methods do monitor the characteristics of hardened cement, there are minimal data that describe what actually happens within hardened wasteforms. One way to understand the success of the encapsulation process is to produce a wasteform containing simulant waste and then cut the product open to visualise the middle of the sample [130, 131]. However, this method is very intrusive and could affect the structural integrity of the sample, and could result in certain aspects being overlooked if only a single slice is taken through a large 3-dimensional wasteform.

Therefore, in order to directly investigate what happens during the encapsulation process and once the product has hardened, a series of experiments were performed at the Diamond Light Source (DLS), which is the UK's national synchrotron facility located on the Harwell Science and Innovation Campus. The proposal for this study received 48 hours of beamtime split between in-situ radiography experiments and tomography analysis. The beamline used was the I12 Joint Engineering, Environment and Processing (JEEP) instrument [132], and the experimental setup was in hutch 2, as shown in Figure 7.1.

Figure 7.1. Image of inside of the experimental hutch for the I12 beamline at the Diamond Light Source.

A synchrotron is a circular particle accelerator (in this case electrons), and works on the basis that when electrons change direction they emit energy. The electrons are accelerated through a series of magnets until they almost reach the speed of light, and are then injected into a polygon-shaped "storage ring" with a bending magnet on each corner and insertion devices in the straight sections that repeatedly alter the direction of the electron beam, creating a more focused and intense beam of synchrotron radiation. If the electron is moving fast enough, the energy is released as an intense light in the X-ray region of the electromagnetic spectrum. The resulting X-rays are directed towards a beamline attached to the synchrotron, and in this case provided the X-ray photons for both the radiography and tomography experiments [133].

Radiography is a technique used for imaging the internal structure of an object using a beam of X-rays [134]. The two dimensional image is constructed as the X-rays are absorbed by the material, where the amount of X-ray absorbed depends on the atomic number density within the sample or structure under analysis. Any X-rays that are not absorbed are captured by a detector and the data collected are used to produce an image. The benefit of using the high intensity and energy of the synchrotron beam is that it enables the analysis of larger samples, which is possible due to the large field of view camera.

Up until now, the infill process that occurs during encapsulation of nuclear waste has only been investigated once the product has hardened and the sample is cut open. In this chapter, for the first time, in-situ radiography experiments were performed to observe the infill process of fresh cement grout in real time.

Tomography is also an imaging method that uses a number of 2D projections (or radiographs) taken at different orientations to produce three dimensional images [135-137]. X-ray computed tomography is used to produce non-destructive cross-sections of a sample to enable 3D reconstructions of a sample or structure. The high energy synchrotron X-rays that were used at the Diamond Light Source allow for the penetration of thicker materials with high spatial resolution [138]. Tomography can be used to determine the size of objects, any cracks, voids or other characteristics of a sample. Tomography was used to analyse hardened products of different formulations, containing simulant nuclear waste, to determine how successful the encapsulation process is. The results of this analysis are presented in this chapter.

7.2 Materials

The cement powders under investigation in this project include GGBS and Calumite sourced from Scunthorpe steel works and Portland cement sourced from the Ribblesdale cement works, which have all been supplied by Hanson. These were the powders the nuclear industry were using when this project started [28]. However, during the 4 year experimental programme, the industry have changed to a different powder supply due to economic changes within the UK cement industry. The Calumite sourced from Scunthorpe continued to be the coarse fraction contribution, but the GGBS was sourced from Port Talbot steel works and the Portland cement originated from Ketton [39]. These new powders were also supplied by Hanson Cement, and were tested alongside the Scunthorpe and Ribblesdale powders in this chapter. The replacement GGBS has a very similar chemical composition to the original powder used, and this is also true for the PC substitution, hence why these powders were chosen as suitable alternatives. However, the particle sizes of the powders are slightly coarser, as shown by the PSDs in Figure 7.2.

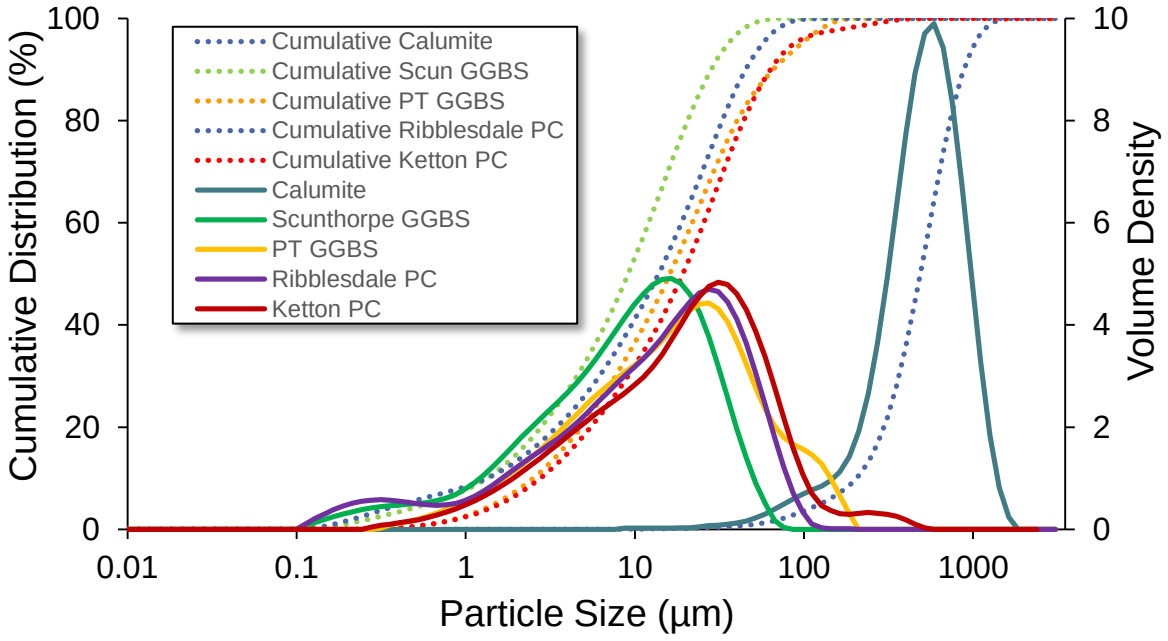

Figure 7.2. Particle size distribution data for Scunthorpe GGBS, Port Talbot GGBS, Ribblesdale PC, Ketton PC and Calumite.

From Figure 7.2, it is clear that the PSD of Port Talbot GGBS is slightly coarser than the Scunthorpe GGBS, this result in slightly more overlap of particles around 100 µm.

One of the aims of this project was to perform larger scale trials on the cement system under investigation, and as such (due to the increased amount of material required) it was not possible to maintain the full mix matrix from Chapter 4 in the experiments presented in this chapter and the mid-scale mixes due to time constraints. Therefore, to reduce the number of mixes and to incorporate the change of powders into the project, a new mix matrix was developed (presented in section 7.3.1.3). The results of the small scale experiments were used to make decisions to reduce the number of mixes of the original Scunthorpe GGBS:Calumite:Ribblesdale PC system. The P72 and P65 blends were considered to be of most interest and were chosen as priority mixes to investigate for these experiments. This is because across the test methods (i.e. mini-slump, rheometry, particle packing, heat of hydration and yield stress measurements) these two blends showed the best performance overall. In addition, as in-situ radiography experiments have not been used to monitor the cement infill process previously, the extremes of the blend (P100 and P0) were explored. This ensured a broader knowledge of the performance of the material during these unusual conditions. Additionally, in

order to capture the effect of the alternative powders, a series of mixes using the new Port Talbot GGBS:Calumite:Ketton PC system were chosen to achieve a rational comparison between the two systems. Finally, a few additional formulations were considered where the two GGBS powders were mixed with each of the PC powders available. Overall, the formulation matrix going forward encompasses the comparison between powder sources, particle size and the water/solids ratio.

7.3 Results and Discussion

7.3.1 In-situ Radiography - Experimental

The radiography experiments were conducted to capture the flow of fresh state cement grout and the infill of simulant nuclear waste. The experimental method mimicked plant operations, whereby the simulant waste was placed in the container and the cement grout was pumped and poured in from above the container. The experimental set-up, from inside the I12 hutch, is shown in Figure 7.3.

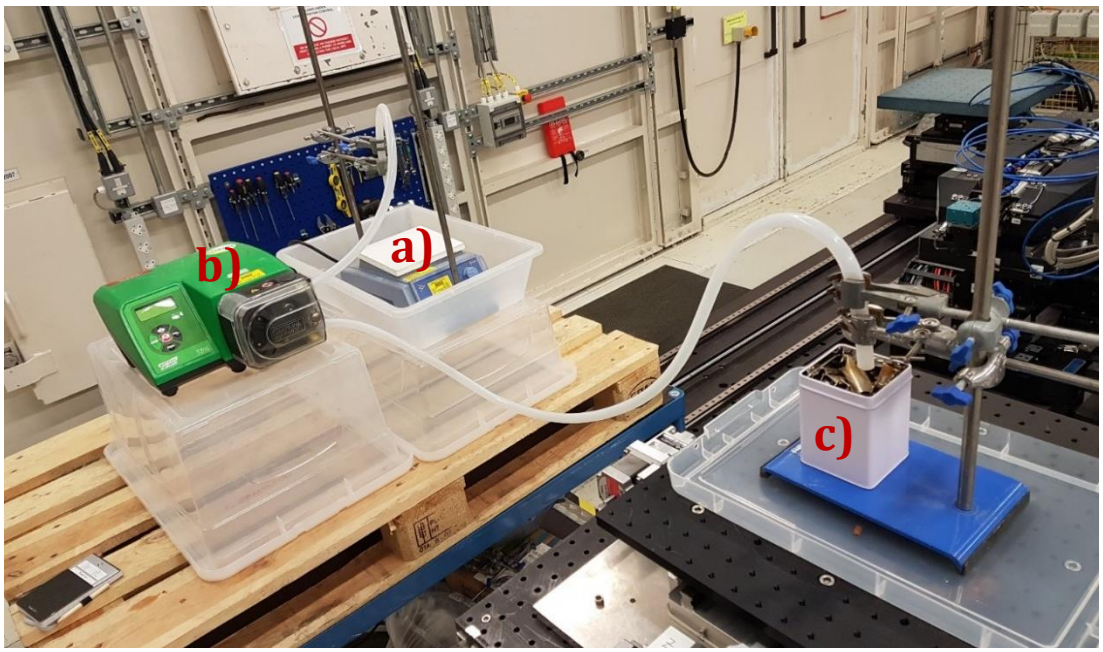

Figure 7.3. Image to illustrate the experimental set-up of the in-situ radiography tests where a) is the location of the cement grout reservoir with magnetic mixer, b) is a peristaltic pump, and c) is the can filled with THORP hulls, to be analysed during filling.

The set-up consisted of three parts which were: a) the source of fresh cement grout, b) a peristaltic pump and c) the sample can for analysis. Fresh grout, mixed in a 1 kg batch, was used for every test and was stirred continuously to maintain agitation throughout

the experiment. Stainless steel tubing (approx. 15 mm in diameter) cut into ca. 50 mm sections, with crimped ends, was used as simulant waste to mimic THORP hulls. The hulls were placed in the sample can prior to the transfer of grout similar to plant operations. The overall set-up was a very close imitation of what occurs on site at a smaller scale, except for the lack of vibration. On plant, the waste filled drums are vibrated to aid the encapsulation process. However, this was not possible as part of this experimental set-up due to the limitations of the sample stage. Following advice from industry experts, simulant Magnox swarf (simulant MEP waste referred to in Chapter 2) was not investigated. The assumption was that the THORP hulls simulant waste would perform better with no vibration, compared with the obscure shape of the Magnox swarf simulant. As such, the THORP simulant would provide more beneficial results considering the short timescale available to perform experiments using the Diamond Light Source facilities.

7.3.1.1 Experimental method

The dry powder components were combined before the addition of water, and were hand mixed for two minutes. The pastes were then subjected to a further 10 minutes of mixing on a Silverson high shear mixer at 5000 rpm to achieve a homogeneous paste. The grout was then transferred from the cement paste reservoir using a Watson Marlow peristaltic pump at flow of 60 mL/min, through the pump and into the sample can. The dimensions of the sample can were; 100 mm (h), 76 mm (w) and 76 mm (d), for each scan the can was positioned in the same place.

7.3.1.2 Scan details

Data were collected using an X-ray beam energy of 124 keV. A large field of view (LFoV) camera was used allowing the analysis of samples of approximately 97 x 25 mm. Two PCO.edge imaging detectors were used with separate optics that view two horizontally adjacent sections of the sample, where there is a small overlap between the two images. The images are processed by aligning them before stitching together using the overlapped region to achieve one large image. A correction is applied by bright field (0.03 s) and dark field (0.2 s) images.

In order to scan the entire can, it was necessary to divide it into sections, as such the sample stage was moved at a speed of 8 mm/s, capturing 6 images on each pass moving down the can. The step of motor movement was 14 mm with an exposure time of 0.2 s per image. The final six images were then stacked and stitched together vertically to achieve a complete image of the sample. The overall temporal resolution for each full can was 25 s and the spatial resolution was 46.9 pixels/mm. This method was repeated

continuously during the infill process, resulting in a series of images capturing the flow of the grout.

7.3.1.3 Mix Matrix

The following 14 formulations were chosen to demonstrate a selection of the blends under investigation. The selection encompasses direct comparisons that will indicate the effect of PSD, powder source and w/s ratio contributions.

Table 7.1. Formulations used in the Radiography experiments containing simulant THORP hulls.

Blend	Powder mix Reference	Powder Source		Water/solids ratio		
		PC	BFS (GGBS:Calumite)	0.33	0.35	0.37
P100	SCR	Ribblesdale	Scunthorpe:Calumite		X	
P80	SCR	Ribblesdale	Scunthorpe:Calumite			
P72	SCR	Ribblesdale	Scunthorpe:Calumite	X	X	X
P65	SCR	Ribblesdale	Scunthorpe:Calumite	X	X	X
P58	SCR	Ribblesdale	Scunthorpe:Calumite			
P52	SCR	Ribblesdale	Scunthorpe:Calumite		X	
P100	PTK	Ketton	Port Talbot:Calumite		X	
P72	PTK	Ketton	Port Talbot:Calumite		X	
P65	PTK	Ketton	Port Talbot:Calumite		X	
P52	PTK	Ketton	Port Talbot:Calumite		X	
P72	SCK	Ketton	Scunthorpe:Calumite		X	
P65	SCK	Ketton	Scunthorpe:Calumite		X	

7.3.2 In-situ Radiography - Results

During the 48 hours of beamtime awarded to this project, only a proportion of the allotted time was designated to radiography experiments. As a result the mix matrix was reduced to 14 formulations that were considered to be of most interest. As part of the experimental setup, it was necessary to set the pump running and exit the hutch before analysis via the beam could begin. As such, trial test runs were conducted (with no beam) to ensure the setup performed correctly. As part of the trial runs, the most and least fluid pastes (P100 and P0, respectively) for the Scunthorpe GGBS:Calumite:Ribblesdale PC blend were tested to monitor their performance whilst it was possible to stay near the equipment. It was discovered that the P0 system had a tendency for the coarser particles to accumulate in the tubing and cause blockages in the setup. Consequently, a total of 14

samples were run during the radiography experiments but it was not possible to measure the P0 system due to the risk of cement paste leakages.

The first system under consideration is the Scunthorpe GGBS:Calumite:Ribblesdale PC blend at a 3:1 BFS:PC ratio and a 0.35 w/s. Figure 7.4 shows samples P65 and P100 following the transfer of cement paste, once the infill is complete.

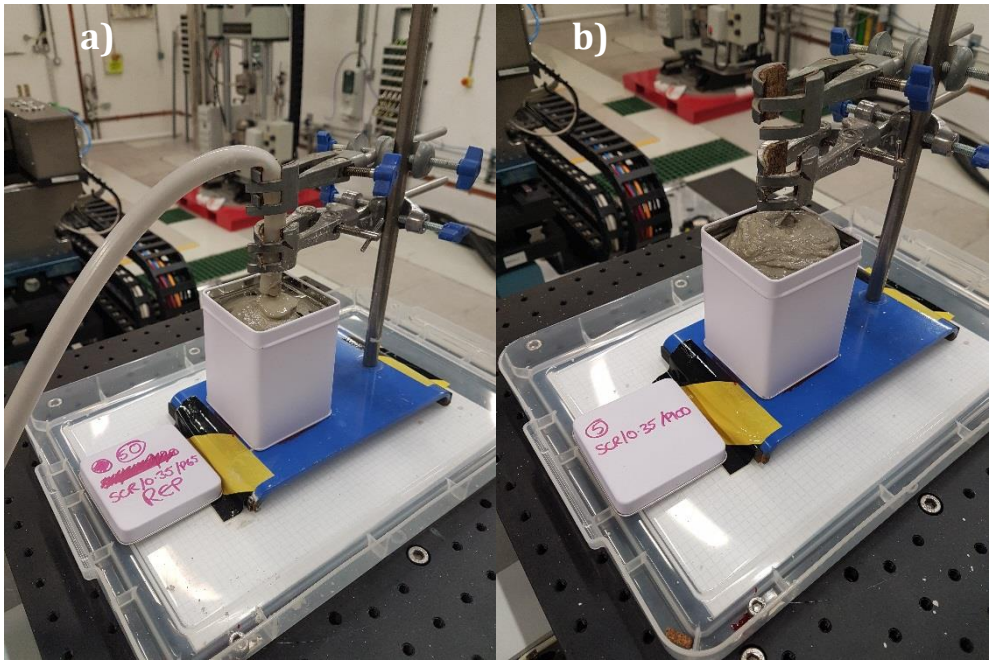

Figure 7.4. Radiography samples at a 3:1 BFS:PC ratio and a 0.35 w/s content following infill: a) P65, and b) P100 GGBS:Calumite blends.

From visual inspection, the cement grout appears to have infilled successfully for both samples (Figure 7.4). However, it is clear that there is more material at the top of the P100 sample can compared to the P65 system, suggesting that a higher THORP hull infill was achieved with the P65 system. This is where the radiography data are essential to understand what is happening inside the container and determine how the cement paste performs.

The infill process of the P65 and P100 systems is presented as a series of images in Figures 7.5 and 7.6. For the P65 system, in the initial image (a), the simulant waste is clearly visible and there is no other material in the container. In the next image (b), the encapsulation process had begun and the cement is demonstrated as a dark mass. As the encapsulation proceeds (images c-h), the cement infills in and around the simulant waste, whilst filling the container. Finally, the last image (i) demonstrates a 'fully encapsulated sample' as shown by dark areas representing cement paste.

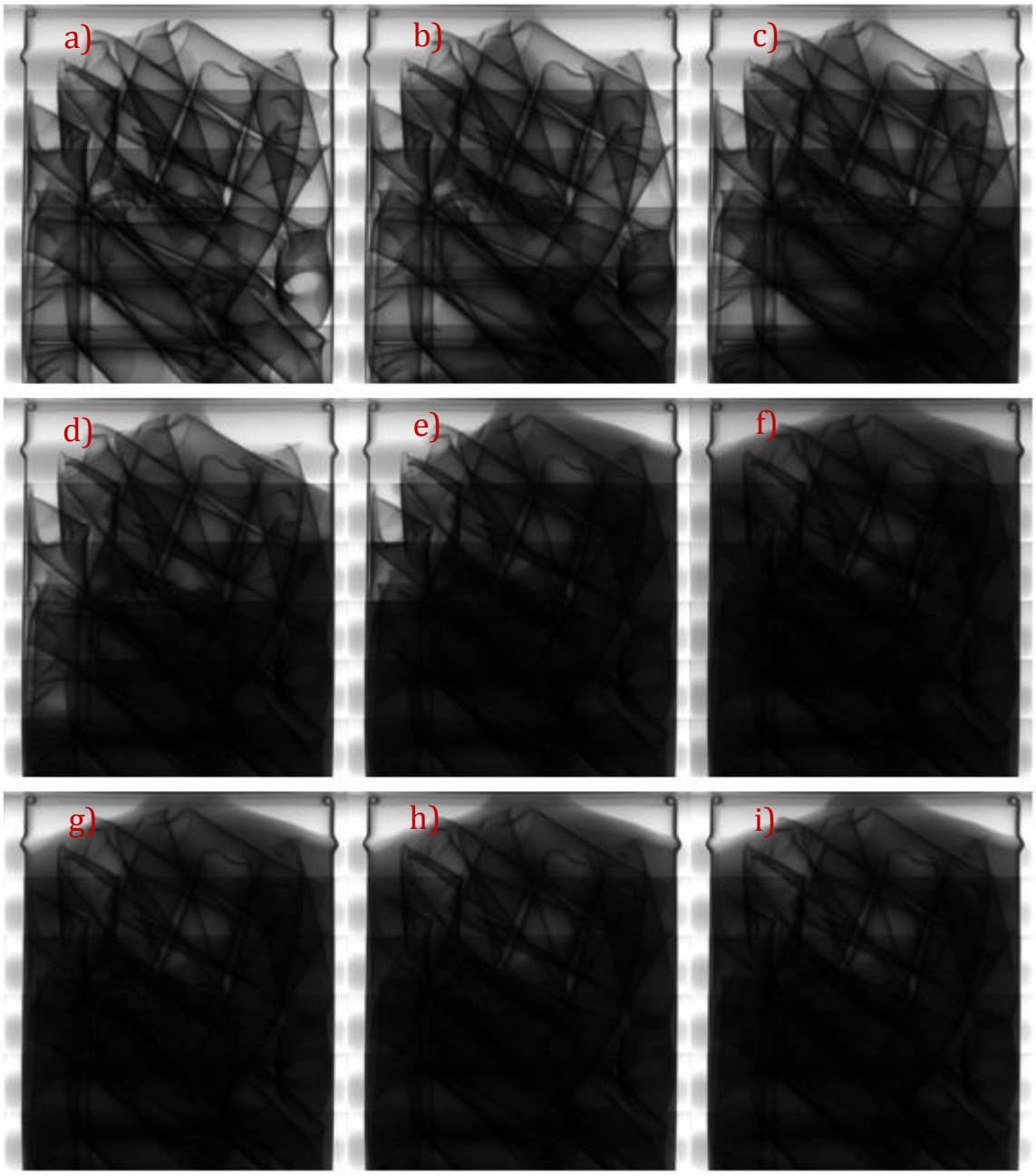

Figure 7.5. Series of radiography sample slices (a-i) of the in-situ infill process for the P65 GGBS:Calumite blend at a 3:1 BFS:PC ratio at a 0.35 w/s content with a timestep of 2.5 mins. (Scunthorpe GGBS, Calumite and Ribblesdale PC)

In Figure 7.5, the images begin to darken from the bottom up, suggesting that the cement paste flows very freely down the can and encapsulates successfully. Full encapsulation is observed fairly quickly and within 5 minutes. The infill process for the P100 system is shown in Figure 7.6, it is clear from the sequence of images (a-i) that the cement paste does not flow freely down the can, and was blocked by the simulant waste. By the final image (30 mins post start), the cement paste was still clearly blocked by the simulant waste, this confirmed that the high surface area of the P100 system results in a material

that is not fluid enough for the encapsulation process. This agrees with data presented in Figure 4.2, where the P100 system achieves the lowest fluidity compared to the P65 blend that produces increased flow. It also demonstrates the effectiveness of this experimental method and that the visual appearance of the samples can be misleading.

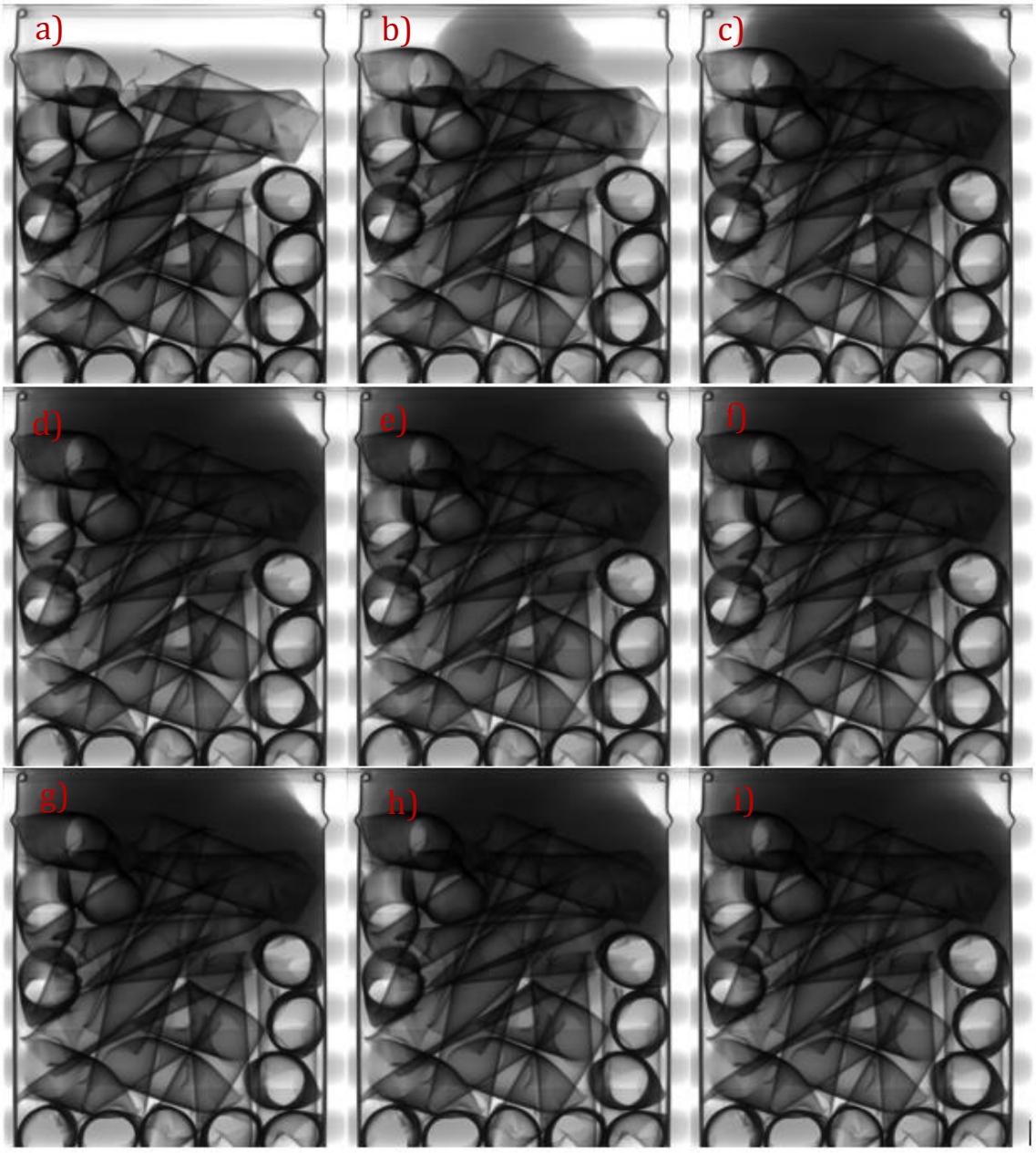

Figure 7.6. Series of radiography sample slices (a-i) of the in-situ infill process for the P100 GGBS:Calumite blend at a 3:1 BFS:PC ratio at a 0.35 w/s content with a timestep of 2.5 mins. (Scunthorpe GGBS, Calumite and Ribblesdale PC)

Trials were also carried out on the P65 system at w/s ratios of 0.33 and 0.37, and a direct comparison can be made to assess the effect of w/s ratio on the flow of cement pastes

during encapsulation. The final image of the trials for each w/s ratio are shown in Figure 7.7.

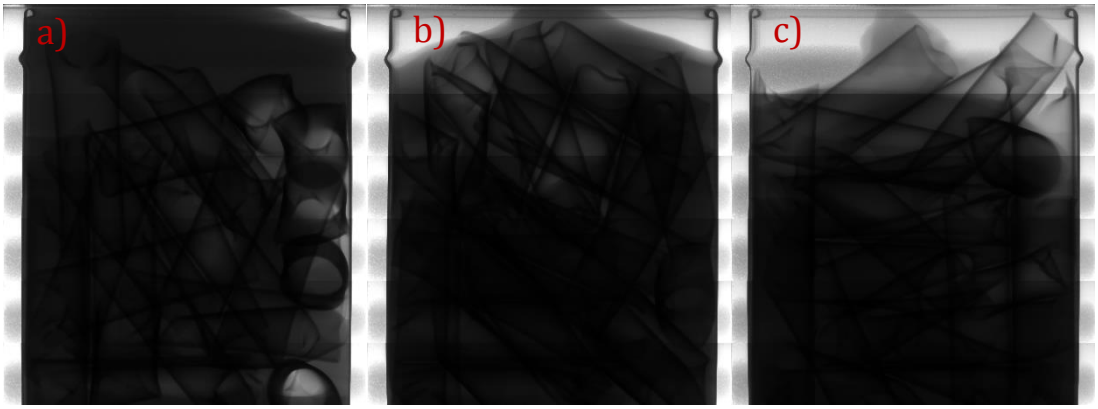

Figure 7.7. Radiography sample slices for the P65 GGBS:Calumite blend at a 3:1 BFS:PC ratio at a) 0.33, b) 0.35 and c) 0.37 w/s content. (Scunthorpe GGBS, Calumite and Ribblesdale PC)

In Figure 7.7, it is clear that all three formulations have infilled the cans to a certain extent. However, the 0.33 w/s sample appears to have gaps that have not infilled successfully along the right hand side of the sample. This is due to the decreased fluidity of the system and confirms with results presented in Figure 4.2. The 0.35 and 0.37 w/s systems show very similar encapsulation but when the series of images are studied in detail, the 0.37 system does encapsulate slightly quicker than the 0.35 equivalent sample. Although, there appears to be less cement grout infilled into the can at a w/s of 0.37, which can be explained by some experimental observations. During the P65 formulation trial at 0.37 w/s content, a small amount of water segregation was observed and the piping was blocked, which forced the trial to be temporarily stopped. The trial was restarted and the data continued to record, however the water segregation meant it was not possible for all of the cement material to be transferred into the sample can. Therefore, while the higher water-to-solids ratio successfully encapsulated the waste, it is unreliable and may cause issues during the encapsulation process at larger scale and on site.

As discussed in section 7.2, these trials incorporated the new powder sources and as such, the Port Talbot GGBS:Calumite:Ketton PC (PTK) system was tested at different GGBS:Calumite blends (Table 7.1) to provide a comparison to the original formulation. The in-situ radiography results for the PTK system are presented in Figure 7.8. The results show successful encapsulation of the simulant waste in a very similar manner to the Scunthorpe/Ribblesdale system.

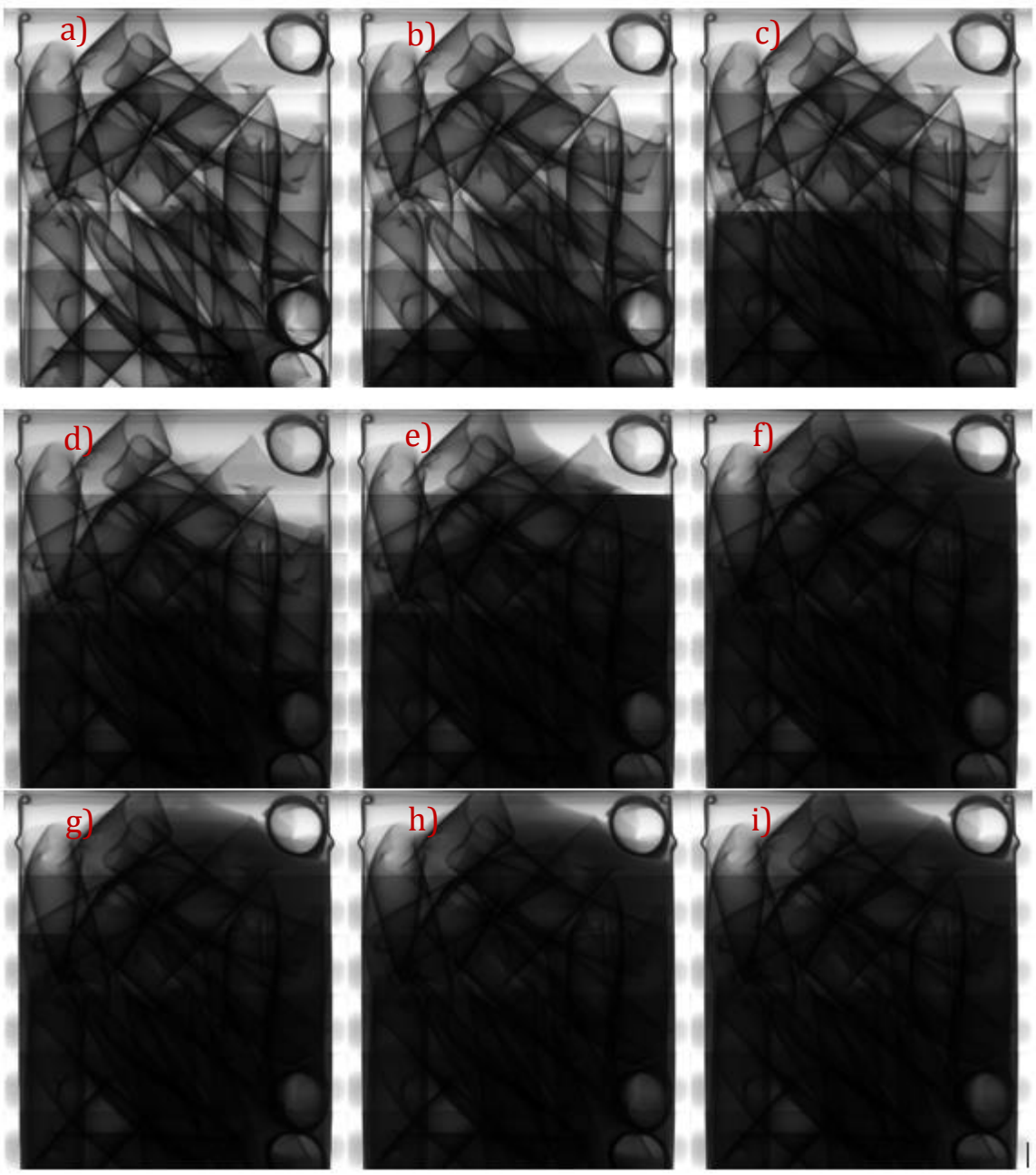

Figure 7.8. Series of radiography sample slices (a-i) of the in-situ infill process for the P100 GGBS:Calumite blend at a 3:1 BFS:PC ratio at a 0.35 w/s content. (Port Talbot GGBS, Calumite and Ketton PC)

The cement paste flows freely down the can and infills from the bottom up. However, an interesting observation obtained from this data was that horizontal hulls do not infill very well compared to the vertically aligned hulls. At the bottom right hand corner of the images, there is a horizontal hull and as the encapsulation occurs it appears that the cement paste does not penetrate the steel tubing. Unfortunately, there is no control over how the simulant waste falls into the waste drum (or can in this case) and this suggests that even with a very fluid system there may be hulls that do not encapsulate fully. On

plant, this is addressed by vibrating the wasteform, but considering that these trials were conducted as static samples the cement pastes have performed extremely well.

In addition to visually inspecting the images produced, it was possible to estimate the voidage for each sample. This was achieved by calculating the volume filled with cement grout and simulant waste (from their weight and density), measuring the empty volume before and finally subtracting both of those values from the total volume of the container used. The effect of water on the voidage of the system is considered by comparing the P72 and P65 Scunthorpe GGBS:Calumite:Ribblesdale PC, shown in Figure 7.9.

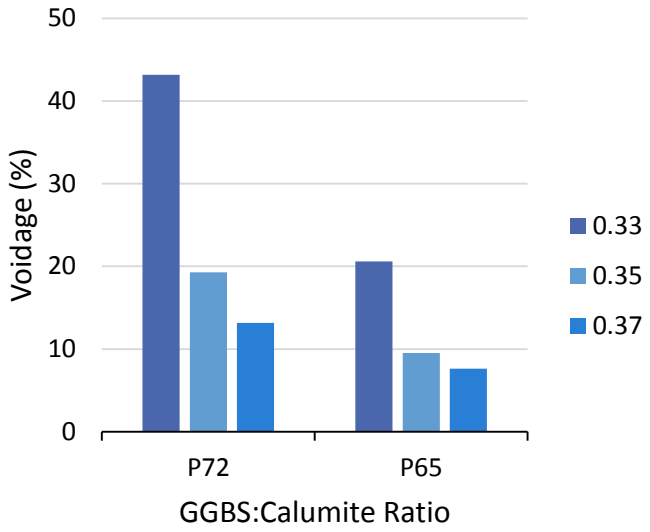

Figure 7.9. Estimated voidage (± 10 vol. %) for the P72 and P65 GGBS:Calumite blends at a 3:1 BFS:PC ratio and a 0.33, 0.35 and 0.37 w/s content. (Scunthorpe GGBS:Calumite: Ribblesdale PC system)

The comparison between w/s contents demonstrates that as the water increases, and therefore increasing fluidity, less voidage was observed. Interestingly, the effect caused by the change in water content was much greater between the lower (0.33) and 0.35 systems, compared to the 0.35 to the higher (0.37) w/s ratio. The 0.33 w/s mix resulted in twice as much voidage compared to the 0.35 w/s system in both the P72 and P65 formulations. This effect was caused by the decreased fluidity. However, the difference between the higher w/s systems (0.35 and 0.37) was not affected to the same extent, but as previously mentioned there were other issues associated with the 0.37 w/s mix. Another observation was made between the P65 and P72 system, where the voidage was almost doubled as the water demand increased. This trend was seen consistently across all three w/s ratios for the P72 and P65 formulations, suggesting that the particle size contribution affected the voidage in the same manner regardless of water content. The

increase of voidage between the P65 to P72 blends validates the decrease in fluidity observed in the mini-slump test results, shown in Figure 4.2.

The effect of particle size and the effect of different powder sources on the voidage of the system was also compared, and is presented in Figure 7.10. When comparing the GGBS:Calumite blends, the P65 appeared to have the lowest voidage, with an increase in voidage either side of that mix. However, it can be stated that as the GGBS content increases, the voidage becomes greater but with no further data below the P52 system this cannot be fully confirmed. Unfortunately, there is no data for the SCK system at a P100 GGBS:Calumite blend but considering the large increase in voidage observed for the SCR or PTK powder systems, it can be assumed that it would also show high voidage.

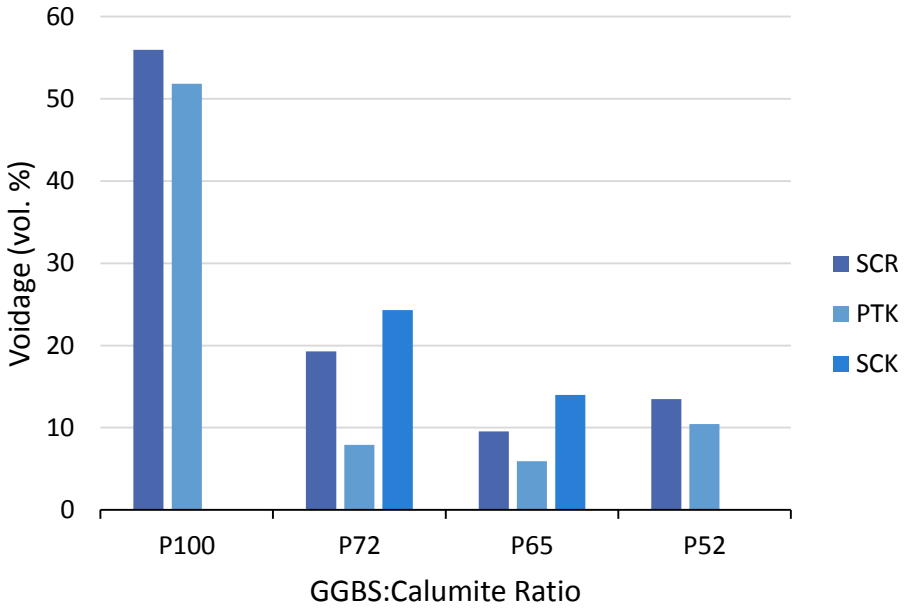

Figure 7.10. Estimated voidage (± 10 vol. %) for varying powder sources at 4 different GGBS:Calumite blends, a 3:1 BFS:PC ratio and a 0.35 w/s content.

The final information to be extracted from these results is the comparison between the powder sources. The PTK system achieved the lowest voidage across all of the GGBS:Calumite blends, suggesting that it has the highest fluidity and would be the preferred material for encapsulation. This is expected following the PSD data presented in Figure 7.2, where the Port Talbot GGBS and Ketton PC have the greater PSD compared to their Scunthorpe and Ribblesdale equivalents, and as such a lower surface area causing increased fluidity due to a decrease in water demand. This increased fluidity is confirmed in Chapter 8 during the mid-scale trials where PTK achieves a higher Colflow measurement than the SCR/SCK systems. Overall, it is fair to conclude that the particle

size of the cement powder used during the infill process has a significant effect on the encapsulation process. The results have shown that this effect can be caused by varying the GGBS:Calumite blend, or by changing the powder source.

7.3.3 Tomography of Hardened Samples – Experimental

Tomography experiments were performed on hardened cement samples containing simulant waste. The samples were cast in metal containers to mimic a full scale wasteform in order to investigate and understand how the cement paste sets in and around the unusual shaped wastes. Both THORP hulls and Magnox simulant waste were used during these experiments. As discussed in section 2.3.1, Magnox is an alloy consisting of 99.2 wt. % magnesium and 0.8 wt. % aluminium. An example of the hardened samples is shown in Figure 7.11. Cylindrical cans were used because the samples were rotated during analysis. As previously mentioned, the full scale wasteforms are vibrated on plant to encourage full encapsulation but this has to be carried out via remote handling operations. Therefore, in order to understand the effect of vibrogrouting, a selection of samples were vibrated and some were left to set with no vibration. The formulations that were tested compared; the effect of different powders, the ratio of GGBS:Calumite and the w/s content of the system, as in the previous section.

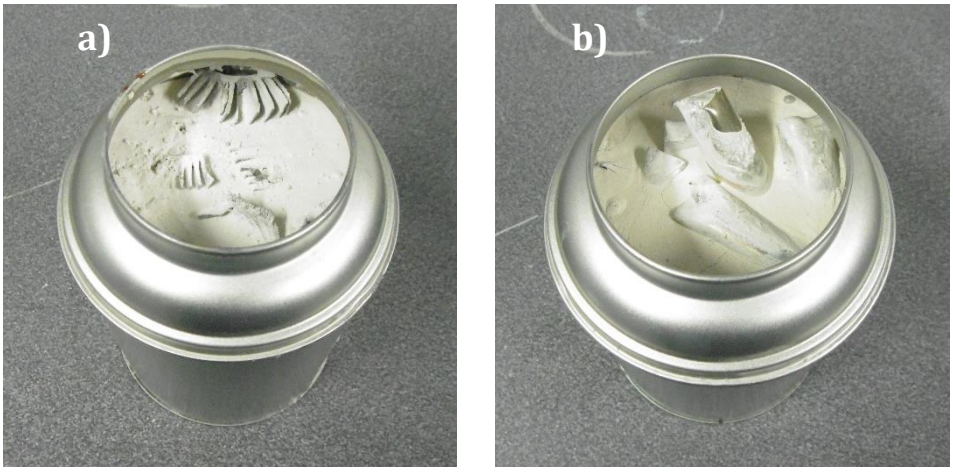

Figure 7.11. Images of the hardened cement samples containing a) Magnox and b) THORP hulls simulant waste.

7.3.3.1 Experimental method

The dry components were combined before the addition of water, and were hand mixed for two minutes. The pastes were then subjected to a further 10 minutes of mixing on a Silverson high shear mixer at 5000 rpm to achieve a homogeneous paste. The cement pastes were poured into cans that were pre-filled with simulant waste. Certain samples

were vibrated for 2 minutes using an ELE International Vibration Table. All of the samples were then cured and kept static for 28 days at 25 ˚C. The dimensions of the cylindrical sample can were 133 mm (h) and 93 mm (d), and the can was positioned in the same place for each tomographic scan.

7.3.3.2 Scan details

In order to scan the entire can it was necessary to scan in sections, i.e. the sample stage was moved down and rotated, capturing 4 sections of data in total per sample. The data were collected using an X-ray beam energy of 124 keV. The same detector was used as previously discussed (Section 7.3.1.2) to collect tomographic data. However, the sample was rotated collecting 3600 vertical projections over 0 - 180˚ resulting in a 0.05˚ step. These cross sections were manipulated to form images of a horizontal slice of the sample. These slices were stacked to produce a reconstruction of one section of the sample. Finally, the four sets of data for each section were combined to create a 3D reconstruction of the full sample.

7.3.3.3 Mix Matrix

The formulations chosen to demonstrate a selection of the blends under investigation are detailed in Tables 7.2 and 7.3. The selection encompasses direct comparisons between powder sources, water/solid ratios, simulant wastes, and the effect of vibration on the sample.

Table 7.2. Formulations used in the tomography experiments containing simulant THORP hulls.

Blend	Mix Reference*	Simulant Waste	Vibration	Water/solids ratio 0.33	0.35	0.37
P100	SCR	THORP hulls	No		X	
P72	SCR	THORP hulls	No	X	X	X
P65	SCR	THORP hulls	No	X	X	X
P52	SCR	THORP hulls	No		X	
P0	SCR	THORP hulls	No		X	
P65	SCR	THORP hulls	Yes	X	X	X
P72	PTK	THORP hulls	No		X	
P65	PTK	THORP hulls	No		X	
P65	PTK	THORP hulls	Yes		X	

*SCR = Scunthorpe GGBS:Calumite:Ribblesdale PC
PTK = Port Talbot GGBS:Calumite:Ketton PC

Table 7.3. Formulations used in the tomography experiments containing simulant Magnox.

Blend	Mix Reference*	Simulant Waste	Vibration	Water/solids ratio 0.33	0.35	0.37
P100	SCR	Magnox	Yes		X	
P72	SCR	Magnox	Yes		X	
P65	SCR	Magnox	Yes		X	
P72	SCR	Magnox	No		X	
P65	SCR	Magnox	No		X	
P72	PTK	Magnox	Yes		X	
P65	PTK	Magnox	Yes		X	

*SCR = Scunthorpe GGBS:Calumite:Ribblesdale PC
PTK = Port Talbot GGBS:Calumite:Ketton PC

7.3.4 Tomography of Hardened Samples – Results

In total, 22 samples were analysed and prioritised to encompass the effect of w/s content, the GGBS:Calumite blend and, how vibration of the sample encouraged encapsulation. Following the tomography scan, the data were processed to produce horizontal slices of the sample. A slice from a sample containing THORP hulls simulant and cement paste made from Scunthorpe GGBS:Calumite:Ribblesdale PC at a 3:1 BFS:PC ratio a P65 GGBS:Calumite blend and a 0.35 w/s content is shown in Figure 7.12. The bright shapes are the steel simulant waste, the dark grey is non-filled volume, and the mid-grey is the cement paste.

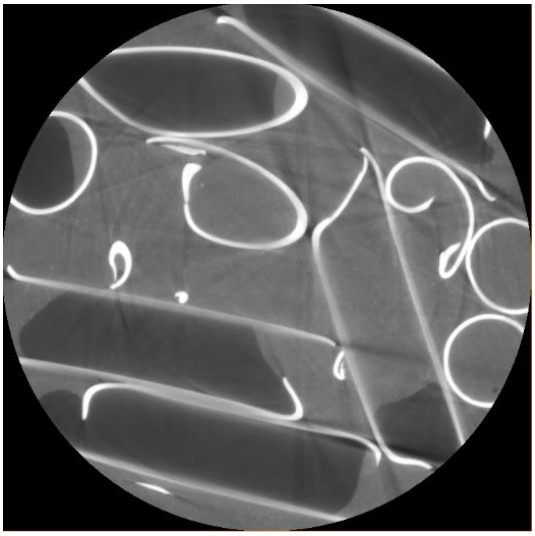

Figure 7.12. Sample slice from tomography data for a hardened sample containing THORP hulls simulant and cement grout at a 3:1 BFS:PC ratio a P65 GGBS:Calumite blend and a 0.35 w/s. This sample was not vibrated.

From Figure 7.12, the processed data show that although there were some voids, the sample was encapsulated, with roughly 64 % of the sample slice demonstrating successful infill. It is also reveals that vertically orientated hulls (which appear in the slice as circles) infill fully, compared to horizontal hulls (which appear in the slice as elongated shapes) that are clearly partially encapsulated, or are not encapsulated at all in concurrence with the radiography data discussed in the previous section.

The data were processed further to produce a reconstruction of a section of the sample using Avizo 3D Software. The sample slices were stacked in order to build a 3D representation of the sample, and using the software it was possible to distinguish between the different materials. Figure 7.13 provides an example of the orientation of the hulls inside the sample can.

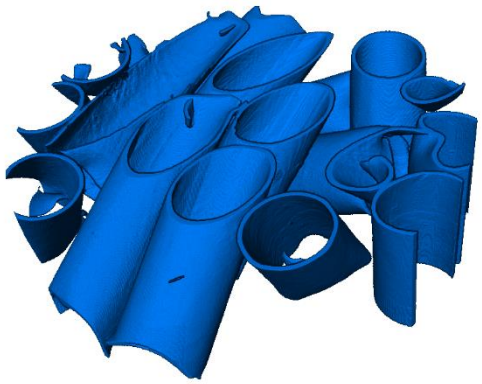

Figure 7.13. Reconstruction of the simulant hulls within a sample.

From the data it was possible to determine how much of the sample can was infilled with cement paste, what was simulant waste and if there was any empty space in the sample can. Each stage of the 3D reconstruction is shown in Figure 7.14 for the P65 sample.

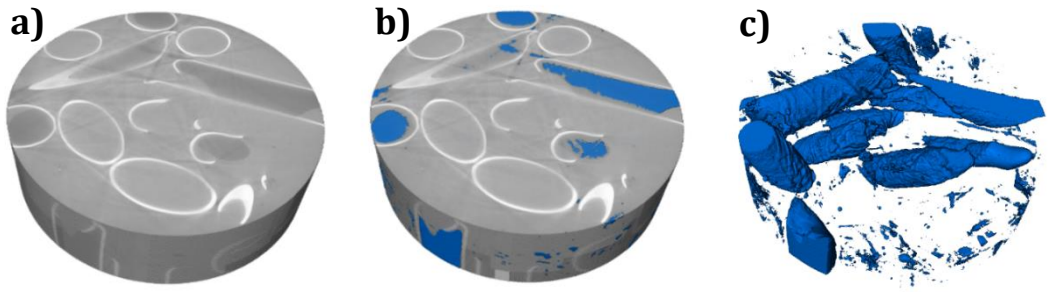

Figure 7.14. Reconstruction of tomography data for a hardened sample containing THORP hulls simulant and a Scunthorpe GGBS:Calumite:Ribblesdale PC cement paste at a 3:1 BFS:PC ratio with a P65 GGBS:Calumite blend and a 0.35 w/s, where a) is a section of the sample, b) highlights the voids in the sample, and c) shows just the voids in the section of sample.

From the reconstruction it is possible to extract the voids in the system, as shown in Figure 7.14c, giving a representative visualisation of how successful the infill process was for each sample. The results confirm that there were a number of hulls which were not infilled, but clearly that some of the hulls were encapsulated completely.

The effect of water on the encapsulation process was investigated by analysing lower (0.33) and higher (0.37) w/s contents, shown in Figure 7.15. When compared to the 0.35 w/s system (Figure 7.12), the sample slice images show voids at all three water contents but there was visibly more empty space in the 0.33 w/s formulation due to poor infill. The results indicate that the optimal formulation (i.e. with the minimal voidage) for infilling was the 0.37 w/s system as the voidage appeared to decrease with higher water content from 0.33 to 0.35 to 0.37 w/s.

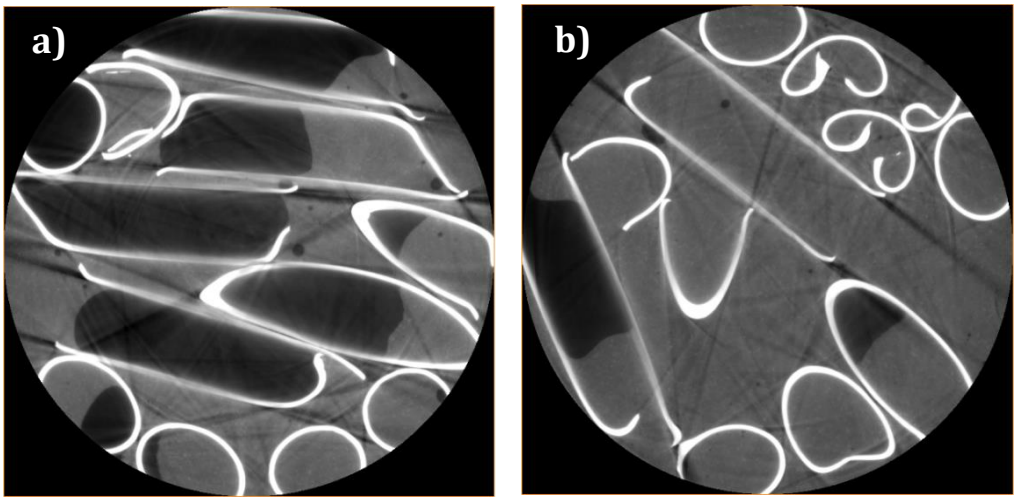

Figure 7.15. Sample slice from tomography data for a hardened sample containing THORP hulls simulant and a Scunthorpe GGBS:Calumite:Ribblesdale PC cement grout at a 3:1 BFS:PC ratio with a P65 GGBS:Calumite blend and a) 0.33 and b) 0.37 w/s. Samples were not vibrated.

The trend caused by changing the w/s ratio confirmed the assumption that at a higher water content, and therefore increased fluidity, the infill was more successful. These data agree with results presented in Chapter 4, where the fluidity was recorded from mini-slump testing in Figure 4.2. However, segregation was also observed at higher w/s ratio and therefore, it may not necessarily be a suitable option to achieve all of the desired performance criteria. This was also highlighted when the bleed of the systems was monitored in Chapter 8.

Another comparison that was investigated was the effect of altering the GGBS:Calumite blend ratio. Figure 7.16 illustrates the sample slice data for a P100 and P0 Scunthorpe GGBS:Calumite:Ribblesdale PC blend at a 3:1 BFS:PC ratio and a 0.35 w/s content. Reconstructions of the voids from those samples are shown in Figure 7.17.

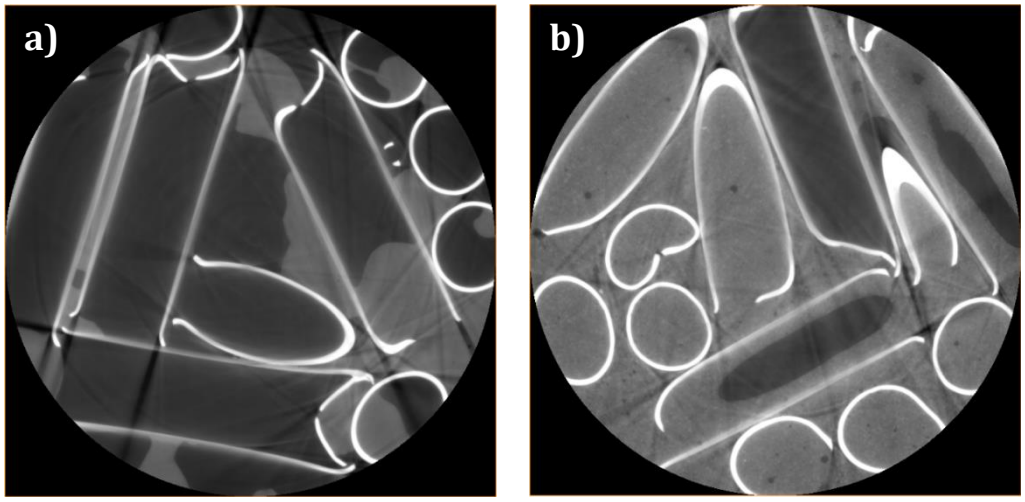

Figure 7.16. Sample slice from tomography data for a hardened sample containing THORP hulls simulant and a Scunthorpe GGBS:Calumite:Ribblesdale PC cement grout at a 3:1 BFS:PC ratio with a) P100 and b) P0 GGBS:Calumite blend and a 0.35 w/s. Samples were not vibrated.

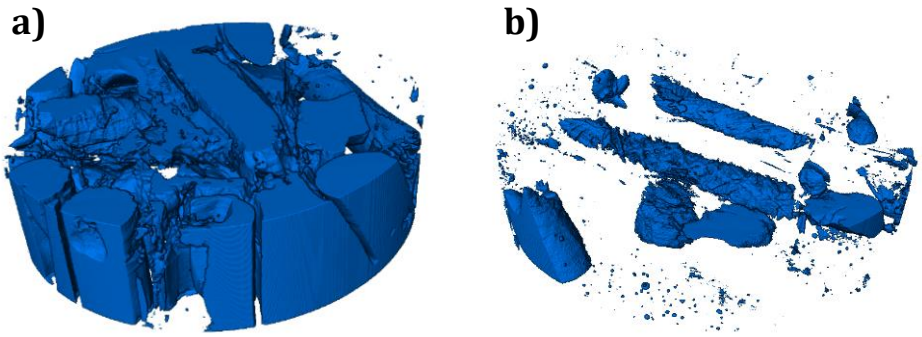

Figure 7.17. Reconstruction of tomography data for hardened samples containing THORP hulls simulant and a Scunthorpe GGBS:Calumite:Ribblesdale PC cement paste at a 3:1 BFS:PC ratio with a) P100 and b) P0 GGBS:Calumite blend and a 0.35 w/s content.

Figures 7.16 and 7.17 demonstrate that changing the GGBS:Calumite blend had a significant effect on the success of the encapsulation process. Figure 7.17a highlights the high volume of voids (blue mass) in the P100 system, and it is clear that the high surface area cement powder has not infilled properly because the majority of the sample is empty space. In comparison, the low surface area cement powder blend, P0, (Figure 7.17b) encapsulated the simulant waste very effectively as there is very little empty space (blue mass) reconstructed from the data. When comparing these two samples to the P65 systems from Figure 7.13, it is fair to conclude that as the GGBS content increases, the voidage in the system increases significantly. These results are in agreement with observations from the radiography experiments, where although the top of the sample container appeared to be encapsulated, it was clear from the images that the cement grout did not infill properly. These results also complement the yield stress values

recorded in Chapter 4, where the P100 system required significant shear stress to achieve any movement.

All of the samples discussed thus far were not vibrated during production. Following this a selection of the sample formulations were duplicated and then vibrated for 2 minutes before allowing them to set. These additional samples were produced in order to investigate the effect of vibration on cement pastes during encapsulation. A vibrated sample with a 3:1 BFS:PC ratio at a P65 GGBS:Calumite blend and a 0.35 w/s content was produced, and the result is shown in Figure 7.18. The most significant feature is that there is very little dark grey (representative of voids) visible in Figure 7.18a, suggesting very minimal voidage in the sample. This was confirmed from the reconstruction of voids within the sample in Figure 7.18b, where the majority of the image was white with very little blue mass especially compared to the equivalent non-vibrated sample in Figure 7.14. This result confirmed that the vibration process carried out during the production of the simulant wasteform influences the encapsulation process quite significantly. Although, the analysis carried out here has shown that decreasing the surface area of the cement powder also improves the infill process. Therefore, if in the future, it is not possible to vibrogrout these products on plant, there is potential that the vibrogrouting may not be an essential step in the encapsulation process for THORP hulls.

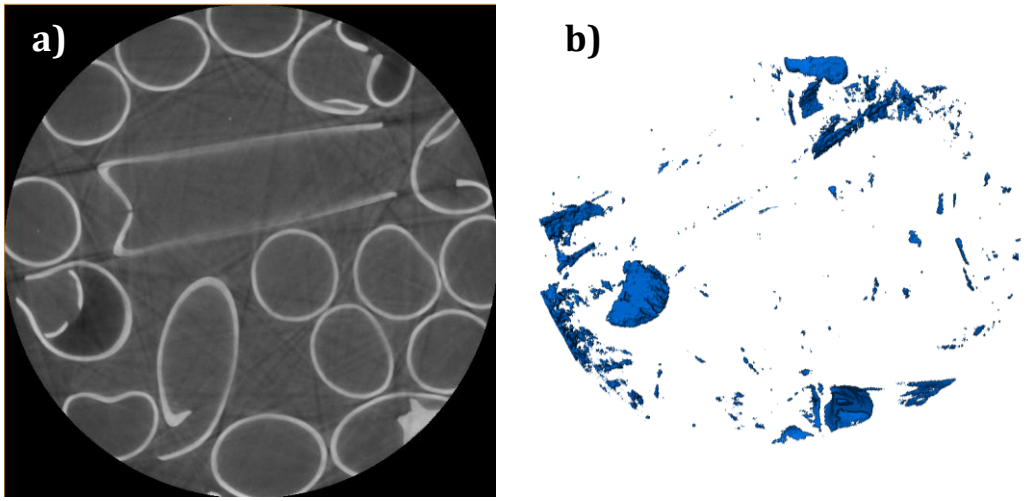

Figure 7.18. Reconstruction of tomography data for a vibrated hardened sample containing THORP hulls simulant and a Scunthorpe GGBS:Calumite:Ribblesdale PC cement paste at a 3:1 BFS:PC ratio with a P65 GGBS:Calumite blend and a 0.35 w/s: a) sample slice, and b) reconstruction of the voids in the sample.

The final comparison to discuss in terms of samples containing THORP hulls as simulant waste is the effect of changing the powder source. Tomographic analysis was also carried

out on a series of Port Talbot GGBS:Calumite:Ketton PC samples. A very similar trend was observed between the different powder sources, i.e. as the Calumite content decreases there is an increase in voidage. This confirms that the Calumite is the major contributing factor in all of these samples. However, the PTK system does have less voidage when a direct comparison is made between the GGBS:Calumite blends. Therefore, in agreement with the radiography experiments presented in the previous section, this would suggest the Port Talbot GGBS:Calumite:Ketton PC is a slightly more fluid system, which was expected due to the wider PSD of the Part Talbot GGBS.

The next set of samples under discussion, investigate the encapsulation of simulant Magnox swarf. The simulant itself consists of a metal 'back-bone' structure with thin fins attached and as such, forms small and difficult to access spaces. This in turn makes it quite a difficult material to encapsulate. This was investigated by generating samples with different parameters. The most interesting comparison to discuss was the effect of vibrating the sample or not. Analysis was carried out on the Scunthorpe GGBS:Calumite:Ribblesdale PC formulation using a 3:1 BFS:PC ratio with a P65 GGBS:Calumite blend at a 0.35 w/s content, where one sample was vibrated and the other left to set immediately after casting the product. The comparison between the two samples is presented in Figure 7.19. Instantly, the first observation between the two sample slice images (Figures 7.19a and 7.19d) shows that there was practically no voidage in the sample that was vibrated. In comparison, the non-vibrated sample highlights that the metal fins do not encapsulate effectively. The reconstruction of the voids in Figures 7.19c and 7.19f depicts the severe difference in empty space between the two samples. The vibrated sample contains nearly no blue mass at all, suggesting that the encapsulation was very successful, unlike the non-vibrated sample where there is a large volume of empty space.

From the data collected for the simulant Magnox samples, it is clear that the P65 system is not fluid enough to encapsulate the waste successfully without the aid of vibration during the casting process. The results also confirmed that if vibration is used the encapsulation process can be very effective, thus providing strong evidence for the nuclear industry that the vibration process is working and that it can applied to Magnox samples with the confidence that the fins will be fully encapsulated.

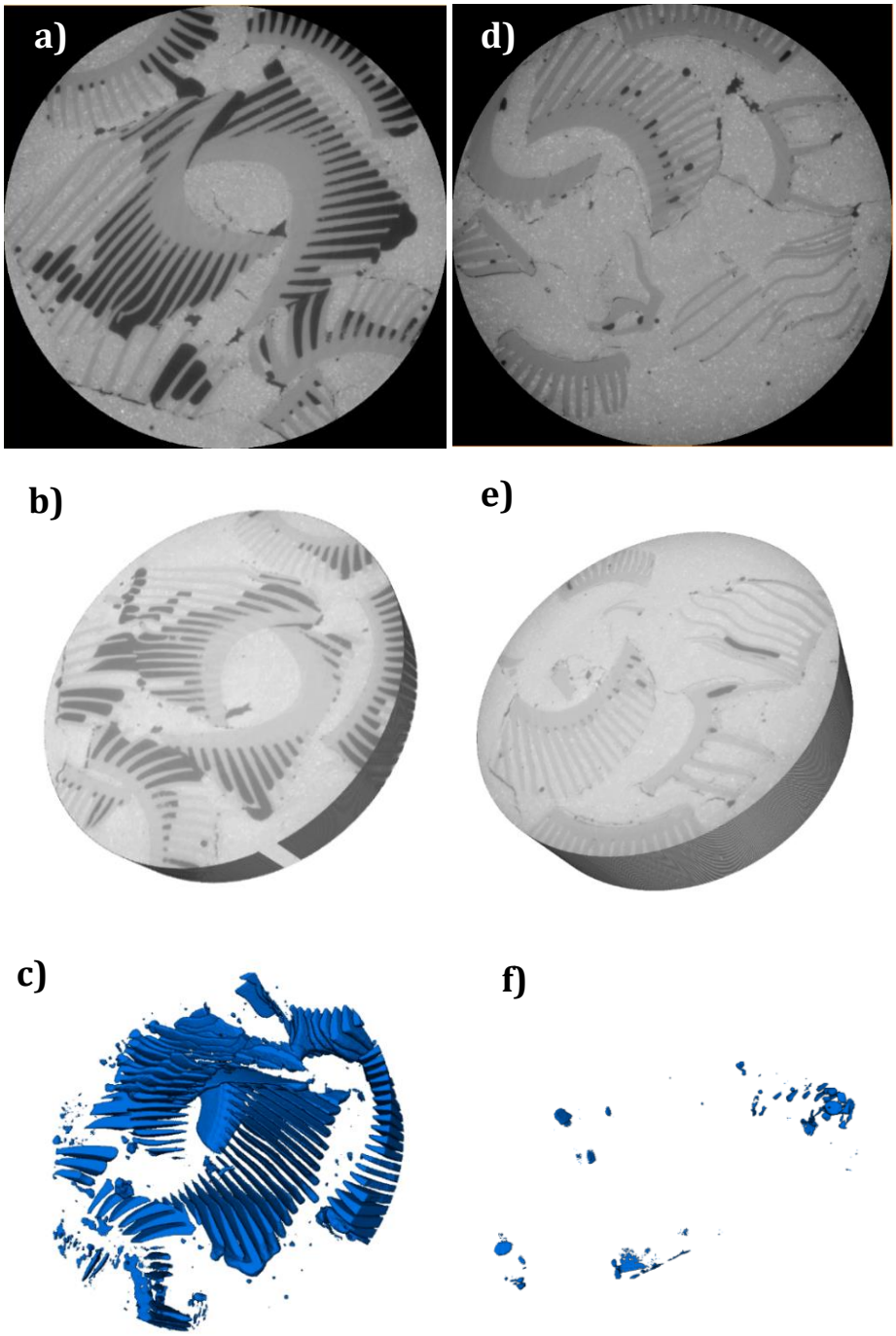

Figure 7.19. Reconstruction of tomography data for hardened samples containing Magnox simulant and a Scunthorpe GGBS:Calumite:Ribblesdale PC cement paste at a 3:1 BFS:PC ratio with a P65 GGBS:Calumite blend and a 0.35 w/s, where in a-c the sample was not vibrated and in d-f sample was vibrated. a+d) sample slice, b+e) reconstruction of the sample and c+f) reconstruction of the voids in the sample.

7.3.5 Full Reconstruction

In order to obtain a fuller reconstruction and analysis of the tomographic samples, further processing was carried out by 3Dmagination, who are a professional imaging

company based at the Rutherford Appleton Laboratory, Harwell. Acknowledgments go to Kamel Madi and Loic Courtois for the data processing. The images produced are presented in this section.

The samples investigated were:

1. Scunthorpe GGBS:Calumite:Ribblesdale PC for the P65 GGBS:Calumite blend at a 0.35 w/s containing simulant THORP hulls (*no vibration*)
2. Scunthorpe GGBS:Calumite:Ribblesdale PC for the P65 GGBS:Calumite blend at a 0.35 w/s containing Magnox swarf simulant (*with vibration*)

These samples were chosen because sample 1 represents the baseline mix that has been investigated throughout this thesis and sample 2 was chosen in order to monitor the infill of Magnox swarf. However, due to the findings from analysing sample sections, it was clear that the non-vibrated Magnox swarf sample did not infill and more value would be gained from reconstructing the vibrated equivalent.

A basic reconstruction of the sample containing THORP hulls is presented in Figure 7.20. This was the first step needed to align and stitch the data set together to form the 3D image.

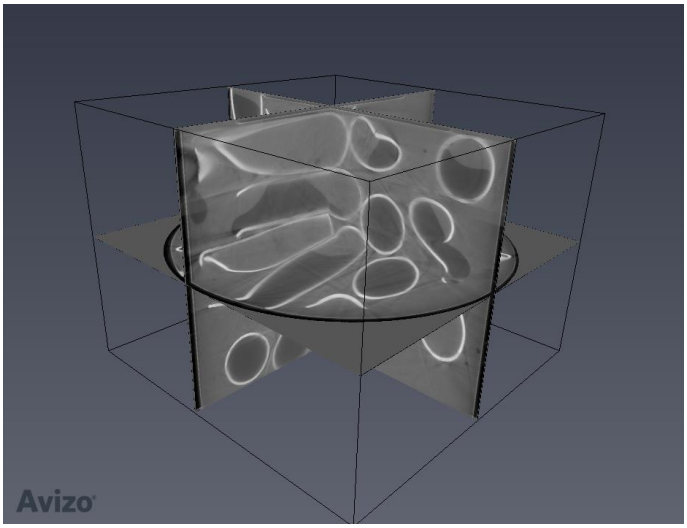

Figure 7.20. Image of the alignment of the full sample in order to stitch the dataset correctly of Sample 1.

Figure 7.20 provides a 3D representation of the full sample. Similar to the images of the sample slices (section 7.3.4), it is possible to distinguish between the cement grout (pale

grey), stainless steel tubing (white) and empty pore volume (dark grey). A cross section of the samples is shown in Figure 7.21.

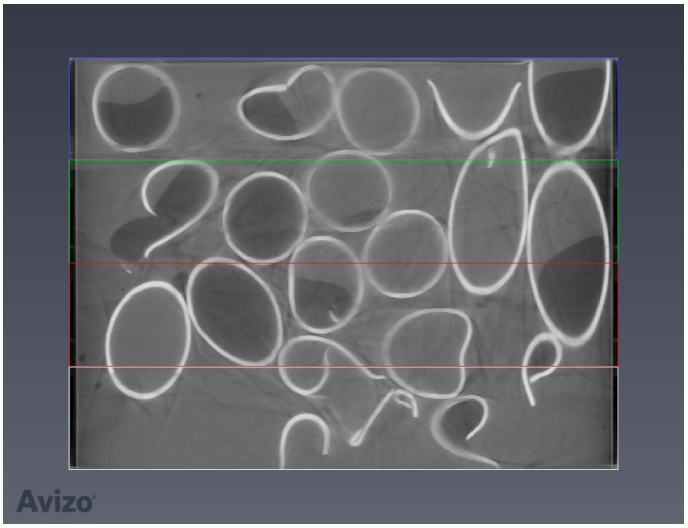

Figure 7.21. Cross section of all four sections of Sample 1 following alignment.

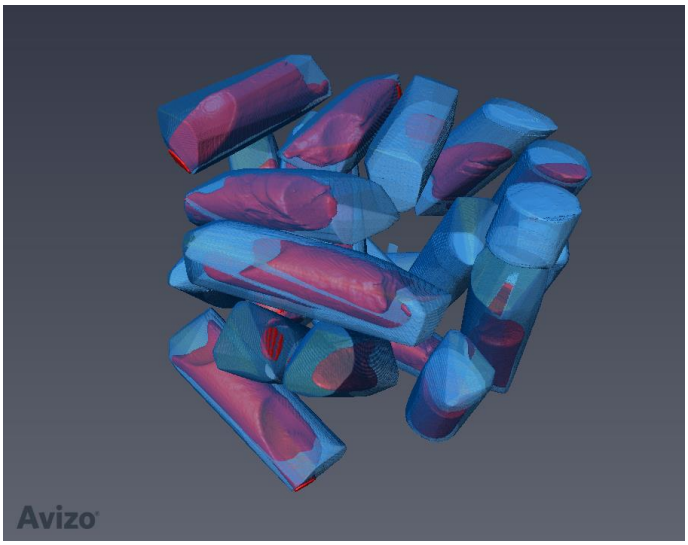

Figure 7.22. 3D visualisation of pores (red) within the simulant THORP hulls within Sample 1.

Figure 7.21 demonstrates a cross section of Sample 1 once the alignment process had been applied. Some of the simulant waste appears to be oblong shaped, but this is due to the angle that the stainless tubing was sitting within the sample. From the cross section, it is fair to conclude that the majority of dark areas (i.e. voidage) occurs within the simulant waste. The next step in the analysis was to determine the volume and location

of empty pores. Figure 7.22 presents a 3D visualization of the simulant THORP hulls with the pore volume highlighted in red.

The 3D visualisation illustrates how the majority of the pores occur in hulls in a horizontal orientation. This was also observed during the radiography experiments. Further manipulation of this data would provide the volume of empty pores and relationship between hull orientation and voidage.

The second sample that was analysed by 3Dmagination contained the Magnox swarf simulant. The full reconstruction clearly shows that the Magnox simulant waste does not encapsulate fully because voids are visible in between the metallic fins of the cladding. A full cross section of the sample is shown in Figure 7.23.

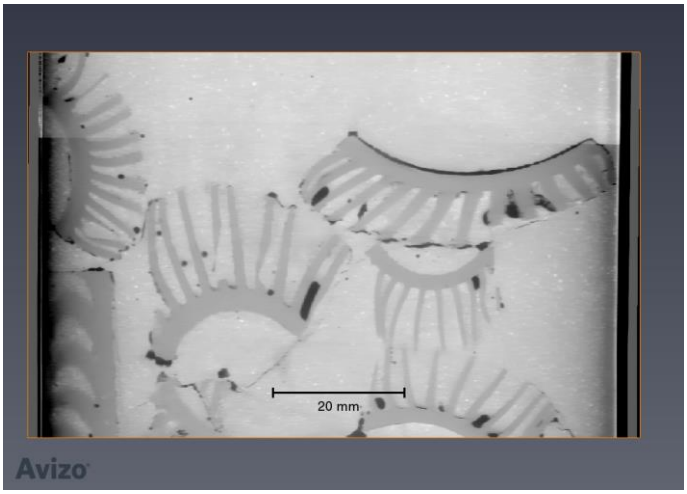

Figure 7.23. Cross section of all four sections of Sample 2 following alignment.

Figure 7.24 demonstrates a full 3D image of sample 2 where the cement is in blue, metal pieces are silver and the pores in the sample are represented in orange. By distinguishing the different components, it is possible to highlight that the majority of the pores are near the surface of the simulant Magnox waste.

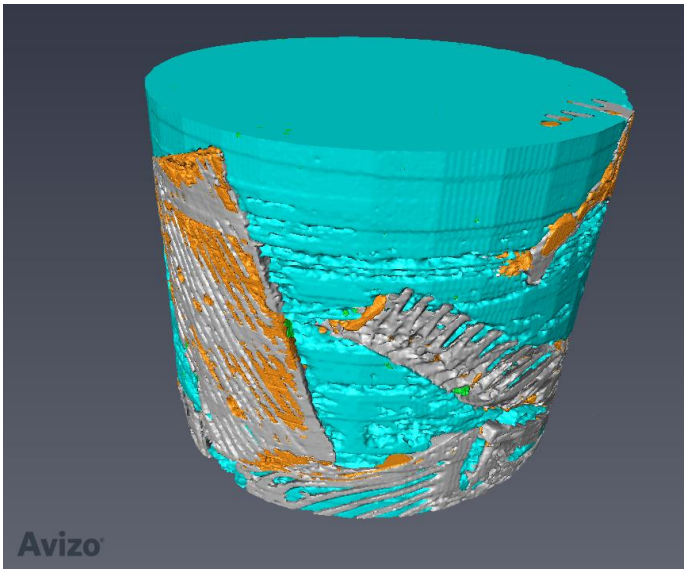

Figure 7.24. 3D image of Sample 2, where the cement is coloured blue, metal is silver and orange represents the pores/voids.

An artifact that was much more common in the sample containing Magnox waste was the formation of cracks. Data to illustrate these cracks has been extracted and is shown in Figure 7.25. The large pores near the metallic pieces are shown in yellow and it appears that the cracks link between them (shown in red). It is likely that these pores cause stress concentration and act as a driving force for crack propagation. The metallic pieces behave as obstacles for the cracks preventing them from growing any further.

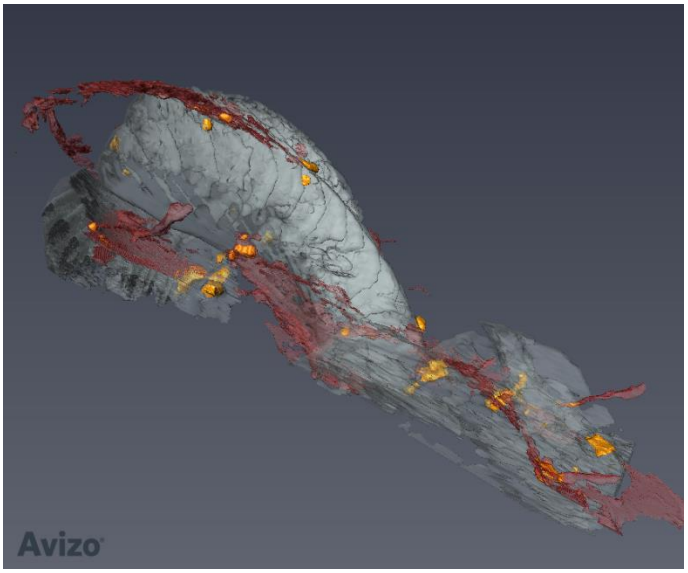

Figure 7.25. 3D visualisation of Sample 2 to illustrate interaction of cracks with the simulant Magnox waste.

7.4 Conclusions

In this chapter, beamline-based analysis was used to investigate the encapsulation process used by the nuclear industry, both in-situ in 2D, and ex-situ in 3D. A series of in-situ radiography experiments were carried out where the real-time infill of simulant nuclear waste was captured in a series of images. This is the first time anyone has successfully conducted time resolved X-ray tomography of cement flowing in and around objects in a nuclear waste immobilisation context. The experiments were a very close representation of the process used on plant and were very successful, producing interesting and reliable results.

The results show that although the top of a sample can could appear to have encapsulated fully, this does not necessarily represent the whole sample. It was found that the 'stiffer' material with a high surface area (P100) did not infiltrate the simulant hulls and just set at the top of the can. In comparison the P65 systems infilled fluidly to the bottom of the can, and this was found in both the SCR and PTK cement systems. The PTK system produced a slightly lower voidage overall compared to the SCR equivalent, and this is likely due to the broader PSD of the cement powder as analysed in the previous chapters. In terms of water content, the 0.33 w/s system did not infill quite as effectively as the higher water ratios, but still infiltrated the hulls fairly well. However, regardless of the cement system used it was clear that the orientation of the simulant THORP hulls influenced the encapsulation. Hulls that were vertical in the can infilled much more effectively than those that were horizontal.

Tomographic analysis was carried out on hardened samples that were cured for 28 days. A series of parameters were investigated including the powder sources, GGBS:Calumite blend and w/s content. The effect of vibration and non-vibration of the samples was also investigated to understand the importance of that additional step in the encapsulation process. The data show that as the Calumite content decreases, the voidage in the samples increases, and this is true across different powder sources. It was also found that as the w/s content increases, the empty space within the sample decreased.

Overall, both sets of experiments highlight the importance and the effect of changing the PSD of the cement paste used on the encapsulation process. This chapter has also provided the UK nuclear industry with more in-depth detail about how successful the encapsulation process is, and some evidence to support the current process they are using.

8 Scale up Trials

8.1 Introduction

As discussed in Chapter 2, the nuclear industry has a required performance specification [61] that cement grout must conform to, for it to be used as part of the encapsulation process. These properties are measured by a series of test methods collectively known as an 'acceptance test'. The acceptance test requires a 3 litre batch and follows a strict mixing regime in order to assess the fluidity, setting time and bleed of the cement grouts. Understanding the behaviour of the cement grouts as a function of the PSD of the systems will strongly underpin the science behind the need to blend the GGBS and Calumite materials. In this chapter, having considered the results of the small scale trials and the experiments carried out at the Diamond Light Source, mid-scale trials were carried out on a smaller selection of mixes.

The second section of this chapter discusses the large scale trials (500 L) carried out at the National Nuclear Laboratory (Workington Site) to complete the experimental programme of this project. The plant scale products mimic the wasteforms produced on the Sellafield site. Large scale trials, such as the ones carried out here, are not conducted very often but are crucial in understanding the effect of the PSD between laboratory and plant scale. They also provide the opportunity to try different options such as infill parameters and formulation to then observe how successful the infill is as a result.

8.2 Results and Discussion

8.2.1 Mid-scale Trials

The mid-scale trials were carried out on 3 litre mixes, which is the standard amount of grout used in the acceptance test at NNL. The BFS:PC ratio was maintained at 3:1 throughout these trials, and three w/s ratios were considered: 0.33, 0.35 and 0.37. In order to accommodate the additional powder sources requested for investigation by the industrial sponsors (Ketton PC; Port Talbot GGBS blended with Calumite, and historic Redcar BFS), the formulation matrix described in Chapter 3 was developed further to incorporate reasonable comparisons between different grout mixes. The formulations chosen for acceptance testing are identified in Table 8.1, indicated by an 'X'.

Table 8.1. Formulation matrix for 3 litre acceptance mixes.

Blend	Mix Reference	Powder Source		Water/solids ratio		
		PC	BFS (GGBS:Calumite)	0.33	0.35	0.37
P100	SCR	Ribblesdale	Scunthorpe:Calumite	X	X	X
P80	SCR	Ribblesdale	Scunthorpe:Calumite		X	
P72	SCR	Ribblesdale	Scunthorpe:Calumite	X	X	X
P65	SCR	Ribblesdale	Scunthorpe:Calumite	X	X	X
P58	SCR	Ribblesdale	Scunthorpe:Calumite		X	
P52	SCR	Ribblesdale	Scunthorpe:Calumite	X	X	X
P42	SCR	Ribblesdale	Scunthorpe:Calumite		X	
P32	SCR	Ribblesdale	Scunthorpe:Calumite		X	
P22	SCR	Ribblesdale	Scunthorpe:Calumite		X	
P0	SCR	Ribblesdale	Scunthorpe:Calumite	X	X	X
P72	PTR	Ribblesdale	Port Talbot:Calumite		X	
P65	PTR	Ribblesdale	Port Talbot:Calumite		X	
P100	PTK	Ketton	Port Talbot:Calumite		X	
P72	PTK	Ketton	Port Talbot:Calumite		X	
P65	PTK	Ketton	Port Talbot:Calumite		X	
P52	PTK	Ketton	Port Talbot:Calumite		X	
P72	SCK	Ketton	Scunthorpe:Calumite		X	
P65	SCK	Ketton	Scunthorpe:Calumite		X	
-	Redcar	Ribblesdale	Redcar*	X	X	X

* Redcar makes up the whole BFS fraction and is therefore not blended with Calumite.

The selection of 31 mixes encompasses the comparison between w/s ratio, PC supply, GGBS supply and the effect of the GGBS:Calumite blend across these parameters.

8.2.1.1 Colflow Measurements

One of the main performance criteria required for successful encapsulation is the fluidity of the system. This was measured using the Colflow method, applied to all the formulations stated in Table 8.1, as one of the acceptance test methods. The results for the 10 blends of GGBS:Calumite at a 3:1 BFS:PC ratio and a 0.35 w/s content are presented in Figure 8.1. The results show that as the Calumite content increases, an increase in the fluidity is observed which is due to a decrease in surface area of the powder, resulting in a lower water demand. This effect caused by the PSD of the system agrees with the observations in the small scale trials described in Chapter 4, in agreement with laboratory scale measurements, the fluidity reaches an optimum point.

The optimum blend of GGBS:Calumite material at small scale in Chapter 4 was found to be the P22 system, compared to the mid-scale trials where this point was achieved in the P32 formulation. This suggests that there are fluidity changes observed when the cement grouts are scaled-up to 3 litres.

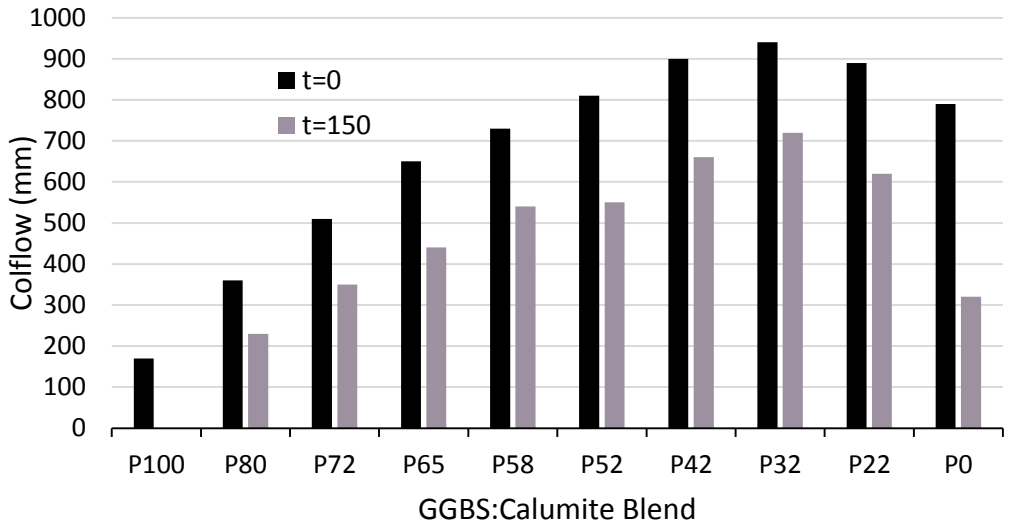

Figure 8.1. Colflow fluidity for the 10 GGBS:Calumite blend ratios at 3:1 BFS:PC ratio and at a 0.35 w/s content for t=0 and t=150. Ribblesdale PC and Scunthore GGBS were used.

The fluidity of the systems was measured immediately following mixing (t=0) and after a 'hold-up' of 150 minutes (t=150). During the hold-up period, the cement grouts are kept agitated for the whole duration. The significance of monitoring the material during this time is to ensure that the grout remains useable and conforms to specification requirements in the event of any unforeseen/unexpected plant hold-ups. Ideally, the cement grout would be used immediately, represented by t=0 measurements but this is not always possible. This is highlighted by the P100 system where at t=150, it was not possible to record a measurement because it did not flow out of the tundish in order to take a flow reading. Generally, the drop in fluidity between t=0 and t=150 becomes greater with decreasing GGBS content and this can be attributed to the reactivity of the system which was observed in the calorimetry data presented in Chapter 6. At t = 150 in Figure 6.1, the cement mixes with a high GGBS content have a greater total heat evolution because the reactivity of the system increases with increasing slag content. However, the P0 system does not have the lowest total heat evolution at this early stage and this is illustrated by a decrease in workability observed in Figure 8.1. This is validated as a significant drop in flow is observed for the P0 system which is because the only contributing binder at t=150 is the Portland cement. These observations confirm that

behaviour seen at large scale can be explained by fundamental science at small scale. In order to compare between the Scunthorpe GGBS:Calumite:Ribblesdale PC and the Port Talbot:Calumite:Ketton PC formulations, the fluidity of the latter system was analysed using fewer GGBS:Calumite blends. A similar trend was observed with the P100 system at t=150, which did not flow at all (data shown in Appendix D).

The Colflow method was also carried out at different w/s ratios in order to monitor the effect of water on the systems. Five GGBS:Calumite blend ratios were considered at 3 different w/s contents (0.33, 0.35 and 0.37), data shown in Figure 8.2.

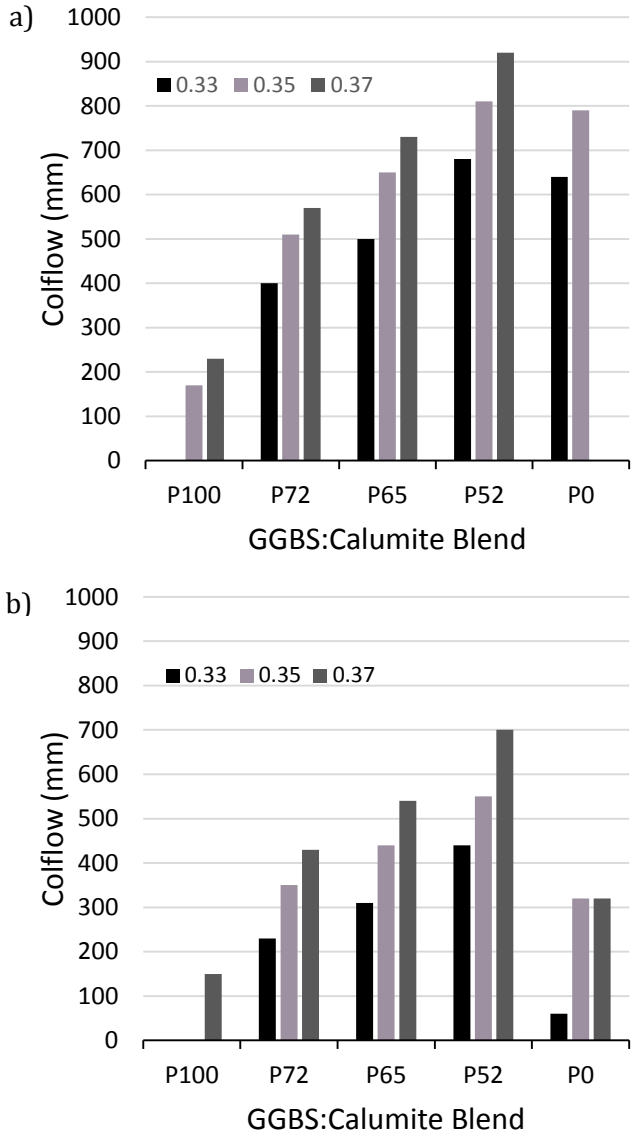

Figure 8.2. Comparison of Colflow fluidity of grouts with w/s ratios of 0.33, 0.35 and 0.37 for 5 GGBS:Calumite blend ratios at 3:1 BFS:PC ratio. a) t=0 and b) t=150. Ribblesdale PC and Scunthorpe GGBS were used.

The results demonstrate that as the water content increases the fluidity of the system increases, which is to be expected. However, as previously discussed in Chapter 4, simply increasing the w/s ratio is not a suitable solution for plant operations due to the possible formation of bleed and the complications that could arise as a consequence (i.e. the generation of secondary wastes). As with the results observed in Figure 8.1, there is a clear loss of fluidity between the t=0 and t=150 data. This is highlighted by the lack of results obtained for some formulations, for example in the P100 system, there was no flow recorded for the 0.33 w/s system, confirming the increased water demand of the fine particles. At t=150, the only P100 system to produce a tangible result was the 0.37 w/s system however there is no data for the P0 system at a 0.37 w/s content. This is because the Colflow measurement was greater than the length of the test channel (1020 mm) and severe water segregation was observed. The differences captured by these tests display the sensitivity of the grouts: changing the PSD and the w/s ratio slightly can cause significant changes in the performance of the system.

The final Colflow comparison to consider is the change of powder source and the effect it has on fluidity of the system. The results are shown in Figure 8.3 for the different powder combinations, using a formulations fixed to the P65 GGBS:Calumite blend at a 0.35 w/s ratio.

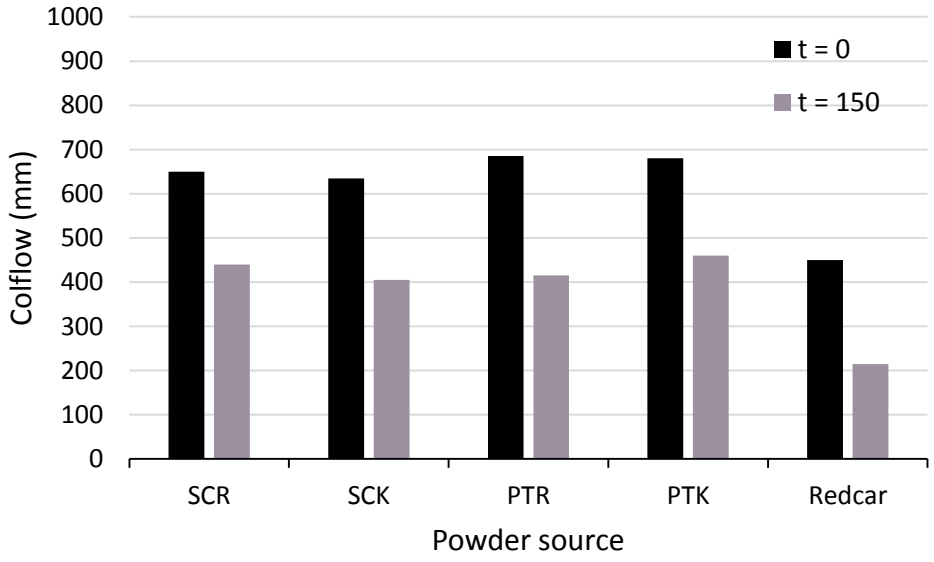

Figure 8.3. Comparison of Colflow fluidity of different powder sources for GGBS:Calumite P65 blend ratios at 3:1 BFS:PC ratio and a 0.35 w/s.

The GGBS:Calumite systems, regardless of powder source, show very similar results and again show a substantial loss of fluidity after the hold-up time. Interestingly, when these

formulations are compared to the cement grout containing Redcar GGBS:Ribblesdale PC, the powder that the specification [58] was originally written for and was used historically, the original material has a much lower flow than the powders that are currently in use on plant. This means the current grout will perform better during plant hold-ups/delays than the original formulation. A very similar result was observed for the P72 system but a decrease in fluidity was observed due to an increase in the powder surface area (data shown in Appendix D).

8.2.1.2 Bleed Measurements

The segregation of water within a cement grout can cause settlement of supernatant at the top of the sample. This supernatant is known as bleed [108, 139], and is monitored as part of the acceptance test methods. Aliquots of 100 mL were taken from the 3 litre grout mixes at 30 minutes intervals (after the termination of mixing) for the entire hold-up duration, then each was tested after 24 hours as described in Chapter 3. Therefore, each mix has 6 bleed samples and these were monitored at 24 hours in order to understand the behaviour of the bleed property. Figure 8.4 shows the results for the ten GGBS:Calumite blends at a 3:1 BFS:PC ratio and a 0.35 w/s content. Many of the formulations showed no bleed at all, but as the Calumite content increased, the observation of water settlement became more prominent. At t=0, bleed was observed for the P58 to P0 blends. However, after the hold-up mixing time no bleed was observed on the t=150 samples, with the exception of the P0 system where a 2 vol. % water segregation was still maintained. For the cement grouts to conform to the Sellafield specification, the bleed of the t = 150 samples must be 2 vol. % or less at 24 hours [58]. Therefore, although the P32, P22 and P0 systems technically adhere to the required performance criteria, they should be avoided because the grout is often used immediately and bleed is observed in the samples prior to t = 150 for those formulations.

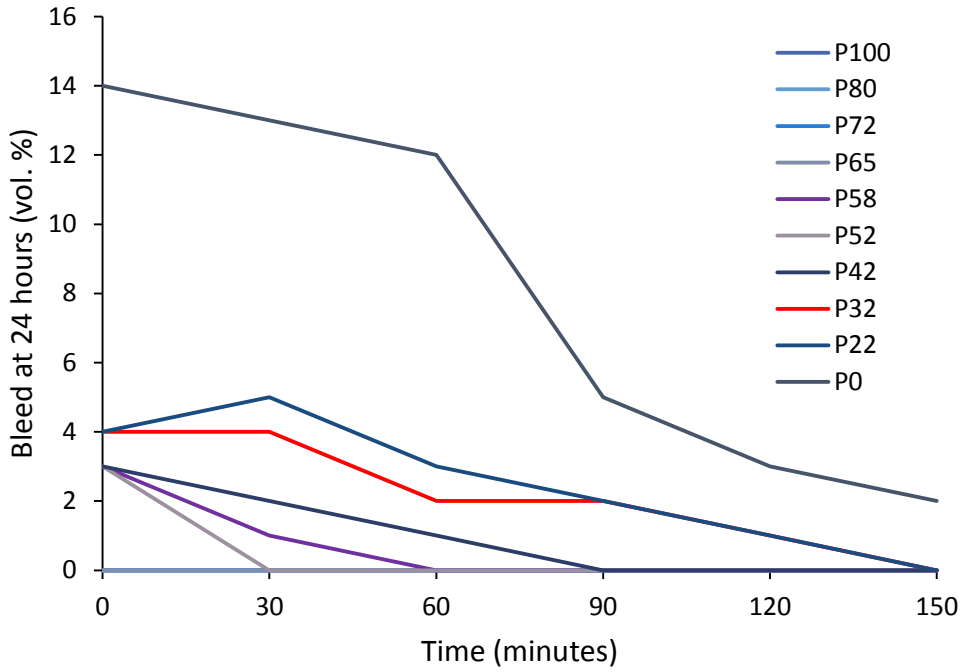

Figure 8.4. Bleed measurements for the 10 GGBS:Calumite blend ratios at 3:1 BFS:PC ratio and at a 0.35 w/s content taken at t=0, 30, 60, 90, 120 and t=150. Ribblesdale PC and Scunthore GGBS were used.

As with the Colflow results, the powder source combinations for the P65 systems at 0.35 w/s content were compared in terms of bleed, shown in Figure 8.5. The samples containing Scunthorpe GGBS exhibited no bleed throughout the mixing time, unlike the Port Talbot GGBS where bleed was observed in the initial samples but this was not seen after 90 minutes. This difference is attributed to the slightly coarser particles within the Port Talbot material resulting in a lower surface area and therefore, a lower water demand. It also highlights the effect that small changes in the PSD of the cement powder used does significantly change the performance of the grouts, which underpins the importance of this research project.

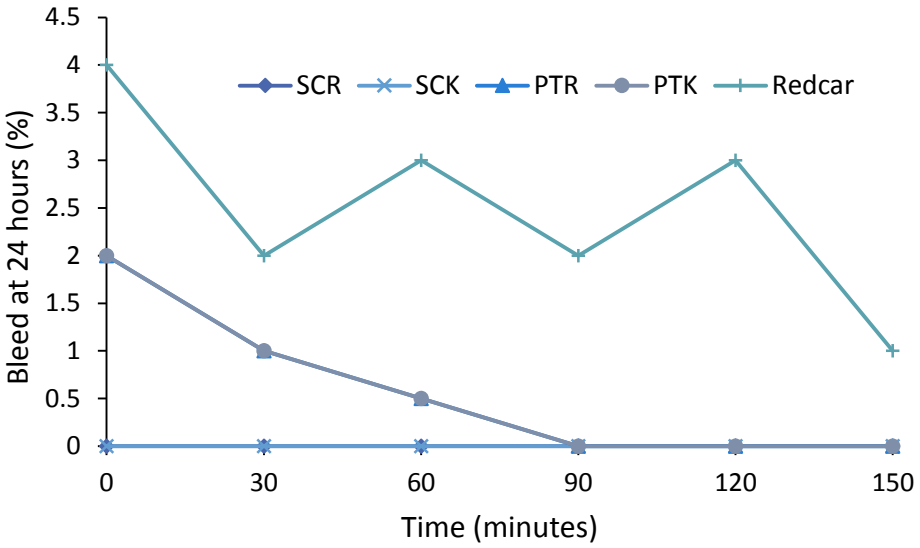

Figure 8.5. Bleed measurements for different powder sources at a P65 GGBS:Calumite blend ratio, a 3:1 BFS:PC ratio and at a 0.35 w/s ratio taken at t=0, 30, 60, 90, 120 and t=150.

The bleed data for the Redcar material is included in Figure 8.5 and does not follow the same linear trend as the other powder formulations. The samples show a constant change of 2.5 ± 0.5 vol. % bleed between measurements at 30 and 120 minutes. Water segregation was observed for every sample measurement, with a 1 vol. % bleed still observed in the final sample at t=150 minutes. This bleed performance does fit within the Sellafield specification but it is desirable to eliminate the presence of any bleed. Particle packing is quite likely to be the reason that the bimodal GGBS:Calumite blends flow much better and do not bleed in the same way the Redcar systems do. This is because of the ability for smaller particles to pack in between larger ones, increasing reactivity and reducing water demand, when a bimodal distribution is observed inducing better flow. Whereas, Redcar is closer to monosized and so in comparison does not pack so closely and is more similar to a fuller distribution which results in a decrease in fluidity [92, 93].

8.2.1.3 Setting Time

The setting time for all of the cement pastes was monitored both manually and using automatic apparatus. The results of the manual Vicat tests demonstrated that all of the formulations from Table 8.1, at a 3:1 BFS:PC ratio and a 0.35 w/s content, meet the Sellafield specification of an initial setting time greater than 4 hours and a final setting time less than 24 hours.

Automatic Vicat testing was carried out in order to get an estimate for the initial set of the cement systems. If the ten baseline GGBS:Calumite blends at a 0.35 w/s content are

considered, it shows that in general as the Calumite content increases the setting time is lengthened, as shown in Figure 8.6. This confirms reported literature that as the content of coarse material increases the cement matrix will have a delayed setting time, but will likely achieve set at a lower degree of hydration [140, 141]. The trend and values obtained are similar to those reported by previous studies investigating GGBS and PC systems at different particle sizes. However, the data obtained for the system under investigation here are slightly higher which is to be expected as the PSD of Calumite is greater than that used in the reported literature [142].

This method defines the initial set to be when a depth value of 5 mm (distance above the bottom of the mould to which the needle penetrates) is achieved, the time taken for this to be achieved, is reported in Figure 8.6. Although there are values for the P0 and P22 systems, when the results are analysed further, the depth does not increase linearly as it does with the rest of the ten GGBS:Calumite systems. This suggests that the high coarse material content of the P0 and P22 systems is affecting the reliability of this test method, and the true setting time is likely to be longer than stated here.

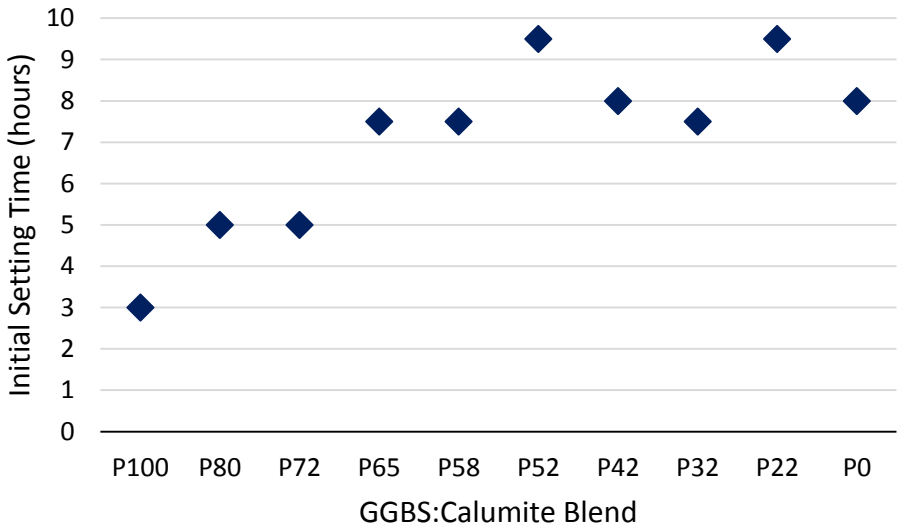

Figure 8.6. Automatic Vicat setting time measurements for the 10 GGBS:Calumite blend ratios at 3:1 BFS:PC ratio and at a 0.35 w/s content. Measurement started at t=150.

The automatic Vicat testing was carried out in a laboratory environment and as such could be affected by ambient temperature. In order to monitor this, the temperature of the lab was recorded during every mix. The temperatures reported for these mixes were ± 2 ˚C of each other. However, there was a significant 5 ˚C drop in temperature for the P52 mix compared to the rest of the mixes, which would have contributed to the

extended time taken for the system to set (9.5 hours compared to ~8 hours for the blends either side).

8.2.1.4 Dimensional Stability

The dimensional stability of a material or structure is the property used to describe the ability to maintain or retain its shape and size [143]. Shrinkage can affect the stability of hardened cements and attributed to delayed hydration, microstructure rearrangement and also alters strength progression [144]. During this study, dimensional stability measurements were carried out to monitor the behaviour of the cement grouts over the curing period (90 days) and any shrinkage/expansion of the products was recorded. The results for the ten baseline GGBS:Calumite blends at a 0.35 w/s ratio are shown in Figure 8.7.

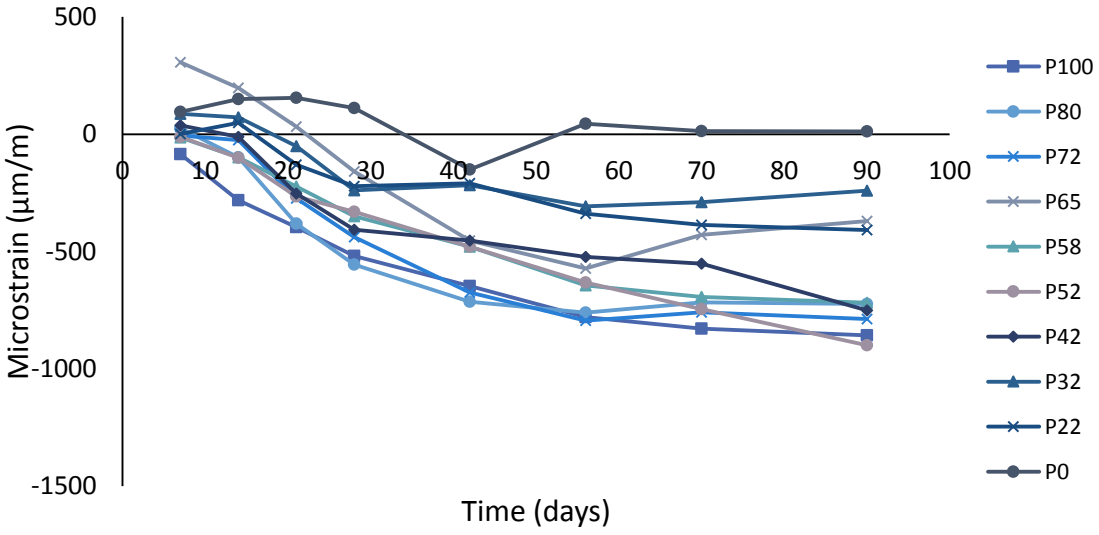

Figure 8.7. Dimensional stability data for ten GGBS:Calumite blends at a 3:1 BFS:PC ratio and 0.35 w/s content over 90 days.

All of the ten formulations demonstrated shrinkage initially but this started to plateau after 42 days. An interesting observation is that the systems containing a high wt. % of GGBS reported a greater change in length (expansion) compared to the P0 system that showed the least at 4.4 µm/m. This suggests that the PSD of the system affects the stability of the system over this time period due to the increased reactivity observed within the blends containing the finer GGBS material. Resulting in the presence of hydration products such as C-S-H which occupy less space than water or cement. Therefore, a higher Calumite content system produces fewer hydration products causing less shrinkage. This is supported by XRD data for 28 day samples presented in Chapter 6, where it was found that as the GGBS content increases the degree of hydration is

greater, leading to increased formation of C-S-H causing further shrinkage. It has also been reported that shrinkage in systems containing slag show greater shrinkage compared to PC equivalents [35, 145]. This is due to increased sensitivity to water loss and a higher porosity inducing shrinkage within the hardened materials [146]. This again agrees with the blends under investigation, where the P0 is predominantly controlled by the PC fraction and shows least shrinkage compared to the other systems containing GGBS that is causing a change in stability.

In terms of the nuclear industry, an acceptable amount of change is considered to be within a 2000 (µm/m) strain range which represents a movement of 0.2 % expansion/shrinkage [147]. All of the products cast, sit comfortably within this range and can therefore be considered a usable system. They also show comparable results to data published during other studies [146, 148, 149].

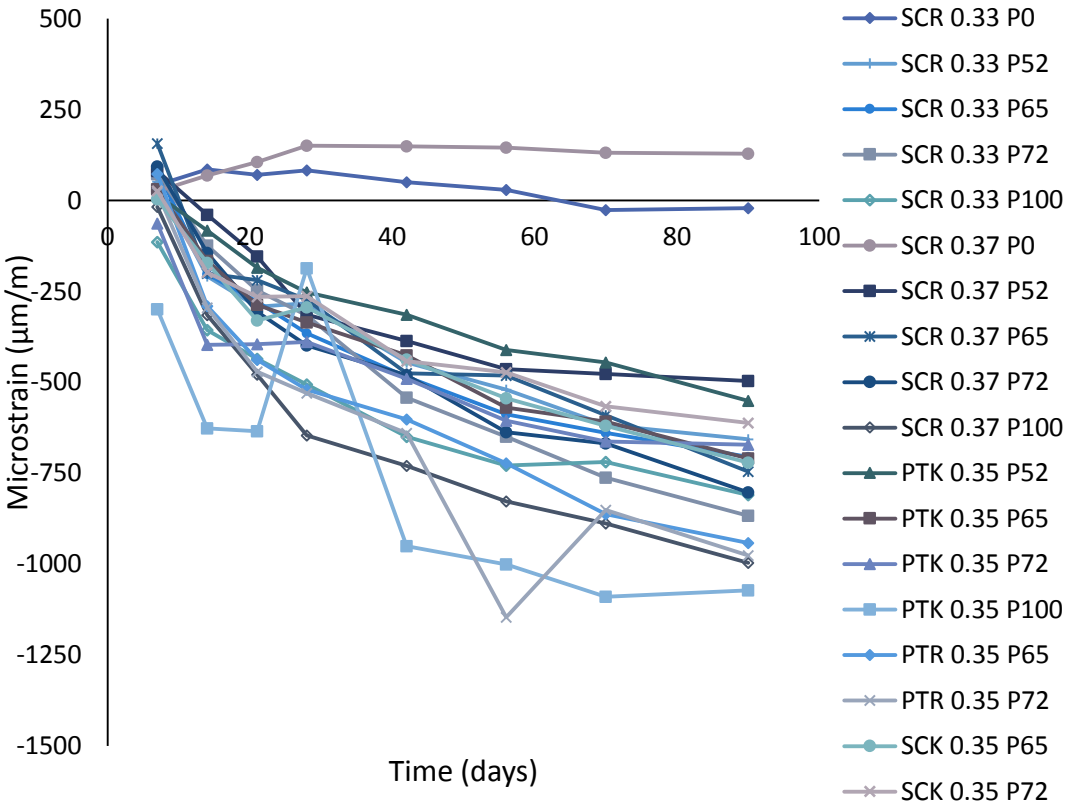

Figure 8.8. Dimensional stability data for mixes that consider different powders sources, combinations and w/s contents from Table 8.1 at a 3:1 BFS:PC ratio and 0.35 w/s content over 90 days.

The dimensional stability results for all of the mixes from Table 8.1 are shown in Figure 8.8. This data highlights that regardless of the powder source, formulation combination or w/s ratio, all of the prisms tested did not exceed the expansion and shrinkage limits.

The P0 system for both the 0.33 and 0.37 w/s content mixes show the same trend as the 0.35 w/s system, where the shrinkage is very little, and so there are higher strain values. As with the Scunthorpe GGBS:Calumite:Ribblesdale PC systems, the general trend shows initial shrinkage before stabilising between 42 and 56 days.

8.2.1.5 Rheometry

Similarly to the small scale trials described in Chapter 4, shear rate-shear stress measurement were recorded for each of the mid-scale 3 Litre trials. The measurements were recorded using a Lamy Rheology RM200 rheometer on samples taken following the initial 20 minute mix period (i.e. t=0). The results for the 10 formulations from Table 3.4 (Chapter 3) at a 3:1 BFS/PC ratio and 0.35 w/s content are presented in Figure 8.9.

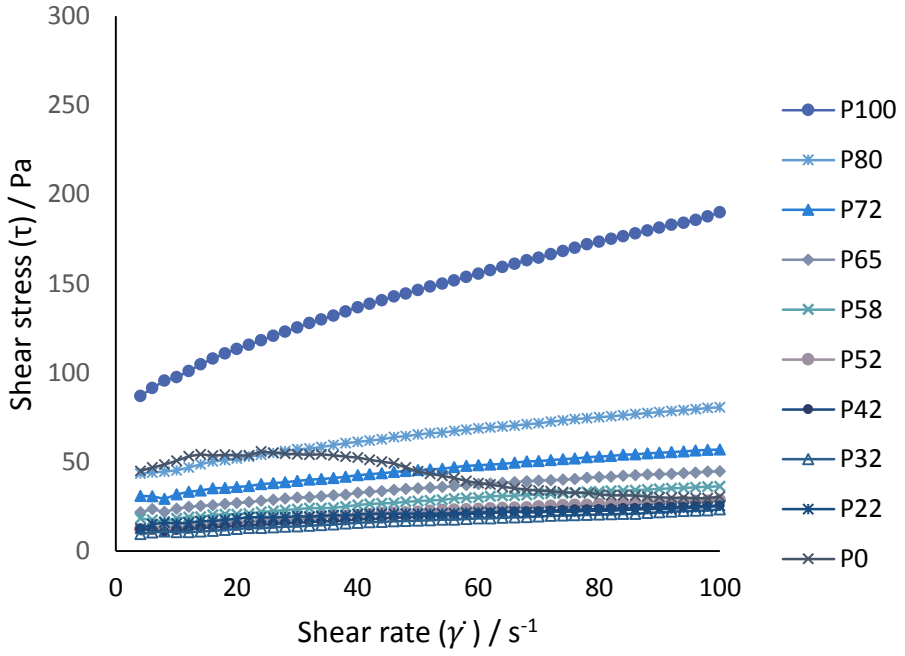

Figure 8.9. Rheometer data for all 10 GGBS:Calumite SCR blends at a 3:1 BFS:PC ratio and a 0.35 w/s content (3 Litre trials).

The results found at mid-scale are very comparable to the data obtained at small scale, discussed in Chapter 4. All 10 formulations follow the Bingham model fairly well but as the Calumite content increases, the results start to deviate from the linear part of the ideal. Similarly, to the small scale trials, the P0 system deviated from the Bingham model and falls out of trend. This was also observed for P0 at a 0.33 and 0.37 w/s content, shown in Figures 8.10 and 8.11 (measured on a smaller selection of formulations).

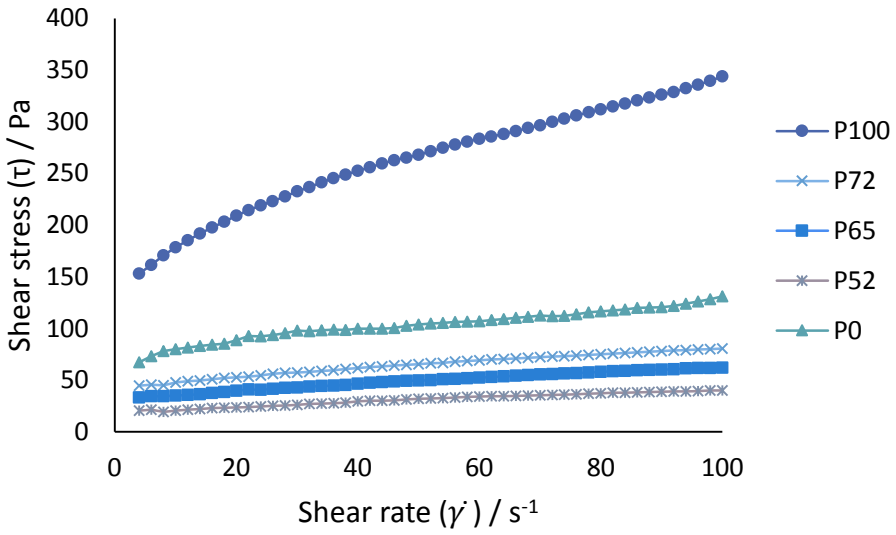

Figure 8.10. Rheometer data for 5 blends of GGBS:Calumite SCR at a 3:1 BFS:PC ratio and a 0.33 w/s content (3 Litre trials).

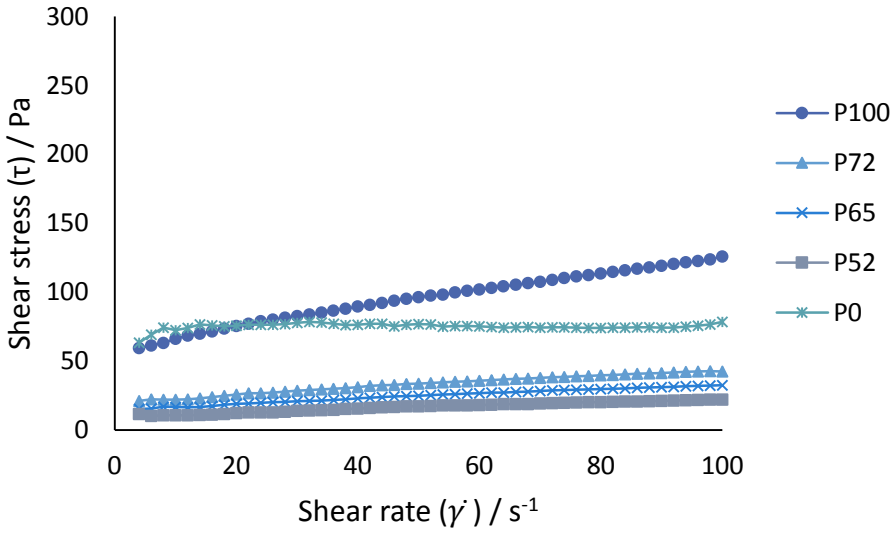

Figure 8.11. Rheometer data for 5 blends of GGBS:Calumite SCR at a 3:1 BFS:PC ratio and a 0.37 w/s content (3 Litre trials).

The yield stress was calculated for each of the formulations and the results are shown in Table 8.2. As the Calumite content increases the yield stress decreases, this is true until blends P22 and P0. These results confirm the divergence from the Bingham model observed in Figures 8.9 and also replicate the data observed at small scale. Another interesting observation is that the yield stress values obtained here are very comparable to those recorded on a different instrument at small scale. This suggests that the method used was appropriate for the material being measured and that smaller scale samples can be used to predict yield stress.

Table 8.2. Yield stress values measured by extrapolation of the Bingham model for a selection of the GGBS:Calumite blends at a 3:1 BFS:PC and a 0.33, 0.35 and 0.37 w/s ratios (3 Litre batch trials). Values in italics are considered unphysical or unreliable.

Mix	Yield Stress (Pa)		
	0.33	**0.35**	**0.37**
P100	171.7	92.5	61.8
P80		44.4	
P72	45.6	30.5	21.1
P65	33.5	22.4	15.2
P58		17.1	
P52	19.8	12.6	9.9
P42		11.2	
P32		9.8	
P22		*15.9*	
P0	*77.0*	*58.8*	*74.6*

As part of the 'acceptance mix' procedure, the 3 litre batch formulations were mixed or 'held-up' for 150 minutes following the initial mixing period. During this time, aliquots of cement paste were taken at 30 minute intervals to monitor the rheology of the system.

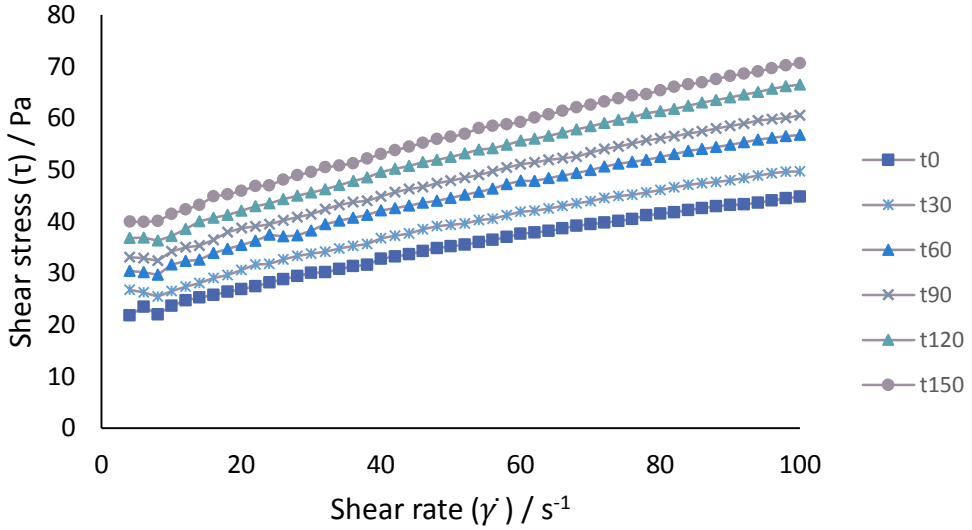

Figure 8.12. Rheometer data for P65 (GGBS:Calumite) at a 3:1 BFS:PC ratio and a 0.35 w/s content at t=0, 30, 60, 90, 120 and 150 minutes (3 Litre trial).

The rheometer results are shown in Figure 8.12 and the correlating yield stress values are presented in Table 8.3.

Table 8.3. Yield stress values measured by extrapolation of the Bingham model for blend P65 (GGBS:Calumite) at a 3:1 BFS:PC and a 0.35 w/s ratios at t=0, 30, 60, 90, 120 and 150 minutes (3 Litre batch trials).

Time (minutes)	Yield Stress (Pa)
0	22.4
30	25.6
60	29.7
90	32.4
120	35.8
150	39.4

As the length of the grout mixing time increases, the yield stress also increased. This is to be expected because fluidity is lost as the 'hold-up' time increases due to chemical reaction and shear thickening. It appears to occur in a linear manner suggesting there isn't a sudden increase in the yield stress over the required acceptance mix period. This trend is observed across all of the 10 GGBS:Calumite blends with the exception of the P0 system. As with many of the other results, the P0 system produces inconsistent unreliable data.

Overall, the rheology of the system behaves very similarly from small to mid-scale. Therefore, going forward, small/bench scale trials could be used with confidence to predict the yield stress of the systems and as such removing the need for trials using large masses of material.

8.2.2 Plant Scale Trials

The full scale trials were carried out in 500 L drums using stainless steel tubes cut into lengths of ca. 50 mm and partially crimped at the ends as simulant waste to mimic THORP hulls produced from reprocessing. It was clear from the Diamond Light Source grout infilling data described in Chapter 7, that at typical plant fluidities vibration was required for successful encapsulation of the Magnox swarf but may not be as crucial for the THORP hulls. Therefore, to fully investigate the results observed at small-scale, the wasteform was produced without vibrogrouting and used THORP hulls as a simulant. The drums were filled with simulant prior to infill, as shown in Figure 8.13.

Figure 8.13. Image of 500 L drum filled with simulant THORP hulls prior to infilling.

Two large scale trials were carried out at a 3:1 BFS:PC ratio and at a 0.35 w/s content. Although this is not the set point used on plant, it is the ratio that has been used throughout this project and therefore provided a direct comparison between small and large scale results. Continuity of the project was also the reason that one of the cement grouts used was based on the Scunthorpe GGBS:Calumite:Ribblesdale PC (SCR) formulation. The second formulation was a blend of Port Talbot GGBS:Calumite:Ketton PC (PTK) because it is the current formulation being used on plant. In terms of the ratio of GGBS:Calumite used, ideally the optimum blend would have been predicted using the model described in Chapter 5 with further testing to confirm its performance. However, this did not prove a reliable enough method, and therefore the logical blend to take forward from results obtained in this project was the P65 blend. Even though the Port Talbot:Calumite blend is used at a 70:30 ratio on plant, the P65 GGBS:Calumite blend was used for both trials in order to get a direct comparison between the powders. The infill process was carried out using the same parameters stated in the plant settings manual [54] and therefore provides a direct comparison to wasteforms produced on site, with the exception of vibrogrouting. The infilling for both trials took ca. 12.5 minutes; both were carried out on the same day and were left to cure for 7 days at 25 ˚C.

As with the mid-scale mixes, fresh state properties of the cement grout used were measured during the trial, data shown in Table 8.4. The Colflow results measured for the large scale trials were much lower than the equivalent at mid-scale. The SCR and PTK

systems achieved Colflows of 650 and 680 mm respectively in the 3 litre mixes compared to 480 and 530 mm at large scale. This difference from medium to large scale is likely due to different mixing intensities, transfer times and most likely the change in the amount of cement being mixed in one batch. It is well reported that the hydration kinetics, rheological features and agglomeration of cement pastes are affected by different speed and intensities of mixing [150-153]. More vigorous mixing of the cement paste leads to greater hydration. Although a substantial difference is observed during scale up, the coarser PTK system still achieves a higher fluidity compared with the SCR formulation, which agrees with results observed at small scale. Therefore, the behaviour and effect of the PSD on the cement grout remains consistent regardless of scale but this observed loss of fluidity in large-scale trials should be taken into account when choosing the correct GGBS to Calumite blend.

Table 8.4. Fresh state properties of the two large scale trials.

Mix Reference	w/s	Bleed at 24 hours in 100 mL (vol. %)	Colflow (mm)		Setting (hrs)	
			t = 0	t = after infill	Initial	Final
SCR 0.35 P65	0.35	0	480	470	<24	<24
PTK 0.35 P65	0.35	2 (0 at 48 hrs)	530	530	<24	<24

The bleed of the large scale products was recorded (using the same method as mid-scale) and replicated the results observed at mid-scale, where no bleed was seen for the SCR system but a small amount of bleed was observed for the PTK mix. When the products were cast, the surface of the samples were covered to prevent evaporation and when the products themselves were checked at 24 hrs, there was no settlement of water observed on either wasteform, as shown in Figure 8.14. In terms of setting time, the results show an agreement between the mid and large scale trials where, both systems set within the desired 24 hours. Due to the similarity in the results observed for these physical properties during scale up experiments, it confirms the suitability of the chosen test methods and their reliability.

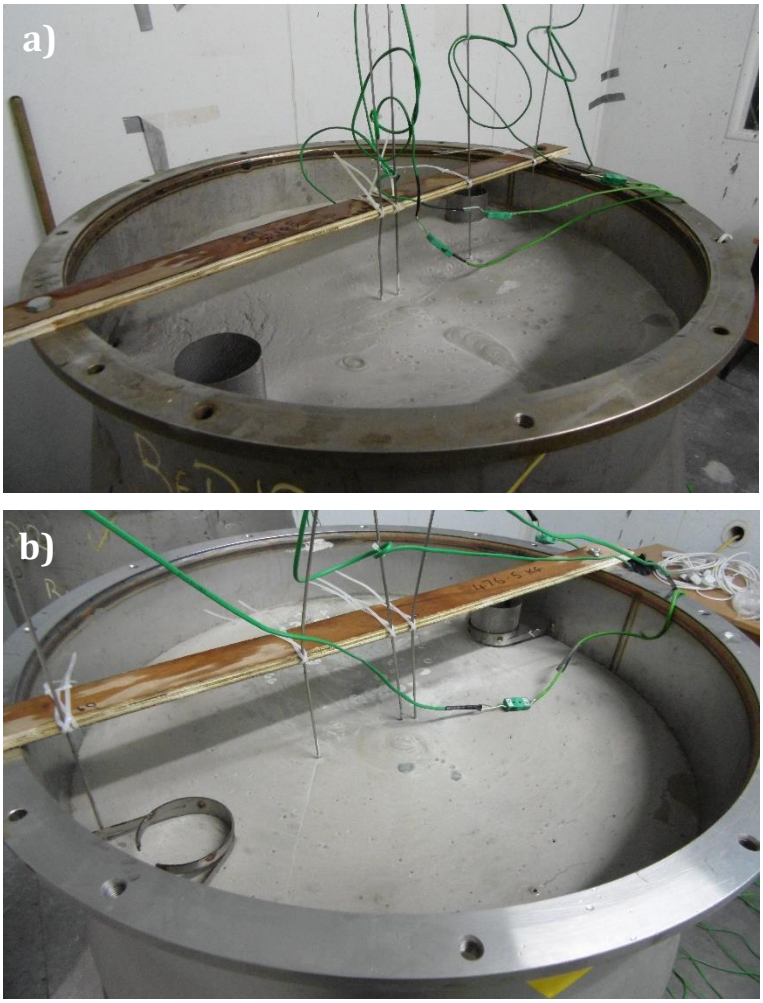

Figure 8.14. Image of drums infilled with a)Scunthorpe:GGBS:Calumite:Ribblesdale PC and b)Port Talbot GGBS:Calumite:Ketton PC after 24 hours curing at 25 ˚C.

Figure 8.14 shows that thermocouples were inserted into the drums before the infill in order to monitor the heat evolution of the products over a 120-hour period. Four thermocouples were placed into each drum; two at the centre point, one at the edge of the drum and one mid-way between the two (the 'mid-point'). The measurements were taken from half way down the drum, i.e. about 500 mm below the top of the hulls. The temperature profiles obtained for the products are shown in Figure 8.15. The data obtained provide a good indication of the hear evolution during the cement setting reaction within such a large mass of cement. If the centre points of both drums are considered, the SCR system shows a higher peak heat temperature closer to 70 ˚C compared to the PTK product, which is just below 60 ˚C. This is sensible in terms of PSD contribution, because the fineness of the SCR system causes increased reactivity and resulted in a higher thermal output. Both systems illustrate that there is very little

difference in terms of thermal output between the very centre of the product and the mid-point.

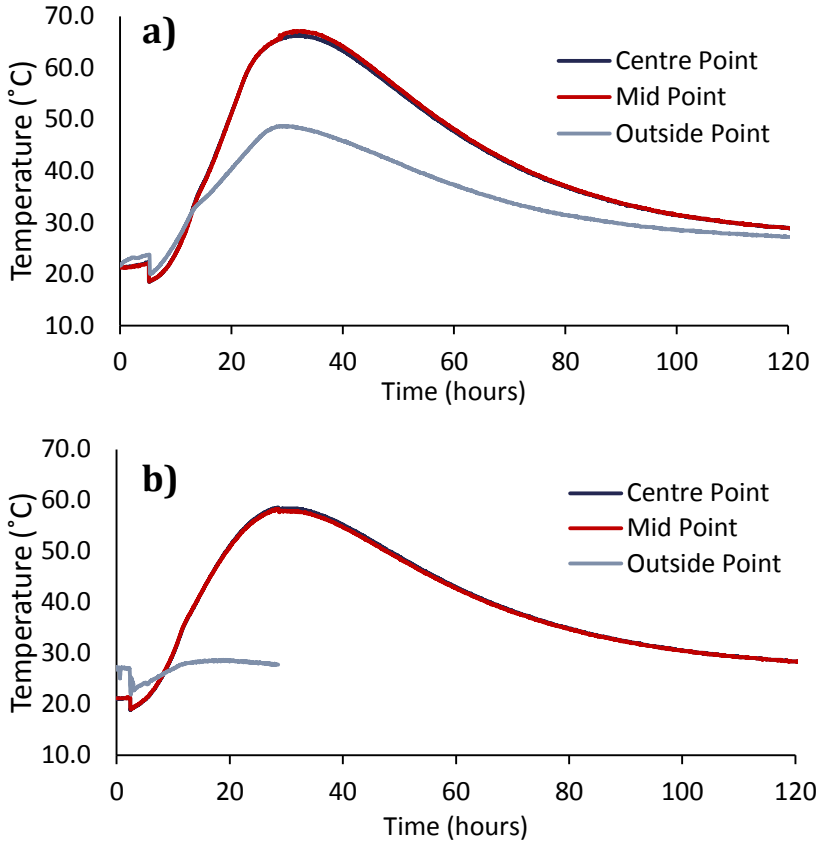

Figure 8.15. Temperature profiles of large scale products containing a) SCR and b) PTK cement grout formualtions at a P65 GGBS:Calumite blend, a 3:1 BFS:PC ratio and a 0.35 w/s content.

This is not the case for the outer point where a significant drop in temperature was observed. Unfortunately, the outer thermocouple in the PTK system failed and therefore the data were lost after 30 hours. The SCR system shows a peak heat difference of 20 °C at around 30 hours before both temperature profiles return down to the curing temperature. One primary concern due to this difference in temperature would be the effect thermal stress could have on the wasteform. Thermal expansion of the metal simulant could potentially cause cracking of the cement as it sets due to movement. Following the seven day curing period, the products were cut in half using a diamond wire saw and photographs of the set wasteforms are shown in Figure 8.16 and 8.17.

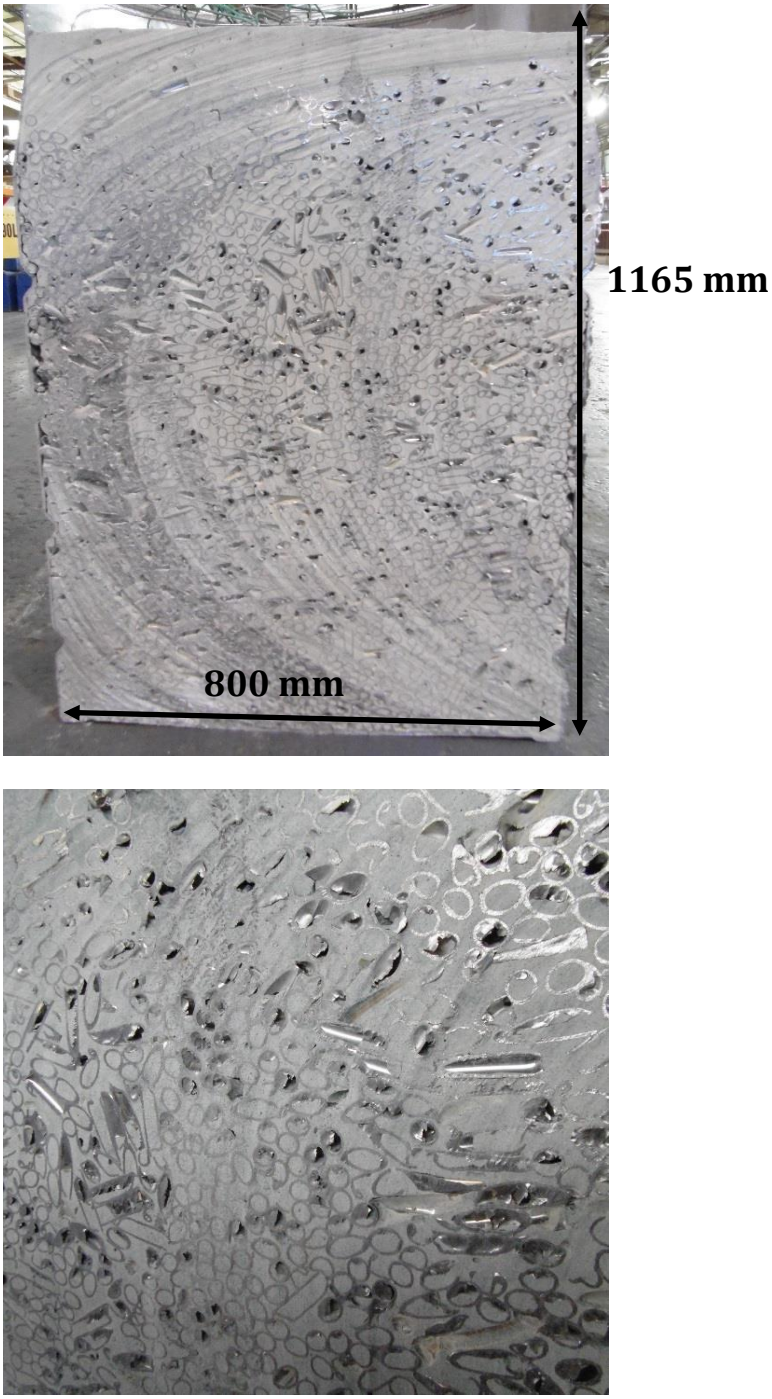

Figure 8.16. Cured 500 L sample drum of Scunthorpe GGBS:Calumite:Ribblesdale PC cement system cut in half.

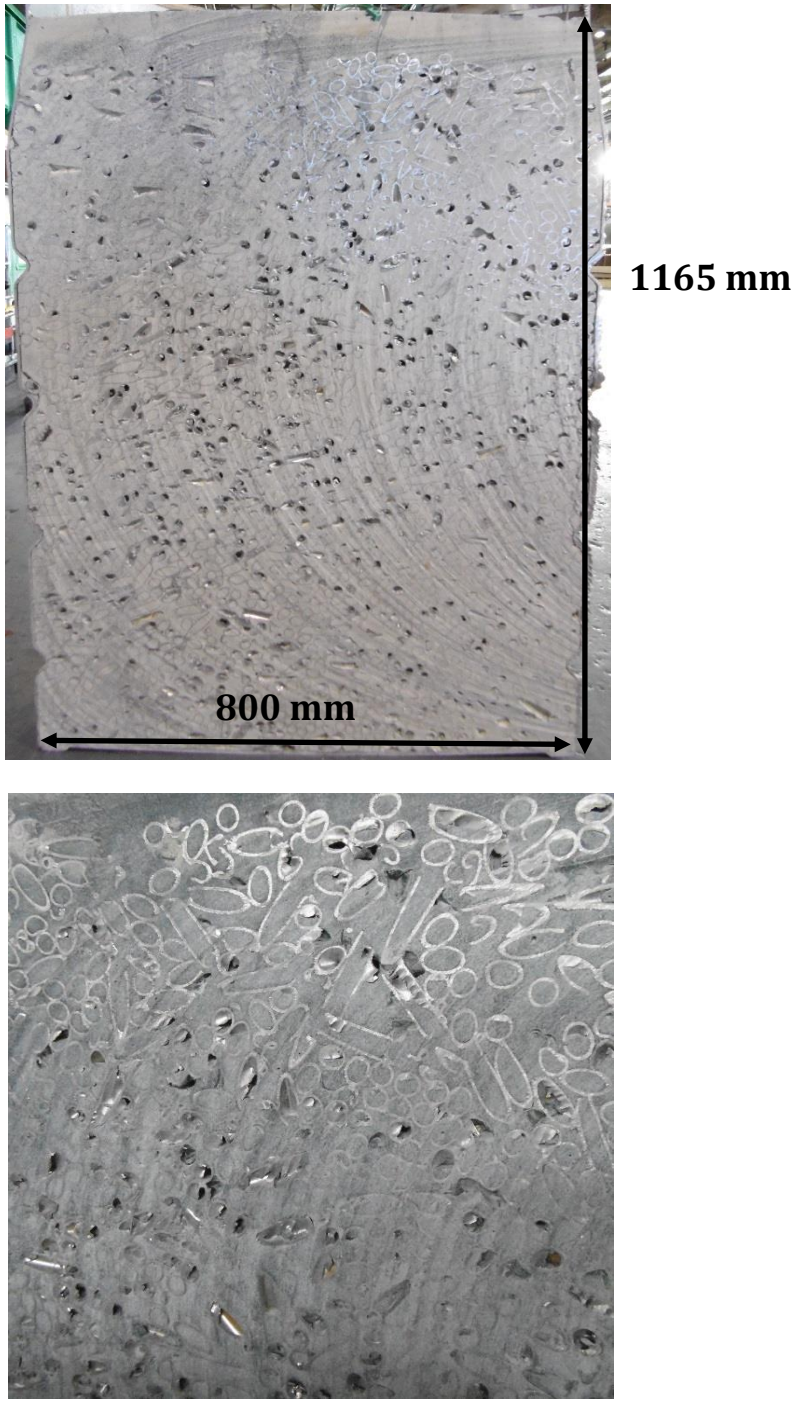

Figure 8.17. Cured 500 L sample drum of Port Talbot GGBS:Calumite:Ketton PC cement system cut in half.

The images show that there are no major signs of cracking, suggesting that any thermal stress caused by the metal simulant was minimal. Thermal cracking can be seen in mass cement forms which can also be caused by temperature change. This is when the maximum difference in temperature is exceeded and contraction due to cooling at the surface of a sample causes thermal cracking [154]. Although a change in temperature

was observed within both of the large scale products from these trials, it did not appear to cause any defects in the wasteforms. The photographs illustrate that both samples have infilled very well. Although there are some visible voids, the majority of the simulant THORP hulls have encapsulated fully, which agrees with the results observed from the radiography experiments described in Chapter 7. This confirms the possibility of not vibrogrouting in the future if this becomes difficult during remote handling operations.

During the large scale trials, 100 mm cubes were cast from the two grout mixes used. The cubes were cured at 20 ˚C and the compressive strength was measured in duplicate at 2, 7, 28 and 90 days. The results are shown in Figure 8.18 for both the SCR and PTK systems.

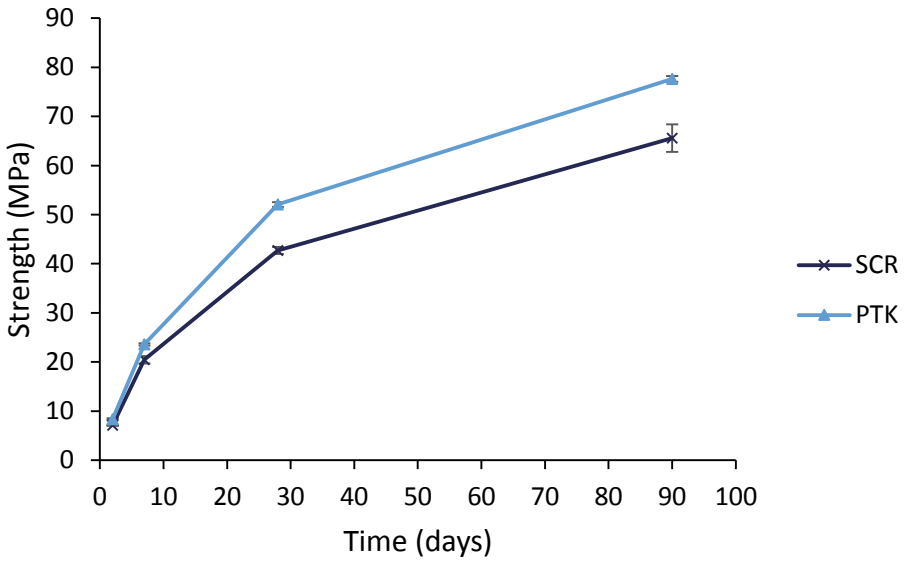

Figure 8.18. Compressive strength development of Scunthorpe GGBS:Calumite:Ribblesdale PC compared to Port Talbot GGBS:Calumite:Ketton PC over 90 days.

The data in Figure 8.18 show that the Port Talbot GGBS based grout achieved higher compressive strength at all ages compared to the Scunthorpe GGBS formulation. Therefore, although the SCR system would be expected to be more reactive due to the finer particles, the wider PSD range produced a stronger product. The main difference, from a PSD perspective, between the two formulations is that there is more overlap of particles around 100 μm within the Port Talbot GGBS:Calumite system compared to the Scunthorpe GGBS equivalent. This suggests that although gap-graded powders do

produce cement products that show reasonable strength, the sample strength is improved by using a less severe bimodal distribution.

8.3 Conclusions

In this chapter, the effects of the scale-up of the GGBS:Calumite:PC formulations are discussed following a series of tests carried out at mid and large scale. In order to determine whether a cement grout conforms to the requirement specification stated by the nuclear industry, all of the 3 litre mixes were subject to an acceptance test which provided performance criteria on the fluidity, setting time and bleed of the systems. The fluidity results obtained for the 10 baseline GGBS:Calumite blends correlate with the data collected at small scale, where in general, as the Calumite content increases, the fluidity of the system improves, until a point when the fluidity begins to decrease again. This is in agreement with the small scale trials. However, the optimum fluidity was achieved at P32 in the mid-scale trials compared to P22 in small scale experiments. In terms of w/s content, upon increasing the w/s ratio, the fluidity increased in concurrence with the small scale trials. A direct comparison was made between the different powder sources using the P65 blend, which demonstrated that there was very little change in the fluidity as a result of different supplies of powder. Although, it did highlight that the current formulations used on plant are much more fluid compared to those based on the powder used historically. As part of the acceptance test, the mixes were subjected to a 150 minute hold up time to observe how the material would behave if for some reason the cement grout could not be used immediately on plant. In terms of fluidity, there is a consistent decrease observed across all of the formulations, to the point where it was not possible to achieve a measurement at all. The P100 – P65 blends from the 10 baseline formulations showed no bleed after 24 hours, whereas the P58 - P0 mixes produced a small amount of bleed which was not visible on the final sample taken at 150 minutes hold-up. The exception to this was the P0 blend, whereby high water segregation was noted and bleed was still observed on the final sample. When comparing the mixes with different powder sources, the mixes containing Port Talbot GGBS showed a small amount of bleed initially but this was not present in the final samples. All of the mix formulations investigated in this chapter conformed to the Sellafield specification in terms of setting times and all achieved final set within 24 hours.

Alongside the acceptance test, the cement grouts were also tested for dimensional stability where prisms were cast and monitored over the course of 90 days. Generally,

the products showed a small amount of shrinkage but they all stayed within the limits considered suitable for nuclear waste encapsulation.

Finally, large scale trials were conducted resulting in products that are direct replicas of the wasteforms that for which the cement systems investigated in this project are utilised. The two formulations chosen for these trials were a Scunthorpe GGBS:Calumite:Ribblesdale PC for continuity of this project as a whole and a Port Talbot GGBS:Calumite:Ketton PC, because they are the powders currently used on plant, at a P65 PSD blend. The cement grouts produced during these trials were also tested in their fresh states. There was a substantial loss in fluidity for both systems at larger scale compared to the mid-scale trials and as such this should be taken into consideration when deciding on future grout formulations. No bleed was observed on the large products at 24 hours, suggesting the PSD of the system was optimum for the water content used. The heat output was monitored using thermocouples and revealed a difference in temperature between the centre of the drum compared to the outer point of the sample. However, after the samples were cured for 7 days, they were cut in half and no visible cracking was observed, suggesting the product did not experience thermal stress regardless of the temperature difference. Simulant THORP hulls were used during these trials as they were not going to be vibrated as a result of the data obtained during the tomography experiments, and the drums were cut in half which allowed visible analysis of the infill success. Both drums displayed very good infill, suggesting that if in the future the industry would like to remove vibrogrouting from the encapsulation process, that it is a viable option.

Overall, this chapter has shown that the effect of PSD on cement grout performance is consistent between small, mid and large scale trials. However, there are some differences in where the optimum balance of fine and coarse powders lies, which should be taken into consideration when varying the PSD of the system.

9 Conclusions

The main objective of this work was to investigate the optimisation of blends of blast furnace slag and Portland cement for the immobilisation and encapsulation of nuclear waste. This was achieved by investigating varying formulations of BFS and PC, where the BFS fraction comprises of GGBS and Calumite. The BFS components have a very similar chemical composition, but their particle size differs significantly where the GGBS powder contains particles that are sub 100 μm in size, compared to Calumite, which comprises material between approx. 40 to 1800 μm. The reason behind this project is that the powder used historically became unavailable, and as such the supply of cement powders to the nuclear industry has been inconsistent. The powders and cement grouts used for encapsulation have to conform to strict performance specifications and must exhibit certain properties.

One feature that is for certain, is that any blend of GGBS, Calumite and PC will produce a bi-modal particle size distribution. The effect of this particle size contribution was investigated by changing the blend ratio of GGBS:Calumite within the BFS fraction, and the performance of various cement grouts was recorded. Following a series of fresh state test methods a series of trends were observed. It was found that as the GGBS content increases, the yield stress and the packing density of the blend systems increased, whilst the fluidity subsequently decreased. In addition, to the effect of particle size of the cement powders used, the consequence of altering the w/s ratio was also monitored throughout the project. It was found that, as the w/s ratio was increased, the yield stress and particle packing density decreased, whilst the fluidity increased. The exception to this is the P0 (i.e. 100 wt. % Calumite) blend, which consistently falls out of trend and is unpredictable or under performs. This is due to the large particles in the material, highlighting the requirement and importance of incorporating both GGBS and Calumite cement powders.

An important conclusion drawn from these experiments was with regards to measuring yield stress. It was shown that the value for yield stress obtained from the mini-slump tests and the vane method were very comparable, providing confidence in the results reported, especially considering the difficulty reported in literature with measuring yield stress.

In conjunction with experimental methods, two models were used to predict the yield stress of the cement formulations under investigation. Unfortunately, neither model was considered to produce consistent and reliable yield stress values and as such are not

suitable to be used as a predictive tool for this project. However, the results did illustrate the complexity of the cement powder system under investigation, and that a model that has worked for other materials is not suitable for the bimodal distribution of the GGBS and Calumite blend.

A significant amount of heat of hydration data was collected for the GGBS:Calumite:PC system. The isothermal conduction calorimetry data collected, demonstrated that altering the blend of finer and coarser material affects the heat evolution of the cement pastes as well as the chemical reaction. As the GGBS content increases, the rate of hydration is accelerated. The hydration reaction is also affected by elevated temperatures, whereby the peak heat of reaction occurs much more rapidly as the temperature increases. By using quartz as a replacement for the Calumite fraction (ground to the same particle size) it was possible to understand the contribution of the GGBS powder to the hydration reaction. The results revealed that the Calumite fraction contributed very little to the overall hydration reaction.

Semi-adiabatic calorimetry was also used to monitor the heat evolution, as it is the current standard method to monitor the heat of hydration in the UK. The results correlate closely with the isothermal calorimetry data but in general are slightly less consistent. Due to the large amount of experimental data collected using both calorimetry methods, it was possible to draw comparisons between the techniques. It was concluded that a positive correlation was achieved between the two methods, which supports the use of isothermal calorimetry as a future standard method to measure the heat of hydration of cementitious materials for the nuclear industry.

The main driver for understanding the effect the particle size of cement powders has on the physical performance is to achieve successful encapsulation of nuclear waste. Two aspects of the infill process were investigated using beamline-based analysis. The in-situ experiments demonstrated that the stiffer BFS/PC paste with a high surface area does not infiltrate the simulant waste and just set at the top of the can, compared to the GGBS:Calumite P65 blend, where the cement paste infilled fluidly to the bottom of the can. During these experiments, a different powder source was included, the results showed that the Port Talbot GGBS achieved a lower voidage overall compared to the Scunthorpe GGBS, which is likely due to the Port Talbot GGBS having a broader PSD. The trials also illustrated that the orientation of the simulant THORP hulls has a significant effect on the success of the encapsulation regardless of the cement formulation used. The hulls that settle in a vertical orientation within the sample were more successfully infilled.

Tomographic analysis performed at the Diamond Light Source, was used to reconstruct 3D images of hardened samples that were prepared using different parameters containing simulant nuclear waste. The data revealed that as the Calumite content decreases, the voidage observed in the sample increases. This trend was observed across the different powders sources investigated. The main outcome from these results was to determine the effect of vibration and non-vibration of the samples once they were poured. Vibrogrouting is an additional step in the encapsulation process and it was observed that for the samples containing Magnox swarf simulant, vibration was essential to ensure minimal voidage was achieved. However, if the correct cement formulation is used, there is the potential to remove the vibration step for samples containing THORP hull simulant. This would be advantageous for the plant process due to the remote handling environment, where any adjustments or repairs to the system is very problematic.

One of the most significant aspects of this project was the application of the research at plant scale. The formulations stated in Chapter 3 were tested at small (200 mL), mid (3 L) and large scale (500 L) providing data illustrating the effects observed when up-scaling the grout mixes from laboratory to plant size. During the mid-scale trials, the fluidity of the systems was tested and the trends observed correlated with the data collected at small scale. In general, the fluidity of the systems improves at the Calumite content increases until a point, when its starts to decrease again. This optimum fluidity was achieved with the P32 system in the mid-scale trials compared to P22 in the small laboratory experiments. A comparison between different powder supplies displayed very little change in the fluidity, confirming that changing the supplier should not affect the physical properties significantly. It did highlight that the powders currently used on plant are much more fluid compared to the Redcar material that was used historically. This suggests that the bimodal powders flow more when compared to the Redcar material, which is closer to a monosized material. The PSD also affects the bleed in the system which is related to the particle packing of the system, where the Redcar material produced more bleed than bimodal BFS powders. For a bimodal system, the smaller particles pack in between the larger particles allowing for more flow, whereas the monosized powder does not pack as successfully due to the narrow particle size distribution.

Two large scale trials were conducted using the 3:1 BFS:PC formulation that has been used throughout this project. Both trials were carried out using THORP hulls simulant waste, and following the recommendation from the Diamond Light Source infilling

results, the drums were not vibrated to fully understand the effect of removing the vibrogrouting step in the encapsulation process. At the time of casting the simulant wasteforms, the grout used was tested for fluidity to monitor effects of mixing, and a significant loss of fluidity was observed compared to the small scale trials. Nonetheless, the cement grouts infilled successfully to the correct encapsulation level required on plant, but this needs to be taken into consideration when collecting data at small scale. The large scale products were cut in half following 7 days of curing. No visible cracking was observed suggesting there was no thermal stress in the products regardless of the temperature difference observed between the peripheral and centre of the drums. Both drums also displayed very good infill, suggesting that the removal of the vibrogrouting step in the encapsulation process could be possible in the future.

Overall, the experiments carried out throughout this project demonstrate that altering the particle size distribution significantly changes how the resulting cement formulation behaves and, ultimately the wasteform produced. A blend of the finer GGBS and coarser Calumite is essential because during all of the test methods used, the P100 and P0 systems consistently under-performed. By investigating different powders, it was demonstrated that providing the chemical composition is similar, the particle size controls a large proportion of the performance properties and as such, the PSD should be the main focus when using new or alternative powders. As a result of using multiple analytical and data acquisition techniques throughout this project, including scale-up trials, it is possible to conclude that the optimum blend of GGBS:Calumite is between P72 and P58, where the balance is weighted in favour of the finer material but there are sufficient coarser particles to conform to the Sellafield specification.

Future work in this area would be to produce a model that is applicable to the bimodal distribution and material used in this project. It would then be possible to predict the optimum PSD of a cement powder that would achieve the optimal performance properties. Alongside this, experimental test methods used here on small scale could be applied to smaller increments of GGBS:Calumite, because the general trend from small to large scale was very similar, suggesting small scale laboratory tests are reliable.

10 References

[1] P.D. Wilson, *The Nuclear Fuel Cycle From Ore to Waste*, Oxford University Press, Oxford, **1996**.

[2] Nuclear Decommissioning Authority, Department for Business Energy & Industrial Strategy, *Radioactive Wastes in the UK: A Summary of the 2016 Inventory,* Prepared by Amec Foster Wheeler plc and Pöyry Energy Limited, **2016**.

[3] Nuclear Decommissioning Authority, Department for Business Energy & Industrial Strategy, *Radioactive Wastes in the UK: UK Radioactive Waste Inventory Report,* Prepared by Amec Foster Wheeler plc and Pöyry Energy Limited, **2016**.

[4] G.A. Fairhall, J.D. Palmer, The Encapsulation of Magnox Swarf in Cement in the United Kingdom, *Cement and Concrete Research*, 22, **1992**, pp. 293-298.

[5] G.A. Fairhall, R.W. Asquith, The Evolution of Waste Management Processes and Tehcnologies in BNFL, *International Conference on Future Nuclear Systems*, Japan, **1997**.

[6] G.A. Fairhall, J.D. Palmer, The Evaluation of the Properties of Immobilised Intermediate Level Wastes, *Radioactive Waste Management*, USA, **1987**, 9.

[7] G.A. Fairhall, W. Heafield, *The Conditioning and Storage of Intermediate Level Waste in the UK,* BNFL,

[8] J.H. Sharp, J. Hill, N.B. Milestone, E.W. Miller, *Cementitious Systems for Encapsulation of Intermediate Level Waste* The 9th International Conference on Radioactive Waste Management and Environmental RemediationOxford, England, **2003**.

[9] M.J. Angus, I.H. Godfrey, M. Hayes, S. Foster, *Managing Change in the Supply of Cement Powders for Radioactive Waste Encapsulation - Twenty Years of Operational Experience*, WM2010Phoenix, , **2010**.

[10] Department of Energy & Climate Change, *Implementing Geological Disposal,* **2014**.

[11] Nuclear Decommissioning Authority, *Geological Disposal Package Evolution Status Report,* NDA/RWMD/031, **2010**.

[12] G.M. Cann, B.H. Mcluckie, *Assessment of Alternative Blast Furnace Slag Supply from Scunthorpe Works,* NNL, NNL (10) 10660, **2010**.

[13] L. Gardner, K. Carruthers, *Assessment of the Suitability of Alternative Slags as Constituents of Sellafield Specification Blast Furnace Slag,* NNL, NNL (13) 12814, **2013**.

[14] J.W. Phair, Green chemistry for sustainable cement production and use *Green Chemistry*, 8, **2006**, pp. 763-780.

[15] British Geological Survey, *Cement - Mineral Planning Factsheet,* BGS, **2014**.

[16] H.F.W. Taylor, *Cement Chemistry*, Academic Press Inc., USA, **1990**.

[17] The British Standards Institution, *Cement*, Part 1: Composition, specifications and conformity criteria for common cements, **2011**, 197-1.

[18] M. Schneider, M. Romer, M. Tschudin, H. Bolio, Sustainable cement production—present and future, *Cement and Concrete Research*, 41, **2011**, pp. 642-650.

[19] E. Lang, *Structure and Performance of Cements*, 2 ed., Spon Press, USA, **2002**.

[20] *Achieving the Goal of Zero-Waste,* Worldsteel fact sheet, **04/08/2014**.

[21] J.-h. Wang, Q.-r. Chen, Y.-l. Kuang, A.J. Lynch, J.-w. Zhuo, Grinding process within vertical roller mills: experiment and simulation, *Mining Science and Technology (China)*, 19, **2009**, pp. 97-101.

[22] N.A. Aydoğan, H. Benzer, Comparison of the overall circuit performance in the cement industry: High compression milling vs. ball milling technology, *Miner. Eng.*, 24, **2011**, pp. 211-215.

[23] H. Wan, Z. Shui, Z. Lin, Analysis of geometric characteristics of GGBS particles and their influences on cement properties, *Cement and Concrete Research*, 34, **2004**, pp. 133-137.

[24] N.C. Collier, *Assessment of Coarse Ground Ordinary Portland Cement Variability,* NNL, NNL (13) 12664, **2013**.

[25] F.T. Olorunsogo, Particle size distribution of GGBS and bleeding characteristics of slag cement mortars, *Cement and Concrete Research*, 28, **1998**, pp. 907-919.

[26] W. Simpson, Calumite slag as a glassmaking raw material for the increase of furnace productivity, *Glass Technology*, 17, **1976**, pp.

[27] N.J. Marriot, *Reduce Furnace Energy Consumption Using Calumite,* Calumite Ltd., UK,

[28] G.M. Cann, K. Carruthers, B.H. McLuckie, J. Borwick, *Scunthorpe GGBS/Calumite blend assessment for use in ILW encapsulation processes,* NNL, NNL (11) 11306, **2011**.

[29] B. Klemczak, M. Batog, Heat of hydration of low-clinker cements, *Journal of Thermal Analysis and Calorimetry*, 123, **2016**, pp. 1351-1360.

[30] J.W. Bullard, H.M. Jennings, R.A. Livingston, A. Nonat, G.W. Scherer, J.S. Schweitzer, K.L. Scrivener, J.J. Thomas, Mechanisms of cement hydration, *Cement and Concrete Research*, 41, **2011**, pp. 1208-1223.

[31] P.C. Hewlett, *Lea's Chemistry of Cement and Concrete*, 4 ed., Elsevier Science & Technology Books **2004**.

[32] B. Kolani, L. Buffo-Lacarrière, A. Sellier, G. Escadeillas, L. Boutillon, L. Linger, Hydration of slag-blended cements, *Cement and Concrete Composites*, 34, pp. 1009-1018.

[33] M. Ben Haha, B. Lothenbach, G. Le Saout, F. Winnefeld, Influence of Slag Chemistry on the Hydration of Alkali-Activated Blast-Furnace Slag — Part II: Effect of Al2O3, *Cement and Concrete Research*, 42, **2012**, pp. 74-83.

[34] S. Liu, W. Han, Q. Li, Hydration Properties of Ground Granulated Blast-Furnace Slag (GGBS) Under Different Hydration Environments, *Materials Science*, 23, **2017**, pp.

[35] Z. Jia, Y. Yang, L. Yang, Y. Zhang, Z. Sun, Hydration products, internal relative humidity and drying shrinkage of alkali activated slag mortar with expansion agents, *Construction and Building Materials*, 158, **2018**, pp. 198-207.

[36] P.Z. Wang, R. Trettin, V. Rudert, Effect of fineness and particle size distribution of granulated blast-furnace slag on the hydraulic reactivity in cement systems, *Advances in Cement Research*, 17, **2005**, pp. 161-166.

[37] F. Lange, H. Mortel, V. Rudert, Dense packing of cement pastes and resulting consequences on mortar properties, *Cement and Concrete Research*, 27, **1997**, pp. 1481-1488.

[38] Radioactive Waste Management, *Geological Disposal: Guidance on the production of encapsulated wasteforms,* RWM, WPS/502/01, **2015**.

[39] S. Farris, E. Miller, E. Wright, H. Shepherd, *Alternative BFS Suppliers,* BNFL, RAT (04) 4134, **2004**.

[40] G.M. Cann, K. Carruthers, *MEP - Source of Product Quality Parameters,* NNL, NNL (12) 10294, **2012**.

[41] P. Ghoddousi, A.A.S. Javid, J. Sobhani, Effects of particle packing density on the stability and rheology of self-consolidating concrete containing mineral admixtures, *Construction and Building Materials*, 53, **2014**, pp. 102-109.

[42] P.F.G. Banfill, Rheology of Fresh Cement and Concrete, *Rheology Reviews*, **2006**, pp. 61-130.

[43] D.A. Williams, A.W. Saak, H.M. Jennings, The influence of mixing on the rheology of fresh cement paste, *Cement and Concrete Research*, 29, **1999**, pp. 1491-1496.

[44] C.K. Park, M.H. Noh, T.H. Park, Rheological properties of cementitious materials containing mineral admixtures, *Cement and Concrete Research*, 35, **2005**, pp. 842-849.

[45] S. Clayton, T.G. Grice, D.V. Boger, Analysis of the slump test for on-site yield stress measurement of mineral suspensions, *International Journal of Mineral Processing*, 70, **2003**, pp. 3-21.

[46] C.F. Ferraris, K.H. Obla, R. Hill, The influence of mineral admixtures on the rheology of cement paste and concrete, *Cement and Concrete Research*, 31, **2001**, pp. 245-255.

[47] A. Kashani, R. San Nicolas, G.G. Qiao, J.S.J. van Deventer, J.L. Provis, Modelling the yield stress of ternary cement–slag–fly ash pastes based on particle size distribution, *Powder Technology*, 266, **2014**, pp. 203-209.

[48] J.D. Palmer, G.A. Fairhall, Properties of Cement Systems Containing Intermediate Level Wastes *Cement and Concrete Research*, 22, **1992**, pp. 325-330.

[49] British Nuclear Fuels Limited, *Decanning process in MEP*, BNFL.

[50] British Nuclear Fuels Limited, *Waste streams from WEP and MEP*, BNFL.

[51] G. M. Cann, D.W. Anderson, *WEP-Sources of Product Quality Parameters,* National Nuclear Laboratory, NNL, NNL(14)9491, **2014**.

[52] G.M. Cann, N.C. Collier, *Effect of High OPC Content on WEP Centrifuge Cake Wasteforms - Phase 2,* NNL, NNL (10) 10896, **2010**.

[53] N.J. Bowmer, K. Carruthers, R. Orr, *WEP - Sources of Product Quality Parameters,* Nexia Solutions, (08) 9491, **2008**.

[54] S. Foster, *MEP Product Quality Assurance Parameters and Plant Control Settings,* Effluents and Encapsulation Plants, Sellafield Ltd, **2016**.

[55] S. Pepper, *Assessment of Alternative Sources of Blastfurnace Slag for use in the Sellafield ILW Encapsulation Plants,* NNL, EP04685/06/04, **2010**.

[56] S. Farris, E. Miller, E. Wright, J. Parr, *Change of BFS Supplier from Castle Cement to North East Slag Cement Redcar Works,* BNFL, RAT (03) 3855, **2003**.

[57] British Standard, *Ground granulated blast furnace slag for use in concrete, mortar and grout*, Part 1: Definitions, specifications and conformity criteria, **2006**, BS EN 15167-1.

[58] G.M. Cann, R.M. Orr, *A Technical Specification for Portland Cement, Blast Furnace Slag and Fly Ash Powders for Use in the Encapsulation/Immobilisation of Radioactive Waste Materials (8th Revision),* NNL, NNL (10) 10653, **2009**.

[59] S. Foster, J. Jowsey, G.M. Cann, *Review of Encapsulation Cements*, Meeting, **11 June 2014.**

[60] G.M. Cann, J. Borwick, H. Dixon, *Assessment of Port Talbot Blast Furnace Slag,* National Nuclear Laboratory, NNL, **2016**.

[61] G.M. Cann, *A Technical Specification for Portland Cement, Blast Furnace Slag and Fly Ash Powders for Use in the Encapsulation/Immobilisation of Radioactive Waste Materials (9th Revision),* NNL, NNL (16) 13324, **2016**.

[62] British Standard, *Ground granulated blast furnace slag for use in concrete, mortar and grout*, Part 2: Conformity evaluation, **2006**, BS EN 15167-2.

[63] British Standard, *Methods of testing cement*, Part 6: Determination of fineness, **2010**, BS EN 196-6.

[64] S. Brunauer, P.H. Emmett, E. Teller, Adsorption of Gases in Multimolecular Layers, *Journal of the American Chemical Society*, 60, **1938**, pp. 309-319.

[65] E.F. Osborn, R.C. DeVries, K.H. Gee, H.M. Kraner, Optimum Compositions of Blast Furnace Slag As Deduced from Liquidus Data for The Quaternary System CaO-MgO-Al_2O_3-SiO_2, *Journal of Metals*, **1954**, pp. 33-45.

[66] D.L. Kantro, Influence of Water-Reducing Admixtures on Properties of Cement Paste - A Miniature Slump Test, *Cement, Concrete and Aggregates*, 2, **1980**, pp. 95-102.

[67] N. Roussel, C. Stefani, R. Leroy, From mini-cone test to Abrams cone test: measurement of cement-based materials yield stress using slump tests, *Cement and Concrete Research*, 35, **2005**, pp. 817-822.

[68] W.S. Rasband. ImageJ, U.S. National Institute of Health: Bethesda, Maryland, USA, **1997-2012.**

[69] J.C. Chang, B.V. Velamakanni, F.F. Lange, D.S. Pearson, Centrifugal Consolidation of Al_2O_3 and AI_2O_3/ZrO_2 Composite Slurries vs Interparticle Potentials: Particle Packing and Mass Segregation, *Journal of the American Ceramic Society*, 74, **1991**, pp. 2201-2204.

[70] M. Glavind, E.J. Pedersen, *Packing calculations applied for concrete mix design*, Utilizing Ready Mix Concrete and Mortar, pp. 121-130.

[71] L. Wadsö, M. Arndt, An international round robin test on isothermal (conduction) calorimetry for measurement of three-day heat of hydration of cement, *Cement and Concrete Research*, 79, **2016**, pp. 316-322.

[72] P. Morabito, *Avoidance of Thermal Cracking in Concrete at Early Ages*, Materials and Structures**1997**, pp. 451-464.

[73] P. Livesey, A. Donnelly, C. Tomlinson, Measurement of the Heat of Hydration of Cement, *Cement and Concrete Composites*, 13, **1991**, pp. 177-185.

[74] P. Atkins, J. De Paula, *Atkins' Physical Chemistry*, Oxford University Press, Oxford, **2006**, pp. 702-710.

[75] R.E. Dinnebier, S.J.L. Billinge, *Principles of Powder Diffraction*, in: R.E. Dinnebier, S.J.L. Billinge (Eds.) Powder Diffraction Theory and Practice**2008**, pp. 1-19.

[76] The British Standards Institution, *Methods of Testing Cement*, Part 3: Determination of setting time and soundness, **2016**, 196-3.

[77] *Standard Test Method for Time of Setting of Hydraulic-Cement Paste by Gillmore Needles*, **2015**,

[78] ASTM International, *Standard Practice for: Use of Apparatus for the Determination of Length Change of Hardened Cement Paste, Mortar and Concrete*, **2009**, C 490-00a.

[79] J. Chappuis, Rheological measurements with cements pastes in vicometers: A comprehensive Approach, *Rheology of Fresh Cement and Concrete*, Liverpool, UK, **1990**.

[80] P.F.G. Banfill, D.R. Kitching, Use of a controlled stress rheometer to study the yield stress of oilwell cement slurries, *Rheology of Fresh Cement and Concrete*, Liverpool, UK, **1990**.

[81] A. Bouvet, E. Ghorbel, R. Bennacer, The mini-conical slump flow test: Analysis and numerical study, *Cement and Concrete Research*, 40, **2010**, pp. 1517-1523.

[82] A.W. Saak, H.M. Jennings, S.P. Shah, The influence of wall slip on yield stress and viscoelastic measurements of cement paste, *Cement and Concrete Research*, 31, **2001**, pp. 205-212.

[83] P.V. Liddel, D.V. Boger, Yield stress measurements with the vane, *Journal of Non-Newtonian Fluid Mechanics*, 63, **1996**, pp. 235-261.

[84] N. Roussel, P. Coussot, "Fifty-cent rheometer" for yield stress measurements: From slump to spreading flow, *Journal of Rheology*, 49, **2005**, pp. 705-718.

[85] ASTM International, *Standard Test Method for Slump of Hydraulic-Cement Concrete*, **2012**, C143M - 12.

[86] A.W. Saak, H.M. Jennings, S.P. Shah, A generalized approach for the determination of yield stress by slump and slump flow, *Cement and Concrete Research*, 34, **2004**, pp. 363-371.

[87] T. Kokado, T. Hosoda, T. Miyagawa, Study on a method of obtaining rheological coefficients of high-flow concrete with numerical analysis, *Doboku Gakkai Ronbunshu*, 2000, **2000**, pp. 109-125.

[88] Z. Tan, S.A. Bernal, J.L. Provis, Reproducible mini-slump test procedure for measuring the yield stress of cementitious pastes, *Materials and Structures*, 50, **2017**, pp. 235.

[89] N. Roussel, *Understanding the rheology of concrete*, Woodhead Publishing, Abingdon, **2012**.

[90] D.V. Boger, Rheology and the resource industries, *Chem. Eng. Sci.*, 64, **2009**, pp. 4525-4536.

[91] L. Bergström, C.H. Schilling, I.A. Aksay, Consolidation Behavior of Flocculated Alumina Suspensions, *Journal of the American Ceramic Society*, 75, **1992**, pp. 3305-3314.

[92] T. Zhang, Q. Yu, J. Wei, P. Zhang, A new gap-graded particle size distribution and resulting consequences on properties of blended cement, *Cement and Concrete Composites*, 33, **2011**, pp. 543-550.

[93] T. Zhang, Q. Yu, J. Wei, P. Zhang, P. Chen, A gap-graded particle size distribution for blended cements: Analytical approach and experimental validation, *Powder Technology*, 214, **2011**, pp. 259-268.

[94] A. Wang, C. Zhang, N. Zhang, The theoretic analysis of the influence of the particle size distribution of cement system on the property of cement, *Cement and Concrete Research*, 29, **1999**, pp. 1721-1726.

[95] P.A. Vesilind, The Rosin-Rammler particle size distribution, *Resource Recovery and Conservation*, 5, **1980**, pp. 275-277.

[96] R.J. Flatt, P. Bowen, Yodel: A yield stress model for suspensions, *Journal of the American Ceramic Society*, 89, **2006**, pp. 1244-1256.

[97] Z. Zhou, M.J. Solomon, P.J. Scales, D.V. Boger, The yield stress of concentrated flocculated suspensions of size distributed particles, *Journal of Rheology*, 43, **1999**, pp. 651-671.

[98] R.J. Flatt, P. Bowen, Yield stress of multimodal powder suspensions: An extension of the YODEL (Yield Stress mODEL), *Journal of the American Ceramic Society*, 90, **2007**, pp. 1038-1044.

[99] F. de Larrard, *Concrete Mixture Proportioning*, E. & F. Spon, London, **1999**.

[100] M. Stuer, P. Bowen, Yield stress modelling of doped alumina suspensions for applications in freeze granulation: towards dry pressed transparent ceramics, *Advances in Applied Ceramics*, 111, **2012**, pp. 254-261.

[101] G. Lomboy, S. Sundararajan, K. Wang, S. Subramaniam, A test method for determining adhesion forces and Hamaker constants of cementitious materials using atomic force microscopy, *Cement and Concrete Research*, 41, **2011**, pp. 1157-1166.

[102] The British Standards Institution, *Method of testing cement*, Part 8: Heat of hydration - Solution method, **2010**, 196-8.

[103] The British Standards Institution, *Methods of testing cement*, Part 9: Heat of hydration - Semi-adiabatic method, **2010**, 196-9.

[104] T. Poole, *Revision of Test Methods and Specifications for Controlling Heat of Hydration in Hydraulic Cement,* Portland Cement Association,,, Illinois, 3007, **2007**.

[105] European Comittee for Standardization, *Isothermal Conduction Calorimetry (ICC) for the Determination of Heat of Hydration of Cement: State of Art Report and Recommendations*, **2014**, PD CEN/TR 16632:2014.

[106] ASTM International, *Standard Practice for Measuring Hydration Kinetics of Hydraulic Cementitious Mixtures Using Isothermal Calorimetry*, **2014**, C1679-14.

[107] ASTM International, *Standard Test Method for Measurement of Heat of Hydration of Hydraulic Cementitious Materials Using Isothermal Conduction Calorimetry*, **2015**, C1702-15a.

[108] P.K. Mehta, P.J.M. Monteiro, *Concrete Microstructure, Properties and Materials*, McGraw-Hill, USA, **2006**.

[109] C.A. Utton, M. Hayes, J. Hill, N.B. Milestone, J.H. Sharp, Effect of Temperatures up to 90°C on the Early Hydration of Portland–Blastfurnace Slag Cements, *Journal of the American Ceramic Society*, 91, **2008**, pp. 948-954.

[110] The British Standards Institution, *Cement - Composition, specifications and conformity criteria for very low heat special cements*, **2015**, BS EN 14216:2015.

[111] E. Berodier, K. Scrivener, Understanding the Filler Effect on the Nucleation and Growth of C-S-H, *Journal of the American Ceramic Society*, 97, **2014**, pp. 3764-3773.

[112] K.L. Scrivener, P. Juilland, P.J.M. Monteiro, Advances in understanding hydration of Portland cement, *Cement and Concrete Research*, 78, Part A, **2015**, pp. 38-56.

[113] H. Binici, H. Temiz, M.M. Köse, The effect of fineness on the properties of the blended cements incorporating ground granulated blast furnace slag and ground basaltic pumice, *Construction and Building Materials*, 21, **2007**, pp. 1122-1128.

[114] W.A. Gutteridge, J.A. Dalziel, Filler cement: The effect of the secondary component on the hydration of Portland cement, *Cement and Concrete Research*, 20, **1990**, pp. 853-861.

[115] B. Lothenbach, K. Scrivener, R.D. Hooton, Supplementary cementitious materials, *Cement and Concrete Research*, 41, **2011**, pp. 1244-1256.

[116] T. Oey, A. Kumar, J.W. Bullard, N. Neithalath, G. Sant, The Filler Effect: The Influence of Filler Content and Surface Area on Cementitious Reaction Rates, *Journal of the American Ceramic Society*, 96, **2013**, pp. 1978-1990.

[117] P. Termkhajornkit, R. Barbarulo, G. Chanvillard, Microstructurally-designed cement pastes: A mimic strategy to determine the relationships between microstructure and properties at any hydration degree, *Cement and Concrete Research*, 71, **2015**, pp. 66-77.

[118] F. Deschner, F. Winnefeld, B. Lothenbach, S. Seufert, P. Schwesig, S. Dittrich, F. Goetz-Neunhoeffer, J. Neubauer, Hydration of Portland cement with high replacement by siliceous fly ash, *Cement and Concrete Research*, 42, **2012**, pp. 1389-1400.

[119] V. Kocaba, E. Gallucci, K.L. Scrivener, Methods for determination of degree of reaction of slag in blended cement pastes, *Cement and Concrete Research*, 42, **2012**, pp. 511-525.

[120] M. Whittaker, M. Zajac, M. Ben Haha, F. Bullerjahn, L. Black, The role of the alumina content of slag, plus the presence of additional sulfate on the hydration and microstructure of Portland cement-slag blends, *Cement and Concrete Research*, 66, **2014**, pp. 91-101.

[121] S. Adu-Amankwah, M. Zajac, C. Stabler, B. Lothenbach, L. Black, Influence of limestone on the hydration of ternary slag cements, *Cement and Concrete Research*, 100, **2017**, pp. 96-109.

[122] X. Wu, D.M. Roy, C.A. Langton, Early stage hydration of slag-cement, *Cement and Concrete Research*, 13, **1983**, pp. 277-286.

[123] S.J. Barnett, M.N. Soutsos, S.G. Millard, J.H. Bungey, Strength development of mortars containing ground granulated blast-furnace slag: Effect of curing temperature and determination of apparent activation energies, *Cement and Concrete Research*, 36, **2006**, pp. 434-440.

[124] J. Jowsey, *Blast Furnace Slag for Sellafield Encapsulation Plants: Technical Specification,* **2012**.

[125] C. Medina, I.F. Sáez del Bosque, E. Asensio, M. Frías, M.I. Sánchez de Rojas, New additions for eco-efficient cement design. Impact on calorimetric behaviour and comparison of test methods, *Materials and Structures*, 49, **2016**, pp. 4595-4607.

[126] E. Gruyaert, N. Robeyst, N. De Belie, Study of the hydration of Portland cement blended with blast-furnace slag by calorimetry and thermogravimetry, *Journal of Thermal Analysis and Calorimetry*, 102, **2010**, pp. 941-951.

[127] P.J. Egan, A comparison between semi-isothermal and semi-adiabatic calorimetry of retarded cement mixes, *Advances in Cement Research*, 1, **1988**, pp. 112-118.

[128] A. Durán-Herrera, C.A. Juárez, P. Valdez, D.P. Bentz, Evaluation of sustainable high-volume fly ash concretes, *Cement and Concrete Composites*, 33, **2011**, pp. 39-45.

[129] D. Prentice, S. Bernal, M. Bankhead, M. Hayes, J. Provis, *Phase evolution of slag-rich cementitious grouts for immobilisation of nuclear wastes: an experimental and modelling approach*, **2017**.

[130] R.J. Caldwell, N.J. Bowmer, E.J. Butcher, I.H. Godfrey, Characterisation of Full-Scale Inactive Cement-Based Intermediate Level Nuclear Wasteforms After One Decade of Storage, **2004**, pp. 681-689.

[131] R.J. Caldwell, S. Rawlinson, E.J. Butcher, I.H. Godfrey, *Characterisation of full-scale historic inactive cement-based intermediate level nuclear wasteforms*, in: A. Al-Tabbaa, J.A. Stegemann (Eds.) Stabilisation/Solidification Treatment and Remediation Taylor & Francis Group, London, **2005**.

[132] M. Drakopoulos, T. Connolley, C. Reinhard, R. Atwood, O. Magdysyuk, N. Vo, M. Hart, L. Connor, B. Humphreys, G. Howell, S. Davies, T. Hill, G. Wilkin, U. Pedersen, A. Foster, N. De Maio, M. Basham, F. Yuan, K. Wanelik, I12: the Joint Engineering, Environment and Processing (JEEP) beamline at Diamond Light Source, *Journal of Synchrotron Radiation*, 22, **2015**, pp. 828-838.

[133] *http://www.diamond.ac.uk/Beamlines/Engineering-and-Environment/I12.html*, UK, **5th May 2018**.

[134] O.S. Floyd, O. Stanley, X-Rays for Study of Internal Structure and Microcracking of Concrete, *Journal of the American Concrete Institute*, 60, **1963**, pp. 575-587.

[135] E.N. Landis, S.L. Petrell, E.N. Nagy, Examination of pore structure using three-dimensional image analysis of microtomographic data, *Concrete Science and Engineering*, 2, **2000**, pp. 162-169.

[136] E. Gallucci, K. Scrivener, A. Groso, M. Stampanoni, G. Margaritondo, 3D experimental investigation of the microstructure of cement pastes using synchrotron X-ray microtomography (μCT), *Cement and Concrete Research*, 37, **2007**, pp. 360-368.

[137] M.A.B. Promentilla, T. Sugiyama, T. Hitomi, N. Takeda, Characterizing the 3D pore structure of hardened cement paste with synchrotron microtomography, *Journal of Advanced Concrete Technology*, 6, **2008**, pp. 273-286.

[138] U. Bonse, F. Busch, X-ray computed microtomography (microCT) using synchrotron radiation (SR), *Progress in biophysics and molecular biology.*, 65, **1996**, pp. 133 - 169.

[139] The Aberdeen Group, *Concrete bleeding: Causes, effects and control*, Concrete Construction, **1988**.

[140] D. Bentz, E.J. Garboczi, C. J. Haecker, O. M. Jensen, *Effects of Cement Particle Size Distribution on Performance Properties of Portland Cement-Based Materials*, **1999**.

[141] D. Kim, Effect of Adjusting for Particle-Size Distribution of Cement on Strength Development of Concrete, *Advances in Materials Science and Engineering*, 2018, **2018**, pp. 6.

[142] J. Zhu, Q. Zhong, G. Chen, D. Li, Effect of particlesize of blast furnace slag on properties of portland cement, *Procedia Engineering*, 27, **2012**, pp. 231-236.

[143] E.G. Wolff, *Introduction to the Dimensional Stability of Composite Materials*, DEStech Publications, Inc. , Pennsylvania, U.S.A, **2004**.

[144] H. Ye, A. Radlińska, Shrinkage mechanisms of alkali-activated slag, *Cement and Concrete Research*, 88, **2016**, pp. 126-135.

[145] X.-h. Yuan, W. Chen, Z.-a. Lu, H. Chen, Shrinkage compensation of alkali-activated slag concrete and microstructural analysis, *Construction and Building Materials*, 66, **2014**, pp. 422-428.

[146] R.J. Thomas, D. Lezama, S. Peethamparan, On drying shrinkage in alkali-activated concrete: Improving dimensional stability by aging or heat-curing, *Cement and Concrete Research*, 91, **2017**, pp. 13-23.

[147] Nuclear Decommissioning Authority, *Waste Packaging Specification and Guidance Documentation,* 9699292, **2008**.

[148] H. Ye, C. Cartwright, F. Rajabipour, A. Radlińska, Understanding the drying shrinkage performance of alkali-activated slag mortars, *Cement and Concrete Composites*, 76, **2017**, pp. 13-24.

[149] P.S. Deb, P. Nath, P.K. Sarker, Drying Shrinkage of Slag Blended Fly Ash Geopolymer Concrete Cured at Room Temperature, *Procedia Engineering*, 125, **2015**, pp. 594-600.

[150] D. Han, R.D. Ferron, Influence of high mixing intensity on rheology, hydration, and microstructure of fresh state cement paste, *Cement and Concrete Research*, 84, **2016**, pp. 95-106.

[151] D. Han, R.D. Ferron, Effect of mixing method on microstructure and rheology of cement paste, *Construction and Building Materials*, 93, **2015**, pp. 278-288.

[152] P. Juilland, A. Kumar, E. Gallucci, R.J. Flatt, K.L. Scrivener, Effect of mixing on the early hydration of alite and OPC systems, *Cement and Concrete Research*, 42, **2012**, pp. 1175-1188.

[153] M. Yang, H.M. Jennings, Influences of mixing methods on the microstructure and rheological behavior of cement paste, *Advanced Cement Based Materials*, 2, **1995**, pp. 70-78.

[154] J. Gajda, M. Vangeem, *Controlling Temperatures in Mass Concrete*, Concrete International, **2002**.

Appendix A: List of Figures

Appendix B: List of Tables

Appendix C: Chapter 6 – Heat of Hydration

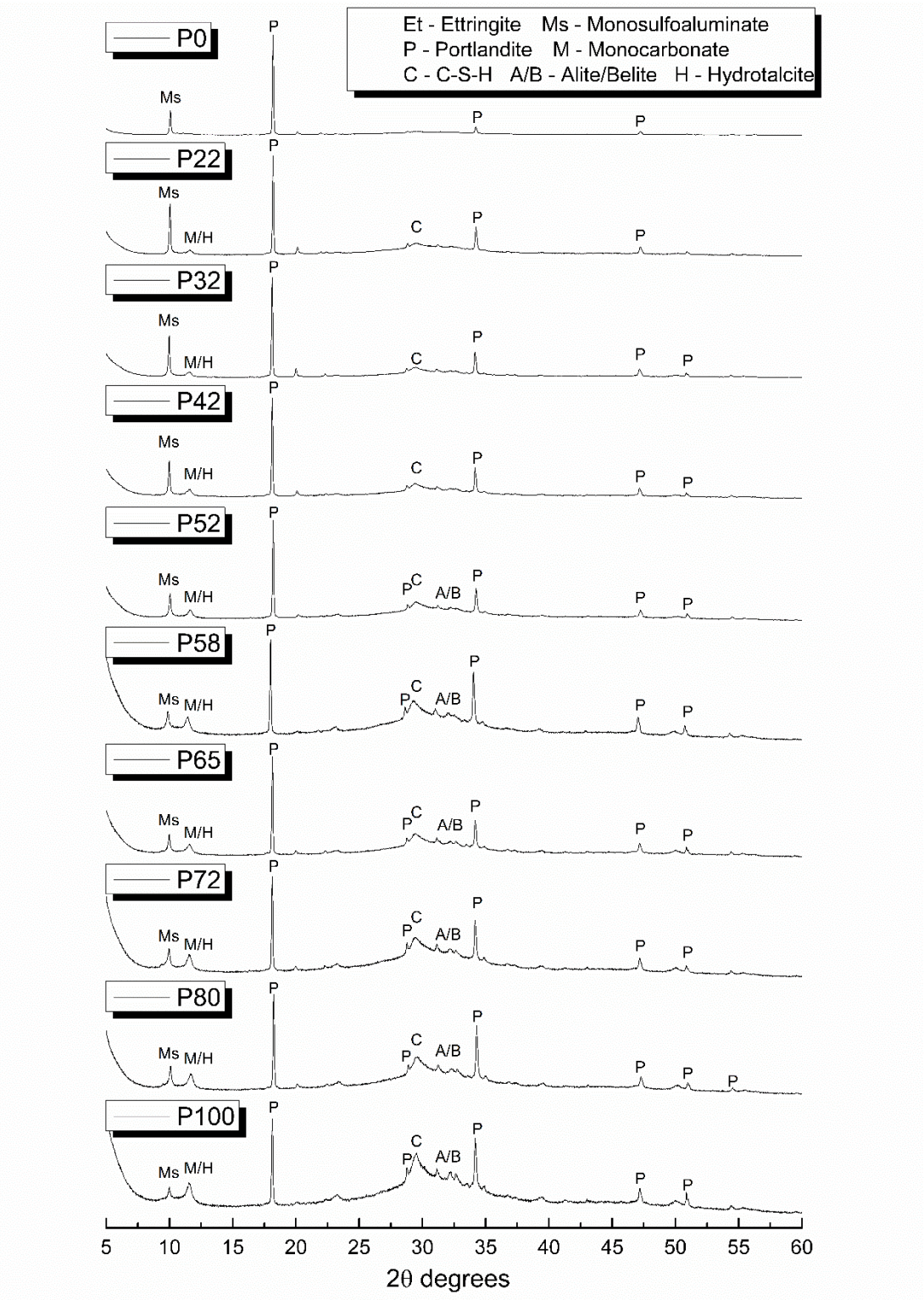

Figure C.0.1. X-ray diffraction patterns of the 10 BFS:PC isothermal conduction calorimetry samples that were measured at 35 ˚C, where the BFS fraction comprises the blends stated in Table 3.4, after 28 days of curing.

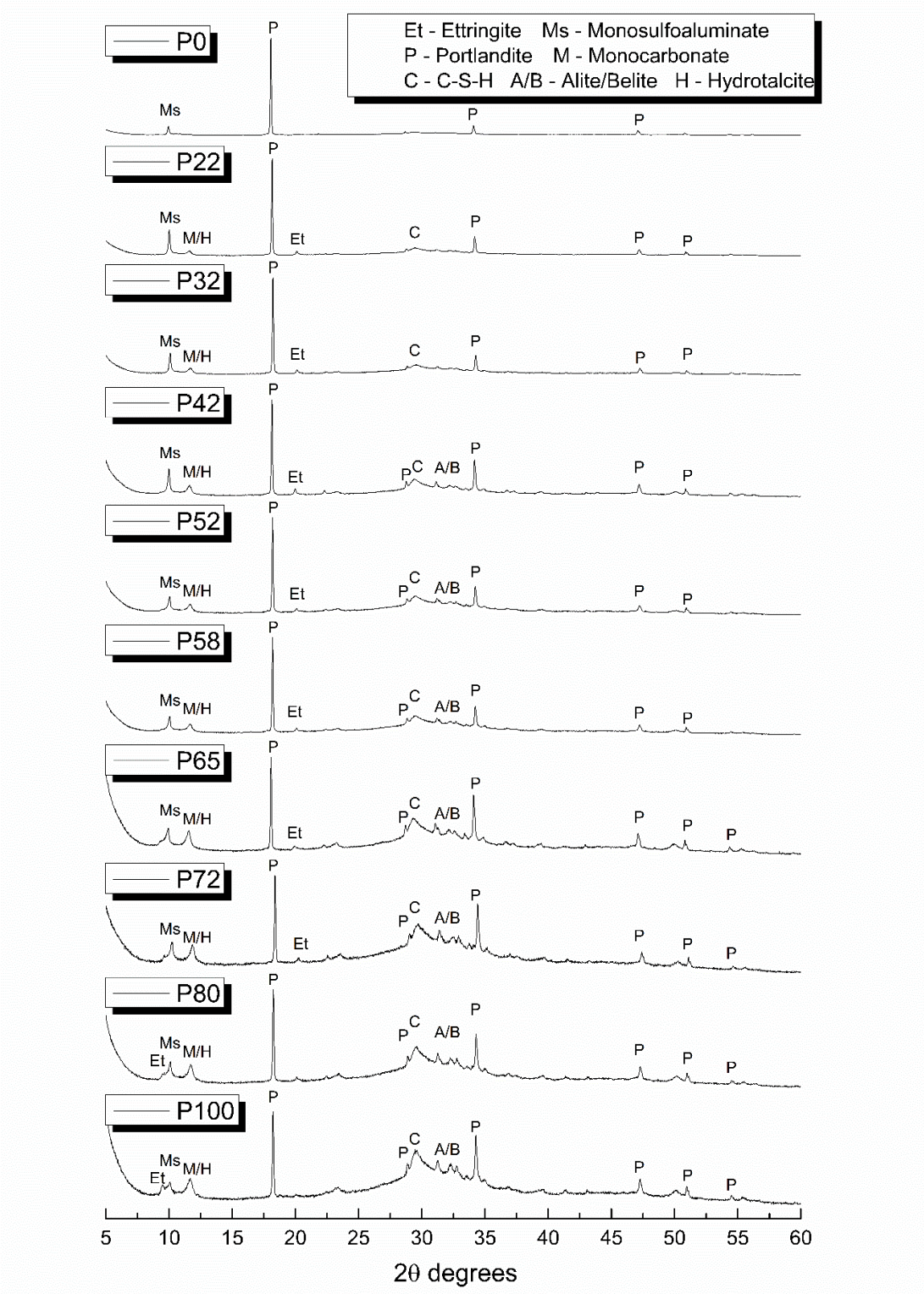

Figure C.0.2. X-ray diffraction patterns of the 10 BFS:PC semi-adiabatic calorimetry samples that were measured at room temperature, where the BFS fraction comprises the blends stated in Table 3.4, after 28 days of curing.

Appendix D: Chapter 8 – Scale up Trials

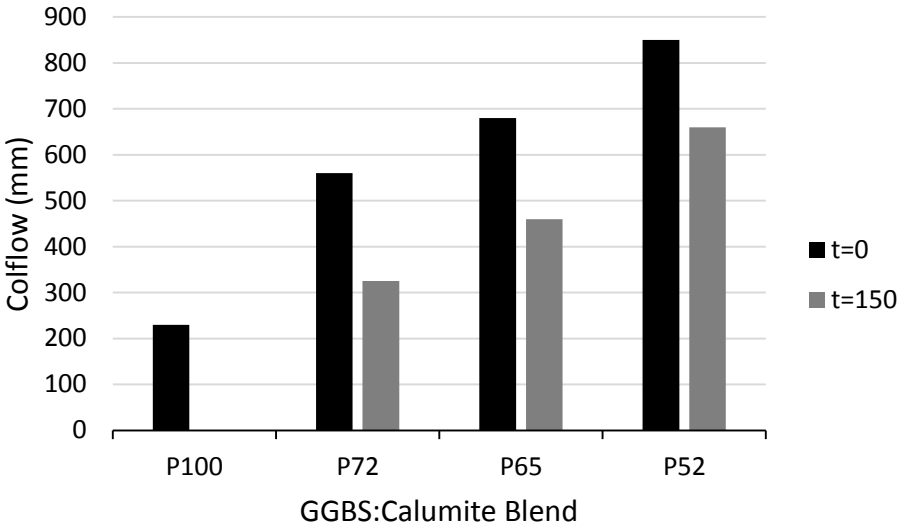

Figure D.0.1. Colflow fluidity for P100, P72, P65 and P52 for the Port Talbot:Calumite:Ketton system at 3:1 BFS:PC ratio and at a 0.35 w/s content for t=0 and t=150.

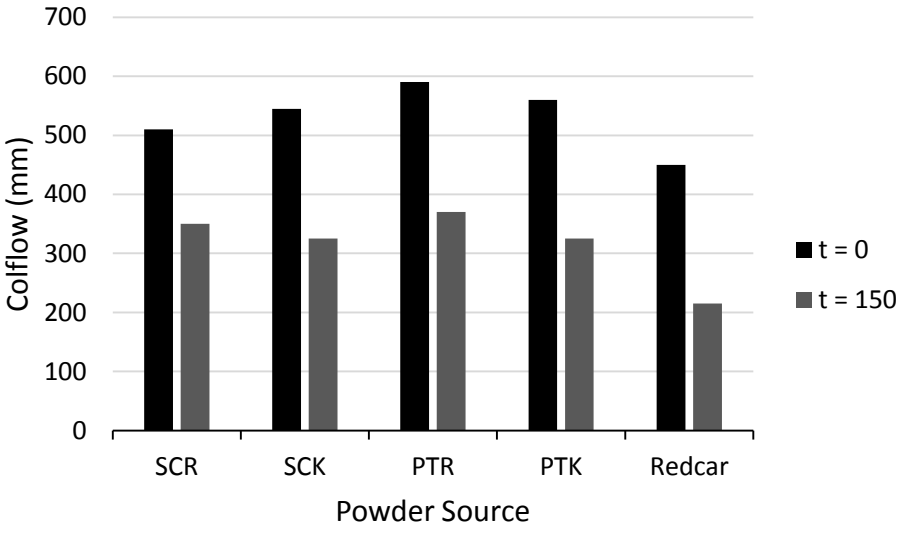

Figure D.0.2. Comparison of Colflow fluidity of different powder sources for GGBS:Calumite P72 blend ratios at 3:1 BFS:PC ratio and a 0.35 w/s.